Identification and Characterization of an

Adaptive Mitochondrial Biogenesis Response to Iron Deprivation

By

Jarred W. Rensvold

A dissertation submitted in partial fulfillment of

the requirements for the degree of

Doctor of Philosophy

(Cellular and Molecular Biology)

at the

UNIVERSITY OF WISCONSIN-MADISON

2015

Date of final oral examination: 9/9/2015

This dissertation is approved by the following members of the Final Oral Committee:

David J. Pagliarini, Associate Professor, Biochemistry
Richard S. Eisenstein, Professor, Nutritional Sciences
Patricia J. Kiley, Professor and Chair, Biomolecular Chemistry
Shigeki Miyamoto, Professor, Oncology
Marvin P. Wickens, Professor, Biochemisty

ABSTRACT

Identification and Characterization of an

Adaptive Mitochondrial Biogenesis Response to Iron Deprivation

By

Jarred W. Rensvold

Under the supervision of Professor David J. Pagliarini

At the University of Wisconsin-Madison

Mitochondrial biogenesis involves the coordinated expression of more than one thousand proteins encoded by two genomes. Defects in this process are associated with a broad range of human diseases and age-related disorders. The transcriptional regulators that control mitochondrial biogenesis, including the PGC-1 family of transcriptional coactivators, are well defined. However, other aspects of the cellular control of mitochondrial biogenesis remain unclear, including epigenetic and post-transcriptional mechanisms that control mitochondrial biogenesis, signals that coordinate gene expression between mitochondria and the nucleus, and the nutritional states that result in decreased mitochondrial production.

To better define the mitochondrial biogenesis program, we performed matched, quantitative proteomics and microarray analyses of mouse muscle cells undergoing PGC-1α-driven mitochondrial biogenesis. From these analyses we find that proteins involved in cellular iron homeostasis are highly coordinated with mitochondrial biogenesis, and that iron deprivation has an equal and opposite effect on mitochondrial biogenesis to that of PGC-1α overexpression. Additional analyses revealed that iron depletion through chelation or active transport in a range of cell lines results in a rapid, dose-dependent loss of nuclear- and mitochondrial-encoded

transcripts, proteins and mitochondrial oxidative capacity that is fully reversible upon iron repletion. Utilizing an RNA labeling approach we determined that the decrease in transcripts encoding mitochondrial proteins is due to a decrease in transcription and not due to increased transcript degradation. We also find that the decrease in mitochondrial proteins precedes this transcriptional dampening, perhaps suggesting a mitochondrial retrograde response. Further, we discover that iron chelation causes dynamic changes in histone acetylation and methylation, with decreases in histone acetylation at nuclear encoded mitochondrial genes. Additionally, the effect of iron chelation on mitochondrial transcript levels is fully reversed with HDAC inhibition, consistent with epigenetic regulation of gene expression. Finally, we find that this response is independent of the well-established PGC-1α-, PGC-1β- and HIF-1α-regulation of mitochondrial biogenesis. Collectively, our research reveals that cellular iron concentration is a key parameter in calibrating the mitochondrial biogenesis program and shows that iron deprivation initiates a reversible, adaptive mitochondrial biogenesis response. Moreover, our work provides a model for how nutrient deprivation can drive epigenetic regulation of mitochondrial biogenesis.

ACKNOWLEDGEMENTS

Graduate school has been an intense, transformative and immensely enjoyable process. I thank the many teachers, mentors, collaborators, friends and family that have supported me in leading up to and throughout graduate school. This thesis would not be possible without you.

First, thank you to my Ph.D. advisor, Professor Dave Pagliarini. I cannot imagine having gone through graduate school with a different mentor. Your scientific passion and vision is inspiring. The attention you give to each of your students and projects is remarkable, and has set an example that I can only hope to emulate. Thank you for providing a rich and exciting research environment, and challenging me to improve in all aspects of science. I am especially grateful for all of the conference travel opportunities, they have not only helped me to advance as a researcher but have exposed me to more of the world, and I am a better person for it. I am proud to have been part of your lab from the beginning and am excited to watch it continue to thrive and to see the new discoveries you will make in the future. Hereafter, no matter where I go or what I do, I will always be mitochondriac.

To my fellow Pagliarini graduate originals, Josh and Amelia, I could not have hoped for better labmates. Your scientific expertise and friendship made graduate school easier and vastly more enjoyable. I especially enjoyed those first semesters in the lab when we were all just trying to figure out what graduate school was about. Paul, your unbridled exuberance kept the lab fun and your writing assistance helped me to develop my own skills. I have had the fortune of sharing a research bay with a several wonderful individuals, including Amelia, Mark, Kelly and most recently Holly. Each of you could not have been more unalike, but those differences brought unique perspectives and fresh ideas that helped to keep my research moving forward. To my mentees, Athavi and Helen, thank you for all of your hard work and letting me practice my

mentorship skills on you. I think that I probably learned more from you than you ever did from me. Natalie and Brendan, thank you for all the helpful high-level research discussions and the specific experimental suggestions on my thesis project. Additionally, none of my thesis research would have been possible without the support of the wonderful undergraduates, including Kate, Anna, Chelsea, Temi, Sarah and Jacob, who worked in the lab at different points during my time as a graduate student and helped to keep the lab and my research going behind the scenes.

Throughout graduate school, I have made friends that I hope I will have for the rest of my life. Their emotional, social and intellectual support helped me to make it though some of the more difficult challenges of my graduate work. Keenan, your easy-going attitude helped to relieve some of the anxiety I felt during our first years as graduate students. I especially enjoyed all the time we spent cycling together, exploring the dairy roads outside of Madison. Matt, you were a fantastic roommate and your humor and cheerfulness was always welcome. Adam, thank you for all your technical advice and the amazing homebrew that seemed to appear just when I needed it the most. I appreciated having someone in lab with which to talk running and thanks for encouraging me to get out once in a while for some races. Andrew, Danielle, Jon and Molly, you are not only labmates but also great friends. Thank you for listening to me vent when my experiments and what seemed to be everything else was working against me. Specifically, thank you to Andrew for picking me up from the ER after my attempt at a face-first bicycle dismount.

I have had the opportunity to work with many great researchers outside of the Pagliarini Lab during my graduate studies. Catie Minogue and Marie Foss, thank you for the opportunity to work with both of you on your respective projects. I learned a tremendous amount in the process. Professor Rick Eisenstein, your insights on iron helped to focus my initial experimental questions and set my research on a clear path, and thank you to your scientists, Christopher Nizzi

and Sheila Anderson, who helped me while I was prepping mouse tissues in your lab. Thanks to Professor John Denu, Kim Krautkramer and James Dowell. Your expertise was critical in advancing my thesis work in a new and exciting direction. Moreover, thank you to my thesis committee. I've always looked forward to your advice at our annual meetings. Your collective wisdom is staggering.

Leading up to graduate school, I have had many great mentors and teachers that have influenced my trajectory toward scientific research and whose lessons and advice have proven invaluable during my thesis work. Specifically, thank you to Professor Dan Gretch. Your biochemistry courses were truly inspirational, and were also my first introduction to metabolism and mitochondrial biology. Thank you for giving me a place in your lab when I was just a freshman undergraduate and providing my first real research experience. I also want to thank Professor Kurt Toenjes and Professor Dave Butler. I am grateful for your help and advice during the graduate school application and interview process. Working in your labs cemented my interest in pursuing a career as a scientist, and the knowledge and skills I gained during that time proved critical for my success as a graduate student.

Finally and most importantly, I thank my family. Thank you for your unconditional love and support. This thesis is dedicated to you. Thank you to my parents, Bill and Louise, for when I was growing up, insisting that I keep studying when I wanted to stop, and for convincing me of the importance of an education, teaching me the value of hard work and instilling in me a deep appreciation for nature. To my sister Liz, you are one of my best friends and I value your advice above anyone else. Thank you for setting examples for which I could strive to follow. Since I have been away from home I cherish the time we all spend together more than ever, and I look forward to the times we will share in the future. Thank you for everything you have done for me.

TABLE OF CONTENTS

CHAPTER ONE: Introduction

1.1 Summary

Mitochondria are ancient and dynamic organelles that are critical for a wide range of cellular processes. The composition, quantity, morphology and function of mitochondria change in response to varying environmental conditions. A substantial body of research has shown that iron deprivation has especially drastic effects on mitochondria, including changes in mitochondrial content, structure and activity in both animal models and cell culture. While the effects of iron depletion on mitochondria are well known, the molecular mechanisms behind these changes as well as how cells adapt to iron deprivation-induced mitochondrial dysfunction are largely undefined. More recent investigations have begun to uncover mechanisms of mitochondrial adaptation in response to iron deprivation. Some of these adaptations include post-transcriptional regulation of the expression of select mitochondrial genes and induction of mitophagy. Additionally, we have found that iron deprivation elicits an adaptive mitochondrial biogenesis response that is rapid and reversible, and involves control of nuclear-encoded mitochondrial gene expression through regulation of histone post-translational modifications. As both mitochondrial dysfunction and iron deficiency are associated with many common human disorders, defining mechanisms of mitochondrial adaptation to iron deprivation could have important implications for understanding disease progression and developing new disease treatments.

1.2 Mitochondria

1.2.1 Overview of Mitochondria

Mitochondria are versatile organelles that are central to a range of key metabolic processes, responsive to changing environmental conditions and critical for the survival of nearly

every eukaryotic cell type. In fact, all eukaryotic cells are thought to contain or have *previously* contained these organelles, suggesting that the formation of mitochondria were critical for the development of eukaryotic life (Lane, 2005; Lane and Martin, 2010). Mitochondria are widely believed to have originated when an archaeon engulfed an α-proteobacteria, which developed an endosymbiotic relationship with its host (Gray, 2012; Lane, 2005). However alternatives to this theory exist, including the autogenous hypothesis and the recent ectosymbiotic inside-out model (Baum and Baum, 2014). Regardless, the formation of mitochondria was likely a key step in the evolution of multicellular organisms and may also be the basis for the overabundance of strictly two sexes in higher organisms (Lane, 2005).

Mitochondria were first observed during the middle to late 1800s (the review by Pagliarini and Rutter from 2013 provides an excellent timeline of the major milestones in mitochondrial research) and based on their appearance, were named using the Greek words mitos and khondrion, meaning thread and small granule (Ernster and Schatz, 1981; Lane, 2005; Pagliarini and Rutter, 2013). Mitochondria are approximately 1 micron in size and most cells in the human body contain hundreds to thousands of mitochondria, while some cells, such as red blood cells, contain virtually none, and egg cells (oocytes) contain the most, at a hundred thousand (Lane, 2005), which is not completely surprising considering the maternal inheritance of mitochondria (Giles et al., 1980; Sato and Sato, 2013). In total, these organelles are estimated to account for 10% of a human's body weight (Lane, 2005). Within each cell, mitochondria form complex reticular structures that are highly regulated and dynamic, with mitochondria undergoing constant fission and fusion (Chan, 2012; Youle and van der Bliek, 2012). Structurally, mitochondria are bound by two membranes, the outer mitochondrial membrane (OMM) and inner mitochondrial membrane (IMM). The area between the membranes is termed

the intermembrane space (IMS) and the area within the IMM is called the matrix. The IMM contains numerous folds called cristae **(**Figure 1A**)**. The large surface provided by the cristae form the staging ground for various biochemical functions of mitochondria, including one of its central roles, the conversion of energy through the process of cellular respiration.

A primary function of mitochondria is to generate the vast majority, greater than 90%, of cellular adenosine triphosphate (ATP) through the mitochondrial processes of fatty acid, amino acid and pyruvate oxidation, the tricarboxylic acid cycle **(**TCA) cycle and oxidative phosphorylation (OxPhos), a role that has earned them the nickname, the "powerhouse of the cell" (Siekevitz, 1957). The OxPhos machinery is comprised of five large, multi-subunit complexes and two electron carriers (cytochrome *c* and coenzyme Q) that are located within or peripheral to the IMM **(**Figure 1A**)**. Complexes I-IV compose the electron transport chain (ETC) and complex V is the ATP synthase. The ETC harnesses energy from the reducing equivalents nicotinamide adenine dinucleotide **(**NADH) and flavin adenine dinucleotide ($FADH_2$), generated from the catabolism of macronutrients, and through a series of redox reactions, the ETC establishes an electrochemical proton gradient across the IMM consuming oxygen in the process. Complex V then utilizes this gradient to generate ATP from ADP **(**Figure 1A**)**.

Mitochondria also contain their own genome (a circular DNA molecule of 16,569 base pairs in humans). The publication of the human mitochondrial DNA (mtDNA) genome sequence in 1981 revealed that it encodes 13 mitochondrial proteins as well as 22 mitochondrial transfer RNAs (tRNAs) and 2 mitochondrial ribosomal RNAs (rRNAs) (Anderson et al., 1981). All 13 of the mtDNA-encoded proteins are integral subunits of OxPhos complexes (with the exception of complex II, which doesn't contain any mtDNA-encoded subunits). The nuclear genome (nDNA)

encodes the remainder of the approximately 76 OxPhos subunits (Figure 1A) (DiMauro and Schon, 2003).

Apart from cellular energy generation, mitochondria are important for many other cellular functions. For instance, mitochondria have a central role in the biosynthesis of a variety of macromolecules such as ketone bodies, pyrimidines, urea, lipids and steroids. Mitochondria also play key roles in programmed cell death (apoptosis), heat generation and cellular signaling through the generation of reactive oxygen species (ROS) and calcium buffering (Scheffler, 2008). The mitochondrion is also critically important for iron metabolism, as it contains enzymes and transporters necessary for heme biosynthesis and iron-sulfur (Fe-S) cluster biogenesis. Heme and Fe-S clusters are necessary for many cellular processes, including the TCA cycle, ETC, DNA maintenance, transcription, ribosome function and translation (Figure 1A) (Furuyama et al., 2007; Lill et al., 2012; Maio and Rouault, 2015; Mense and Zhang, 2006; Netz et al., 2014; Richardson et al., 2010; Rouault, 2015a).

In addition to their diverse roles in cellular function, mitochondria also display extraordinary variation in structure and composition across species, tissues and cell types. The groundbreaking electron microscopy (EM) studies by George Palade, Fritiof Sjöstrand and others, in addition to revealing the structural organization of mitochondria, showed that mitochondria are morphological diverse. Some of these early images showed that some mitochondria contain electron dense inclusions (thought to be stored calcium) (Scheffler, 2008), and other images showed striking variation in the morphology of the mitochondrial cristae, which ranged from lamellar to tubular to angular (Blinzinger et al., 1965; Friend and Brassil, 1970; Revel et al., 1963).

Following the sequencing of the mitochondrial genome (Anderson et al., 1981), a number of innovative studies, enabled by the sequencing of the human nuclear genome (Lander et al., 2001; Venter et al., 2001), the introduction of large-scale protein mass spectrometry (MS) technologies and computational approaches, have contributed to the identification of most (85%) of the estimated 1100-1400 nDNA-encoded mitochondrial proteins (Calvo and Mootha, 2010; Pagliarini and Rutter, 2013). Of these efforts, the MitoCarta compendium, published in 2008, represents the most accurate and comprehensive list of mitochondrial proteins (including 1098 distinct proteins) to date (Pagliarini et al., 2008). This inventory was generated through a combination of an MS-based subtractive proteomics of mitochondria isolated from 14 mouse tissues, computational analysis of 6 additional datasets, microscopy localization using large-scale green fluorescent protein (GFP)-tagging and previous literature annotations. Several recent studies have expanded upon the MitoCarta (Kazak et al., 2013), including the mitochondrial matrix proteome (Rhee et al., 2013) and mitochondrial IMS proteome (Hung et al., 2014). Additionally, other researchers have described dynamic changes in the mitochondrial phosphoproteome and acetylproteome under acute and chronic metabolic transitions (Grimsrud et al., 2012; Hebert et al., 2013a; Kim et al., 2006b; Overmyer et al., 2015; Still et al., 2013; Zhao et al., 2011). Importantly, these proteomic studies have revealed that mitochondria show considerable variation in abundance, protein composition and PTMs across tissues, disease states and in response to stress (Johnson et al., 2007a; Johnson et al., 2007b; Kislinger et al., 2006; Mootha et al., 2003a; Palmfeldt et al., 2009). Based on measurements of cytochrome *c*, heart contains 2 to 5 times more mitochondria than other tissue. Additionally, the protein composition of the mitochondrial ribosome is highly variable between tissues and 50% of the mitochondrial proteome distributed in a tissue specific manner with the remainder being shared by all tissues

(Pagliarini et al., 2008). The molecular controls behind this tissue specificity have largely not been determined, but are likely due to differences in mitochondrial biogenesis (Scarpulla, 2011; Spiegelman, 2007), mitochondrial dynamics (including mitochondrial fission, fusion and intracellular mitochondrial movement) (Chan, 2012; MacAskill and Kittler, 2010) and mitochondrial quality control (Quiros et al., 2015; Youle and Narendra, 2011). Moreover, how the mitochondrial proteome changes during development, differentiation and in response to environmental or nutritional stress, and uncovering the molecular basis behind those changes will require additional research.

1.2.2 Mitochondrial Disease

Following the sequencing of the mitochondrial genome (Anderson et al., 1981), the first disease causing mutations in mtDNA were identified (Holt et al., 1988; Wallace et al., 1988), and to date, over 500 mutations in the mitochondrial genome have been linked to disease (Ruiz-Pesini et al., 2007) (http://www.mitomap.org). However, these maternally acquired syndromes only represent approximately 15-20% of all inherited mitochondrial syndromes, with the remainder due to defects in nuclear-encoded genes (Chinnery, 2003; DiMauro and Davidzon, 2005). Mitochondrial respiratory chain diseases (RCD) (or diseases of OxPhos) occur at an estimated prevalence of 1 in 5000 live births and are the most common inborn error of metabolism (Skladal et al., 2003). RCD show complex inheritance patterns, and the clinical features of RCD are exceedingly variable, affect multiple organs, show amazing tissue specificity and can include seizures, stroke, blindness, deafness, pheripheral neuropathy, ataxia (with Friedreich's ataxia, an iron metabolism disorder, being the most common inherited ataxia) (Campuzano et al., 1996), cardio- and skeletal muscle myopathy, anemia, liver failure and bone

marrow dysfunction (Vafai and Mootha, 2012; Xu et al., 2013). Diseases of OxPhos can arise through defects various pathways (Kirby and Thorburn, 2008), including mutations in mtDNA encoded proteins, rRNAs or tRNAs (DiMauro and Schon, 2003; Pancrudo et al., 2007; Taylor et al., 2004; Uusimaa et al., 2004), nDNA encoded OxPhos protein subunits, proteins involved in import or assembly of the OxPhos subunits, and genes involved in mtDNA replication and expression (Calvo and Mootha, 2010; DiMauro et al., 2013; Vafai and Mootha, 2012). In addition to traditionally defined mitochondrial diseases (those directly affecting mitochondrial respiration), expanding the definition of mitochondrial disease to include any mitochondrial localized protein results in over 150 disorders (Scharfe et al., 2009), including type 2 diabetes and various cancers (Boland et al., 2013; Calvo and Mootha, 2010; DiMauro and Schon, 2003; Lowell and Shulman, 2005; Wallace, 2005). As such, elucidating mechanisms causing mitochondrial alteration would provide valuable insight into disease pathogenesis, as mitochondrial dysfunction occurs in many common disorders.

1.3 Overview of Mitochondrial Biogenesis

Mitochondrial biogenesis, or the production of mitochondria, is a complex process that involves the orchestrated transcription, translation, import and assembly of approximately twelve hundred proteins encoded by the nuclear genome that is coordinated with the expression of the 13 proteins, 22 tRNAs and 2 rRNAs encoded by the mitochondrial genome (Dominy and Puigserver, 2013; Mick et al., 2011; Pagliarini et al., 2008; Scarpulla, 2008; Schmidt et al., 2010). The mitochondrial proteins expressed from the nucleus not only include those involved in metabolic processes, such as OxPhos or heme biosynthesis, but also for those involved in mitochondrial protein import, including subunits of the translocase of the outer membrane

(TOM) and inner membrane (TIM), and assembly, such as OxPhos assembly factors. Moreover, all of the proteins required for mtDNA replication and transcription (e.g., mitochondrial transcription factor A, TFAM) are encoded in the nuclear genome as well as ribosomal proteins and tRNA synthetases required for mitochondrial translation.

The network of nuclear transcription factors and transcriptional coactivators that control mitochondrial biogenesis is well defined, and includes the PGC-1α (peroxisome proliferator-activated receptor γ, coactivator 1 α) family of transcriptional coactivators that integrate the activities of a diverse group of transcription factors, including nuclear respiratory factor 1 (NRF-1), GA-binding protein (GABP or NRF-2), the peroxisome proliferator-activated receptors (PPARs) and estrogen-related receptors (ERRs). Once bound at its transcription factor targets, PGC-1α also acts to recruit transcription-activating complexes, such as histone acetyltransferases, to further enhance gene expression. Additionally, other mechanisms of mitochondrial regulation, including mitochondrial dynamics (via mitochondrial fission and fusion), mitochondrial motility (or intracellular movement) (Chan, 2012; MacAskill and Kittler, 2010), mitochondrial quality control (i.e., the activity and expression of mitochondrial proteases and chaperones) and mitochondrial specific autophagy (mitophagy) (Quiros et al., 2015; Youle and Narendra, 2011) may act in concert with mitochondrial biogenesis or alone to influence mitochondrial function and adaptation to cellular stress. Moreover, post-transcriptional regulatory mechanisms, such as microRNAs (Li et al., 2011) or iron-responsive elements (IREs) (Eisenstein and Ross, 2003), are also known to affect the expression of a select number of mitochondrial genes.

Mitochondrial biogenesis is responsive to changes in environmental conditions and nutrient demands (Hock and Kralli, 2009). For example, caloric restriction and endurance

exercise training induce multiple physiological signals, including norepinephrine, Ca^{2+}, cAMP, nitric oxide and their associated signaling pathways, leading to activation of PGC-1α and increased mitochondrial biogenesis (Civitarese et al., 2007; Irrcher et al., 2003; Ljubicic et al., 2010). Additionally, energy depletion during fasting and exercise increase the AMP:ATP ratio leading to activation of AMPK (AMP-activated protein kinase), which then phosphorylates and activates PGC-1α. Similarly, deacetylation by the NAD^+ dependent deacetylase SIRT1, also activates PGC-1α (Scarpulla et al., 2012). In contrast to these adaptations, long-term hypoxia results in decreased mitochondrial biogenesis through multiple mechanisms (Hoppeler et al., 2003; Semenza, 2013). Hypoxia inhibits the α-ketoglutarate-O_2-Fe^{2+}-dependent hydroxylases that constitutively target the alpha subunit of the transcription factor HIF (hypoxia inducible factor 1 α) for degradation (Schofield and Ratcliffe, 2004). This leads to HIF-1α stabilization, dimerization with the constitutively expressed HIF-1β subunit and the subsequent induction of genes that aid in cell survival under limited oxygen tension. Additionally, ROS generated at complex III during hypoxia may also play a role in stabilization of HIF-1α (Klimova and Chandel, 2008). Hypoxia has been shown to initiate a decrease in mitochondrial biogenesis via HIF-1α repression of PGC-1β expression in renal clear cell carcinoma (RCCC) cells (Zhang et al., 2007). HIF-1α also induces expression of PDK1 (pyruvate dehydrogenase kinase 1), which phosphorylates and inactivates the mitochondrial enzyme pyruvate dehydrogenase (Kim et al., 2006a). Further, HIF-1α induction of the mitochondrial protease LONP1 leads to the degradation of complex IV subunit 4 isoform 1 (COX4I1) and a subunit switch to COX4I2 (Fukuda et al., 2007), and HIF-1α induction of microRNA-210 (miR-210) leads to repression of Fe-S cluster assembly proteins, ISCU1 and ISCU2, and a decrease in the activity of mitochondrial Fe-S cluster proteins (Chan et al., 2009). Increased mitochondrial autophagy, the sequestration of

mitochondria in double-membrane autophagic vacuoles (autophagosomes) and delivery to lysosomes for degradation, has also shown to be an important cellular adaptation to hypoxia (Zhang et al., 2008). Additionally, mitochondrial composition and function is altered in response to iron deprivation (Dallman, 1986). However, unlike endurance exercise or long-term hypoxia, the mechanisms responsible for mitochondrial adaptation during iron deficiency are largely undefined.

1.4 Mitochondrial Responses to Iron Deprivation

1.4.1 Effects of Iron Deprivation on Mitochondria

A large number of studies, performed primarily from 1960 to 1990, have examined the effects of iron deficiency on mitochondrial content, morphology and bioenergetics. These efforts began in 1934 when Eugene Cohen and Conrad Elvehjem, from the University of Wisconsin-Madison, found that iron deficiency caused a reduction in cytochromes in the brain, heart and liver of rats (Cohen and Elvehjem, 1934). Incidentally, this observation occurred before the location of the cytochromes (the respiratory pigments of OxPhos) was demonstrated to be in mitochondria (Ernster and Schatz, 1981). Early studies of cytochrome oxidase (complex IV) activity from iron deficient rats revealed a significant decrease in kidneys, but heart and liver were unaffected (Beutler, 1959; Schultze, 1939). The activity of succinate dehydrogenase was also reduced in heart and kidney but not in liver of iron deficient rats (Beutler and Blaisdell, 1960). A study on iron deficiency in pigs, revealed a decrease in the levels of cytochrome *c* in heart and kidney but cytochrome oxidase activities in heart, kidney and liver were unchanged (Cartwright et al., 1957). Studies of iron-deprived rats found reductions in cytochrome *c* in the liver and kidney (Beutler, 1957; Beutler and Blaisdell, 1958). Another study found significant

reductions in cytochrome *c* in the skeletal muscle and kidney of iron-deprived rats but not in liver or heart (Salmon, 1962). A comparison of cytochrome *c* levels in a variety of tissues from iron deficient rats, found cytochrome *c* loss, in order of increasing severity, in heart, diaphragm, kidney, intestinal mucosa and skeletal muscle (no change was found in brain), and a decrease in succinate oxidation (complex II-dependent) in muscle (Dallman and Schwartz, 1965a). Notably, the change in cytochrome *c* in intestinal mucosa and skeletal muscle returned to control levels upon the reintroduction of iron, with the recovery occurring much faster (after 48 hours) in intestinal mucosa (Dallman and Schwartz, 1965b).

Electron microscopic (EM) analysis of heart, muscle, liver and erythroblasts (red blood cell precursors) of iron deficient rats revealed enlarged, or perhaps swollen, mitochondria with liver mitochondria containing fewer cristae (Dallman and Goodman, 1970). The enlarged heart mitochondria appeared to displace and distort the myofibrils. Liver mitochondria also occupied an increased percentage of cytoplasm due to an enlargement and elongation of mitochondria, and the changes in heart and liver mitochondria returned to normal following iron repletion. Mitochondrial cytochrome concentration was also decreased in the liver (but not heart) and total mitochondrial protein and lipid levels, and measurements of OxPhos coupling remained constant (Dallman and Goodman, 1971; Goodman et al., 1970). Similar effects on mitochondrial morphology were observed in blood lymphocytes from patients with iron-deficiency anemia (Jarvis and Jacobs, 1974).

A series of investigations have reported profound effects on mitochondrial respiration and OxPhos complex activity in a variety of tissues from iron deprived rats. In mitochondria isolated from liver, iron deprivation was found to decrease succinate-cytochrome *c* reductase activity (complex II/III-dependent) but had no effect on NADH-ferricyanide reductase (complex

I), succinate-ferricyanide reductase (complex II), NADH-cytochrome *c* reductase (complex I/III-dependent) or cytochrome oxidase (complex IV) activities (Bailey-Wood et al., 1975). A different report of mitochondrial function in liver found a decrease in mitochondrial iron, a slight decrease in cytochromes, and a moderate decrease in mitochondrial membrane potential ($\Delta\psi_m$), ATP levels (along with an increase in ADP levels), the respiratory control ratio, due to an increase in state 4 (or ADP deficient) respiration, and ADP/O ratio, indicating a partial uncoupling (or reduced efficiency) of OxPhos (Masini et al., 1994a). There was no change in total lipid, cholesterol, phospholipid or fatty acid of the mitochondrial membranes (but there was an increase in total liver lipid). Interestingly, the coupling defect and loss of mitochondrial iron, but not the loss of cytochromes, was recovered with iron supplementation (Masini et al., 1994b). The increase in state 4 respiration and RCR in liver mitochondria from iron deficient rats was replicated in a separate study that also found an increase in mtDNA fragmentation (Walter et al., 2002). A functional study of isolated mitochondria from heart of iron deficient rats found a reduction in respiratory enzyme activities, oxygen consumption and cytochrome levels, but no change in APD/O ratio, suggesting that iron deficiency does not affect the coupling of electron transport and ATP synthesis in that tissue (Blayney et al., 1976). In skeletal muscle of iron-deprived rats, respiratory enzyme activities as well as abundance of mitochondrial cytochromes, flavoproteins and Fe-S clusters were reduced and could be recovered following iron repletion (Davies et al., 1982; Edgerton et al., 1972; Finch et al., 1976; Hagler et al., 1981; McLane et al., 1981). Respiratory control ratios and APD/O ratios were unchanged. Specifically, the activities of NADH dehydrogenase (complex I) and succinate dehydrogenase (complex II) were decreased along with total muscle mitochondrial content, and these measurements returned to control values with the reintroduction of dietary iron (Davies et al., 1982). Similarly, along with

decreases in cytochromes and oxidase activity, and significant decreases in complex I and complex II activity, mitochondria isolated from skeletal muscle of iron-deprived rats had substantial decreases in complex I and complex II Fe-S clusters Complex III Fe-S clusters were also slightly affected but, again, coupling of OxPhos was unaffected (Maguire et al., 1982). Another study showed evidence suggesting that the decrease in complex I and complex II activities are due to decreases in the abundance of those enzymes and not simply due to loss of their cofactors (Ackrell et al., 1984).

Iron deprivation has strong effects on OxPhos activity and its cofactors, however other studies have shown that iron deprivation has little effect on other mitochondrial pathways. Specifically, the activities of several TCA cycle, fatty acid and ketone body oxidation enzymes from skeletal muscle of iron-deprived rats were unaffected (Cartier et al., 1986). Moreover, severe iron deficiency in rats caused an increase in the activity of matrix enzymes in red (slow-twitch) skeletal muscle (but the activity of Fe-S cluster containing mitochondrial aconitase was decreased) (Ohira et al., 1987). The molecular basis for these increases remains unexplored, but these results indicate that the activity of OxPhos and other mitochondrial processes can be independently regulated during iron deprivation.

In addition to animal models, the effects of iron deprivation on mitochondria have also been investigated using cultured cells. Use of the clinically used iron chelator DFO (deferoxamine, desferrioxamine B or desferal) is popular in studies examining the effects of iron deprivation in cell culture. DFO is a siderophore produced by the bacteria *Streptomyces pilosus*, has an extremely high specificity and binding affinity for ferric iron (Fe^{3+}) with a 1:1 stoichiometry (Keberle, 1964), and iron bound by DFO is rendered chemically inactive and cannot participate in the generation of ROS (Bernhardt, 2007; Kalinowski and Richardson,

2005). DFO is poorly membrane permeable, enters cells though endocytosis, accumulates in lysosomes and endosomes (Lloyd et al., 1991), and is thought to chelate intracellular free or labile iron (Richardson et al., 1994). *In vitro* studies show that DFO weakly removes iron from ferritin and hemosiderin, only partially from transferrin (10-21%) and cytochrome *c* but not from hemoglobin and does not inhibit complex I/III- or complex II/III-dependent activity. *In vivo*, DFO stimulates ferritin degradation and iron release in lysosomes (Baker et al., 1992; Keberle, 1964; Kidane et al., 2006; Laub et al., 1985; Yoon et al., 2003). DFO has also been shown to cause cell cycle arrest and senescence resulting in a decrease in cell proliferation, as well as apoptosis via a release of cytochrome *c* from mitochondria leading to caspase activation (Yu et al., 2007). In the human erythroleukemic K-562 cell line, treatment with 200 μM DFO for 24 hours resulted in a decrease in TCA cycle enzymes, including a significant decrease in mitochondrial aconitase, and a slight decreases in citrate synthase, isocitrate dehydrogenase and succinate dehydrogenase (TCA cycle/OxPhos) as well as a small decrease in NADH (Oexle et al., 1999). Another report found that treatment of Chang cells (a HeLa derivative) with 500 μM DFO led to a decrease in ATP, MTT NAD(P)H-dependent activity and a loss of $\Delta\psi_m$ after 24 hours (Im et al., 2007; Yoon et al., 2003). Some of these effects were also observed in Hep3B and Huh7 human hepatoma cell lines. Interestingly, the decrease in ATP was reversed when the cells were switched to DFO-free media after 1 mM DFO treatment for 24 hours but not when the cells were initially treated for 48 hours. Additionally, treatment of Chang cells with 1 mM DFO led to a decrease in complex II/complex III-dependent activity and maximal respiration but not complex I/III-dependent activity. At 500 μM, DFO led to a decrease in the protein level of the complex II-SDHB subunit (Fe-S cluster containing) within 24 hours and a decrease in the mRNA levels of complex II-SDHC (and subunits of complex I and III) after 2-3 days but there was no

decrease in protein levels of the complex II-SDHA subunit, even after 5 days of treatment (Yoon et al., 2003). Decreases in complex I-V proteins and cytochrome *c* were also observed after 3-5 days of iron chelation (Yoon et al., 2003). DFO also decreased the protein and transcript levels of TRAP1 (a mitochondrial HSP90 family member), but not mitochondrial HSP60 or HSP70, in a time and dose-dependent manner, and its levels could be recovered depending on the length of the initial treatment (Im et al., 2007). Further, elongated, interconnected mitochondria were observed in Chang cells after DFO treatment (500 μM) for 1-3 days as assessed by fluorescence microscopy (Yoon et al., 2006). Using EM imaging, the length of mitochondria was also increased despite a decrease in mitochondrial number (Im et al., 2007; Yoon et al., 2006). These changes in mitochondrial morphology were accompanied by an increase in mitochondrial membrane mass (after 1 day of chelation) and a decrease in mtDNA levels (after 3 days of chelation). Notably, this study found no change in the expression of regulators of mitochondrial biogenesis, including TFAM and NRF1, and there was no release of apoptogenic factors, including cytochrome *c* and apoptosis-inducing factor (AIF) to the cytosol of DFO treated cells. Conversely, a study of human colon adenocarcinoma Caco2 cells found a decrease in $\Delta\psi_m$ that was accompanied by cytochrome *c* release from mitochondria and an increase in caspase activity following DFO treatment (200 μM for 1-3 days), indicating an induction of intrinsic mitochondrial cell death (Sun et al., 2009). A decrease in mitochondrial heat shock proteins (HSP60 and HSP70) and a mitochondrial ribosomal protein was also observed via 2-dimensional gel electrophoresis followed by MS but there was no change in complex IV subunit 4.

Cells contain many forms of iron whose levels dictate cellular activity. These forms include protein cofactors such as heme and iron-sulfur clusters and protein bound di-iron and monoiron centers. In addition, iron is found in the chelatable, “labile iron pool” (LIP) and is

stored in the cytosolic protein ferritin and mitochondrial protein mitoferrin (Hentze et al., 2010). Mitochondria also play an important role in the biosynthesis of heme and iron-sulfur clusters (Richardson et al., 2010). A variety of studies have examined how deficiencies in these cofactors affect mitochondrial activity. In the budding yeast *Saccharomyces cerevisiae*, deletion of proteins involved in the synthesis of Fe-S clusters results in decreases in the activity of Fe-S cluster containing proteins, including mitochondrial aconitase, complex II, complex III (*S. cerevisiae* lack complex I) (Adam et al., 2006; Foury, 1999; Garland et al., 1999; Kim et al., 2001; Kispal et al., 1999; Lange et al., 2000; Li et al., 1999; Li et al., 2001; Lutz et al., 2001; Muhlenhoff et al., 2002; Rodriguez-Manzaneque et al., 2002; Rotig et al., 1997; Strain et al., 1998; Voisine et al., 2001; Wiedemann et al., 2006) as well as complex IV (which contains heme cofactors but no Fe-S clusters) (Foury and Cazzalini, 1997; Schilke et al., 1999), heme and cytochromes (Lange et al., 2004; Lesuisse et al., 2003). Some of these studies found reductions in the levels of OxPhos proteins, including subunits of complex II, complex III, complex IV, cytochromes, and mitochondrial aconitase (Adam et al., 2006; Kim et al., 2001; Li et al., 2001; Schilke et al., 1999; Voisine et al., 2001). Others found little to no change in protein levels (Lange et al., 2000; Li et al., 2001; Muhlenhoff et al., 2002; Rodriguez-Manzaneque et al., 2002; Wiedemann et al., 2006). There were no changes in the activity of the non-iron containing mitochondrial enzymes malate dehydrogenase and citrate synthase (Kispal et al., 1999; Muhlenhoff et al., 2002). Moreover, deletion of many Fe-S biogenesis proteins has also been shown to result in mitochondrial iron accumulation (Rouault and Tong, 2005, 2008). Similar effects have been observed in mammalian cells when these proteins are knocked down using RNAi, in knockout mouse models and in patient samples with mutations in Fe-S cluster machinery (Maio and Rouault, 2015; Rouault, 2015b; Stehling and Lill, 2013).

Cellular depletion of heme also results in profound changes to mitochondrial proteins and activity. Treatment of mouse L1210 leukemia cells with succinylacetone (at 2-3 mM), an inhibitor of δ-aminolevulinic acid dehydratase at the second step of heme biosynthesis (Ebert et al., 1979), for 3 days strongly impaired their respiration (Weinbach and Ebert, 1985). Inhibition of ferrochelatase at the last step of heme biosynthesis, using *N*-methyl protoporphyrin IX (NMP) (De Matteis and Marks, 1983) at 10 μM, in a human primary lung fibroblast cell line (IMR90) for 1 week caused a significant decrease in the activity of complex IV and a slight decrease in complex II (Atamna et al., 2001). NMP treatment also resulted in large decreases in the levels of complex IV proteins, including subunits I, II and IV, and a slight decrease in cytochrome *c*. Interestingly, this inhibitor did not cause any change in complex I or complex III proteins, despite complex III containing multiple heme cofactors (Figure 1A). Similar effects on complex IV after NMP treatment have been observed in human neuroblastoma (SHSY5Y) and astrocytoma (U373) cell lines (Atamna et al., 2002).

Overall, iron deprivation has powerful effects on mitochondrial proteins, function, abundance, dynamics and structure. However, there are slight differences in the responses to iron deprivation depending on the cell type, organism or tissue being tested, and on the duration and level of iron depletion. Additionally, many of these effects have been shown to be reversible depending on the initial duration of iron deficiency.

1.4.2 Mitochondrial Adaptation and Regulation in Response to Iron Deprivation

In mammalian cells, iron homeostasis is primarily regulated through the iron regulatory protein (IRP)-iron-responsive element (IRE) system. Under iron limiting conditions, the cytosolic iron regulatory proteins, IRP1 and IRP2, post-transcriptionally control the expression

of a select number of genes through binding to conserved hairpin/stem-loop structures (IREs) located in the 5'- or 3'-untranslated regions (UTRs) of their target mRNAs. The stability of IRP1 and IRP2 are under control of the E3 ubiquitin ligase substrate specificity component FBXL5 (F-box and leucine-rich repeat protein 5) that senses changes in iron levels via a hemerythrin-like, di-iron-oxygen binding domain. Under iron-replete conditions, FBXL5 promotes IRP ubiquitination and subsequent proteosomal degradation. However, when iron levels are low, FBXL5 is degraded (Ruiz et al., 2013; Salahudeen et al., 2009; Vashisht et al., 2009). IRP1 is also controlled by an additional regulatory mechanism. When iron is abundant, IRP1 binds an Fe-S cluster and functions as the cytosolic aconitase, but when iron is scarce, IRP1 losses its Fe-S cluster and becomes an RNA-binding protein. The canonical IRE consists of a 6-nucleotide loop at the end of a base-paired stem containing an unpaired cytosine nucleotide (C8) bulge located 5 base pairs 5' of the loop. Typically, when bound to an IRE located in a 5'-UTR, the IRPs will inhibit translation initiation for that transcript, as is the case for light (L)- and heavy (H)-ferritin. When bound to the multiple IREs located in the transferrin receptor 3'-UTR, the IRPs will inhibit cleavage and degradation of that transcript (Anderson et al., 2012; Hentze et al., 2010). Several mRNAs with IREs or IRE-like elements that encode mitochondrial proteins have been described, and include mammalian mitochondrial aconitase (m-acon or *ACO2*) (TCA cycle), the erythroid isoform of δ-aminolevulinate synthase (eALAS or *ALAS2*), the mammalian complex I (CI)-75 kilodalton (kDa) subunit (*NDUFS1*) and *Drosophila melanogaster* succinate dehydrogenase B subunit (*sdhB*) (OxPhos complex II/TCA) (Cox et al., 1991; Dandekar et al., 1991; Eisenstein and Ross, 2003; Gray et al., 1996; Joshi et al., 2012; Kim et al., 1996; Kohler et al., 1995; Lin et al., 2001; Melefors, 1996). The *NDUFS1* transcript contains an IRE-like

sequence (Lin et al., 2001), and the *sdhB* IRE does not appear not be conserved in mammals (Gray et al., 1996; Kohler et al., 1995).

IRP-IRE mediated control of mitochondrial aconitase expression has been described in detail. IRP1 binds to the *ACO2* IRE, represses its translation and iron can regulate this interaction *in vitro* (Gray et al., 1996). Mitochondrial aconitase levels from mouse or rat liver are decreased in iron deficient mice, IRP-binding activity is increased, and *ACO2* mRNA levels are unchanged (Chen et al., 1998; Chen et al., 1997; Kim et al., 1996). Synthesis of mitochondrial aconitase is rapidly regulated (after just 4 hours of iron chelation) in several mammalian cell types and is directly regulated at the translational level *in vivo* (Schalinske et al., 1998). However, the iron-deprivation induced decrease in mitochondrial aconitase does not seem to affect TCA cycle capacity and the metabolic consequences of IRP regulation of *ACO2* remain largely unclear (although this regulatory mechanism may function to increase citrate export from mitochondria for use in the cytosol) (Eisenstein and Ross, 2003; Ross and Eisenstein, 2002).

The erythroid specific *ALAS2* mRNA also contains an IRE. ALAS2 is the first and rate-limiting step in erythroid heme synthesis. In mouse erythroleukemia (MEL) cells *ALAS2* translation is regulated in response to iron, and *in vitro* IRP1 represses its translation (Bhasker et al., 1993; Melefors et al., 1993). Additionally, loss of glutaredoxin 5 (*glrx5*), a component of mitochondrial Fe-S cluster biosynthesis, in zebrafish leads to activation of IRP1, inhibition of *ALAS2* translation and a block in heme biosynthesis, thereby connecting the production of heme to Fe-S cluster biogenesis (Wingert et al., 2005). These pathways also share another regulatory link as the last step in heme biosynthesis is catalyzed by the mitochondrial Fe-S cluster protein ferrochelatase whose stability is dependent on iron and Fe-S cluster production (Crooks et al., 2010; Taketani et al., 2000). The housekeeping version of δ-aminolevulinate synthase (encoded

by *ALAS1*) does not have an IRE but is under feedback regulation by heme at multiple levels of gene expression (Furuyama et al., 2007; Tian et al., 2011). Notably, one of these negative feedback mechanisms involves the nuclear heme receptor Rev-erbα (reverse orientation c-erbA gene α or *NR1D1*), which recruits the nuclear receptor corepressor-histone deacetylase 3 (NCoR-HDAC3) complex (Yin et al., 2007) to repress the expression of the transcriptional coactivator, PGC-1α (encoded by *PPARGC1A*), an activator of *ALAS1* transcription (and mitochondrial biogenesis) (Wu et al., 2009). Interestingly, inhibition of heme synthesis via succinylacetone (5 mM) leads to an increase in transcript levels of *PPARGC1A* in human HepG2 hepatocellular carcinoma cells (Wu et al., 2009) and succinylacetone has also been shown to decrease cellular respiration (Weinbach and Ebert, 1985), suggesting that in response to heme depletion, cells may try to compensate for decreased mitochondrial function through PGC-1α induced mitochondrial biogenesis. We have also observed similar changes in cellular respiration and *Ppargc1a* transcript levels during DFO-induced iron deprivation (Chapter 2) (Rensvold et al., 2013).

A study published in 2001 found that the levels of NDUFS1 (CI-75 kDa), an Fe-S cluster containing protein subunit of complex I, but not the non-Fe-S CI-39 kDa protein subunit, was decreased 48 to 72 hours following iron deprivation with DFO in monkey COS-7 fibroblast-like kidney cells (Lin et al., 2001). There were no changes in *NDUFS1* mRNA, suggesting that the decrease in protein is the result of post-transcriptional regulation. Additionally, the 5'-UTR of *NDUFS1* mRNA was found to contain a novel IRE-like stem loop sequence and an unidentified cytoplasmic protein bound the IRE in an iron dependent manner. The *NDUFS1* IRE is poorly conserved, as it does not contain a typical bulged C8 nucleotide on the stem, and the terminal loop is formed from 5 nucleotides instead of 6 (Joshi et al., 2012). However the RNA binding

protein was found to be neither IRP1 nor IRP2. Of note, there have been no additional studies confirming or expanding upon these NDUFS1 and 75 kDa-binding protein observations.

An integrative analysis utilizing multiple transcriptome-wide approaches was recently used to identify IRP bound mRNAs and new putative IRE-containing transcripts (Sanchez et al., 2011). These analyses identified novel mRNAs that interact with both IRPs or exclusively with either IRP1 or IRP2. However, transcripts encoding for mitochondrial proteins or pathways did not appear to be enriched. This study also performed a large-scale, MS-based proteomic analysis of protein synthesis via pulsed stable isotope labeling by amino acids in cell culture (pSILAC) (Schwanhausser et al., 2009) under conditions of iron supplementation (100 μM hemin) and iron deprivation (200 μM DFO) in mouse hepatoma Hepa1-6 cells, and in IRP knockout bone marrow-derived macrophage (BMDM) cells. Interestingly, the synthesis of ETC proteins, including 24 subunits of complex I and all 4 subunits of complex II, was decreased in the IRP deficient cells (Sanchez et al., 2011), suggesting that the expression of these proteins is under translational regulation during disruptions of cellular iron-homeostasis (although not likely via direct IRP binding of their transcripts). IRP-liver specific knockout in mice has also been shown to cause mitochondrial functional dysfunction and structural abnormalities (Galy et al., 2010). Similar to iron-deficient mice, IRP-deficiency causes mitochondrial enlargement and cristae defects as well as a decrease in the activity of ETC complexes I-III (while complex IV and complex V activity are unchanged or slightly increased) and several TCA cycle enzymes. Additionally, the level of cellular and mitochondrial iron, total heme and activity of non-ETC and non-mitochondrial Fe-S cluster dependent enzymes are decreased, indicating that IRPs are critical for securing cellular and subsequently mitochondrial iron for Fe-S cluster and heme biosynthesis, and the function of proteins that depend on those cofactors.

Unlike the IRP-IRE system in metazoans, the fungus *S. cerevisiae* regulates iron metabolism through the action of two transcription factors Aft1p and Aft2p. During iron deprivation, decreased mitochondrial Fe-S cluster biogenesis leads to translocation of Aft1p and Aft2p from the cytosol to the nucleus. Aft1p and Aft2p activate the iron regulon, which includes genes involved in iron reduction at the plasma membrane, iron transport and heme oxygenase (Kaplan and Kaplan, 2009). Additionally, iron deprivation in *S. cerevisiae* leads to a widespread, adaptive mitochondrial response. Also induced as part of the iron regulon, the mRNA binding proteins Cth1p and Cth2p bind to and promote the degradation of transcripts that encode proteins involved in iron dependent processes, including many mitochondrial proteins, such as those involved in the ETC and TCA cycle, as well as in heme and Fe-S cluster biosynthesis (Puig et al., 2005; Puig et al., 2008). Similar changes in transcript abundance are observed when components of mitochondrial Fe-S synthesis are depleted (but not when a component of cytosolic Fe-S synthesis is depleted) (Hausmann et al., 2008; Lesuisse et al., 2003). Mammalian cells encode for orthologs of Cth1p and Cth2p, including ZFP36 (also known as tristetraprolin, TTP or TIS11), ZFP36L1 (TIS11B), ZFP36L2 (TIS11D) and ZFP36L3 (in rodents only). The ZFP36 family members have roles in cancer and inflammation (Sanduja et al., 2011) and ZFP36 has recently been reported as having a role in cellular iron metabolism through regulating transferrin receptor mRNA stability (Bayeva et al., 2012).

We recently discovered a similar adaptive transcriptional response to iron deprivation in mammalian cells (Rensvold et al., 2013). The identification of this response is described in Chapter 2 and an important part of its mechanism is described in Chapter 3. Briefly, using microarray and quantitative mass-spectrometry approaches, we found that DFO treatment of C2C12 mouse myotubes leads to a global decrease in the transcript abundance of mitochondrial-

and nuclear-encoded mitochondrial genes and mitochondrial proteins. We found that this response occurs across a broad range of cell types, is rapid, dose-dependent and reversible upon the reintroduction of iron, indicating that the response to iron deprivation is an adaptive cellular response rather than irreversible cellular damage. We have shown that this process is independent of well-established regulators of mitochondrial biogenesis, including PGC-1α, PGC-1β and HIF-1α. Interestingly, while PGC-1β may not function in the repression of mitochondrial biogenesis during iron deprivation, iron uptake has been shown to be critical for PGC-1β driven mitochondrial biogenesis during osteoclast differentiation (Ishii et al., 2009). Our data suggest a similar role for iron during PGC-1α induced mitochondrial biogenesis in muscle cells (Rensvold et al., 2013) and PGC-1α protein levels have also been reported to be decreased in soleus muscle of iron-deprived rats (Han et al., 2011).

In addition to regulating mitochondrial biogenesis, iron deprivation has also been reported to induce mitochondrial specific autophagy (mitophagy) (Allen et al., 2013; Schiavi et al., 2015). In a drug screen using a pH-sensitive mitochondrial targeted GFP expressed in human osteosarcoma U2OS cells and human neuroblastoma SH-SY5Y cells, iron chelators, such as deferiprone (DFP) or deferoxamine (DFO) at 1 mM for 24 hours, were found to cause the strongest mitophagy response (greater than several well known inhibitors of mitochondrial OxPhos). This effect was validated using alternative measurements of mitophagy, including EM imaging, and levels of mitochondrial proteins from each mitochondrial compartment were also reduced with iron chelation, consistent with autophagy. Interestingly, the mitophagy response was dose dependent, with no induction of mitophagy when cells were treated at a concentration of 100 μM DFP. Additionally, iron chelation was found to specifically induce mitophagy rather than general macroautophagy. This response was blocked when core autophagy components

ATG5 or Beclin-1 were knocked-down via RNAi or when cells were cultured in media containing galactose (to force reliance on OxPhos) instead of glucose. Additionally, the iron deprivation mitophagy response was independent of the well-described PINK1/Parkin mitophagy pathway and the HIF-1 regulated autophagy factor BNIP3 (Zhang et al., 2008), suggesting that this response is independent of HIF-1 induced mitophagy. The authors speculate that the purpose of this iron deprivation induced mitophagy response might be to recycle iron to other essential iron-requiring functions (Allen et al., 2013).

Additional accounts of iron deprivation induced mitophagy have been described in *C. elegans* (Kirienko et al., 2015; Schiavi et al., 2015). Silencing the expression of the *C. elegans* PINK1, Parkin, and BNIP3 homologs blocked the *C. elegans* iron-deprivation induced mitophagy response (Schiavi, 2015, Current Biology). Further, iron chelation caused mitochondrial fragmentation, a loss of membrane potential, and a decrease in mitochondrial mass and mtDNA in *C. elegans*, consistent with mitophagy (Kirienko et al., 2015). However, as mitochondrial fission (not fusion) is linked to mitochondrial autophagy, these reports are seemingly at odds with the descriptions of iron deprivation-induced mitochondrial elongation (Dallman and Goodman, 1970) and reported increases in the level of the protein FIS1, a regulator of mitochondrial dynamics that promotes mitochondrial fission (Yoon et al., 2006). Nevertheless, both processes, fission and fusion, could possibly be working in tandem. For example, healthy, functional mitochondria may resist autophagy during iron deprivation through elongation, while damaged, fragmented mitochondria are eliminated via autophagy (Westermann, 2010).

Finally, as the same HIFα hydroxylases that require oxygen also require iron as a cofactor, iron deprivation could theoretically initiate the HIF-1α-dependent mechanisms of

mitochondrial regulation described in Section 1.2. However, many of the iron deprivation induced mitochondrial adaptations described above, including our observations, have been shown to be independent of HIF-1α. Additionally, a microarray analysis of transcript abundance during iron chelation (DFO) and hypoxia in Hepb3 cells showed that only 23% of the DFO induced transcriptional changes were shared with hypoxia (Vengellur et al., 2005), indicating that these treatments can illicit unique cellular responses.

To summarize, iron deprivation is well known to cause extensive changes in mitochondrial function, composition and structure, but the molecular mechanisms that control these adaptation are just beginning to be unraveled. Recent studies have shown that targeted post-transcriptional regulation of select mitochondrial proteins, decreased mitochondrial biogenesis, increased mitophagy and possible regulation of mitochondrial dynamics may have important mechanistic roles in the cellular response to iron deprivation.

1.4.3 Significance

Iron is one of the most abundance elements on Earth. However, iron deficiency anemia is the most common nutritional disorder in the world, affecting an estimated 1.6 billion people, 25% of the world's population (McLean et al., 2009). Iron is an essential cofactor for a wide range of cellular processes, including OxPhos, various metabolic pathways, gene expression, and DNA replication and repair (Furuyama et al., 2007; Mense and Zhang, 2006; Rouault, 2015a). Dysfunction of iron homeostasis directly causes a variety of human diseases, including Friedreich's ataxia, hereditary hemochromatosis, aceruloplasminaemia and neuroferritinopathy (Andrews, 1999; Rouault, 2013), and likely contributes to neurodegenerative disease (including Parkinson's disease and Alzheimer's disease), microbial pathogenesis, various cancers and

cardiovascular disease (Ames and Wakimoto, 2002; Ganz and Nemeth, 2015; Rines and Ardehali, 2013; Torti and Torti, 2013; von Haehling et al., 2015; Ward et al., 2014). Recently, studies have shown a link between iron deprivation (as well as iron overload) and obesity, which is rapidly becoming a worldwide health problem affecting both adults and children, and is associated with the development of diabetes, heart disease, stroke, mental illness and a reduced quality of life (Aigner et al., 2014; Simcox and McClain, 2013). Iron deficiency decreases physical activity and work performance in adults, and may cause decreased motor development and cognition in children and adolescents (Fretham et al., 2011; McCann and Ames, 2007). Additionally, maternal iron deficiency anemia can lead to low birth weight and preterm delivery, increasing the risk of maternal and infant mortality (Zimmermann and Hurrell, 2007). Other known effects of iron deficiency include diminished skeletal and cardiac muscle function, and athletic endurance capacity (Rowland, 2012). Despite the known association of iron deficiency with these and other disorders, many of the basic mechanisms regulating iron homeostasis are unknown, and the direct cellular consequences of iron deprivation are largely uncharacterized. Moreover, the molecular mechanisms that regulate mitochondrial biogenesis in response to the availability of nutrients, such as iron, are not well understood.

1.5 References

Ackrell, B.A., Maguire, J.J., Dallman, P.R., and Kearney, E.B. (1984). Effect of iron deficiency on succinate- and NADH-ubiquinone oxidoreductases in skeletal muscle mitochondria. J Biol Chem *259*, 10053-10059.

Adam, A.C., Bornhovd, C., Prokisch, H., Neupert, W., and Hell, K. (2006). The Nfs1 interacting protein Isd11 has an essential role in Fe/S cluster biogenesis in mitochondria. EMBO J *25*, 174-183.

Aigner, E., Feldman, A., and Datz, C. (2014). Obesity as an emerging risk factor for iron deficiency. Nutrients *6*, 3587-3600.

Allen, G.F., Toth, R., James, J., and Ganley, I.G. (2013). Loss of iron triggers PINK1/Parkin-independent mitophagy. EMBO Rep *14*, 1127-1135.

Ames, B.N., and Wakimoto, P. (2002). Are vitamin and mineral deficiencies a major cancer risk? Nat Rev Cancer *2*, 694-704.

Anderson, C.P., Shen, M., Eisenstein, R.S., and Leibold, E.A. (2012). Mammalian iron metabolism and its control by iron regulatory proteins. Biochim Biophys Acta *1823*, 1468-1483.

Anderson, S., Bankier, A.T., Barrell, B.G., de Bruijn, M.H., Coulson, A.R., Drouin, J., Eperon, I.C., Nierlich, D.P., Roe, B.A., Sanger, F.*, et al.* (1981). Sequence and organization of the human mitochondrial genome. Nature *290*, 457-465.

Andrews, N.C. (1999). Disorders of iron metabolism. N Engl J Med *341*, 1986-1995.

Atamna, H., Killilea, D.W., Killilea, A.N., and Ames, B.N. (2002). Heme deficiency may be a factor in the mitochondrial and neuronal decay of aging. Proc Natl Acad Sci U S A *99*, 14807-14812.

Atamna, H., Liu, J., and Ames, B.N. (2001). Heme deficiency selectively interrupts assembly of mitochondrial complex IV in human fibroblasts: revelance to aging. J Biol Chem *276*, 48410-48416.

Bailey-Wood, R., Blayney, L.M., Muir, J.R., and Jacobs, A. (1975). The effects of iron deficiency on rat liver enzymes. Br J Exp Pathol *56*, 193-198.

Baker, E., Richardson, D., Gross, S., and Ponka, P. (1992). Evaluation of the iron chelation potential of hydrazones of pyridoxal, salicylaldehyde and 2-hydroxy-1-naphthylaldehyde using the hepatocyte in culture. Hepatology *15*, 492-501.

Baum, D.A., and Baum, B. (2014). An inside-out origin for the eukaryotic cell. BMC Biol *12*, 76.

Bayeva, M., Khechaduri, A., Puig, S., Chang, H.C., Patial, S., Blackshear, P.J., and Ardehali, H. (2012). mTOR regulates cellular iron homeostasis through tristetraprolin. Cell Metab *16*, 645-657.

Bernhardt, P.V. (2007). Coordination chemistry and biology of chelators for the treatment of iron overload disorders. Dalton Trans, 3214-3220.

Beutler, E. (1957). Iron enzymes in iron deficiency. I. Cytochrome c. Am J Med Sci *234*, 517-527.

Beutler, E. (1959). Iron enzymes in iron deficiency. IV. Cytochrome oxidase in rat kidney and heart. Acta Haematol *21*, 371-377.

Beutler, E., and Blaisdell, R.K. (1958). Iron enzvmes in iron deficiency. III. Catalase in rat red cells and liver with some further observations on cytochrome C. J Lab Clin Med *52*, 694-699.

Beutler, E., and Blaisdell, R.K. (1960). Iron enzymes in iron deficiency. V. Succinic dehydrogenase in rat liver, kidney and heart. Blood *15*, 30-35.

Bhasker, C.R., Burgiel, G., Neupert, B., Emery-Goodman, A., Kuhn, L.C., and May, B.K. (1993). The putative iron-responsive element in the human erythroid 5-aminolevulinate synthase mRNA mediates translational control. J Biol Chem *268*, 12699-12705.

Blayney, L., Bailey-Wood, R., Jacobs, A., Henderson, A., and Muir, J. (1976). The effects of iron deficiency on the respiratory function and cytochrome content of rat heart mitochondria. Circ Res *39*, 744-748.

Blinzinger, K., Rewcastle, N.B., and Hager, H. (1965). Observations on Prismatic-Type Mitochondria within Astrocytes of the Syrian Hamster Brain. J Cell Biol *25*, 293-303.

Boland, M.L., Chourasia, A.H., and Macleod, K.F. (2013). Mitochondrial dysfunction in cancer. Front Oncol *3*, 292.

Calvo, S.E., and Mootha, V.K. (2010). The mitochondrial proteome and human disease. Annu Rev Genomics Hum Genet *11*, 25-44.

Campuzano, V., Montermini, L., Molto, M.D., Pianese, L., Cossee, M., Cavalcanti, F., Monros, E., Rodius, F., Duclos, F., Monticelli, A.*, et al.* (1996). Friedreich's ataxia: autosomal recessive disease caused by an intronic GAA triplet repeat expansion. Science *271*, 1423-1427.

Cartier, L.J., Ohira, Y., Chen, M., Cuddihee, R.W., and Holloszy, J.O. (1986). Perturbation of mitochondrial composition in muscle by iron deficiency. Implications regarding regulation of mitochondrial assembly. J Biol Chem *261*, 13827-13832.

Cartwright, G.E., Gubler, C.J., and Wintrobe, M.M. (1957). Studies on copper metabolism. XX. Enzyme activities and iron metabolism in copper and iron deficiencies. J Biol Chem *224*, 533-546.

Chan, D.C. (2012). Fusion and fission: interlinked processes critical for mitochondrial health. Annu Rev Genet *46*, 265-287.

Chan, S.Y., Zhang, Y.Y., Hemann, C., Mahoney, C.E., Zweier, J.L., and Loscalzo, J. (2009). MicroRNA-210 controls mitochondrial metabolism during hypoxia by repressing the iron-sulfur cluster assembly proteins ISCU1/2. Cell Metab *10*, 273-284.

Chen, O.S., Blemings, K.P., Schalinske, K.L., and Eisenstein, R.S. (1998). Dietary iron intake rapidly influences iron regulatory proteins, ferritin subunits and mitochondrial aconitase in rat liver. J Nutr *128*, 525-535.

Chen, O.S., Schalinske, K.L., and Eisenstein, R.S. (1997). Dietary iron intake modulates the activity of iron regulatory proteins and the abundance of ferritin and mitochondrial aconitase in rat liver. J Nutr *127*, 238-248.

Chinnery, P.F. (2003). Searching for nuclear-mitochondrial genes. Trends Genet *19*, 60-62.

Civitarese, A.E., Smith, S.R., and Ravussin, E. (2007). Diet, energy metabolism and mitochondrial biogenesis. Curr Opin Clin Nutr Metab Care *10*, 679-687.

Cohen, E., and Elvehjem, C.A. (1934). The Relation of iron and copper to the cytochrome and oxidase content of animal tissues. J Biol Chem *107*, 97-105.

Cox, T.C., Bawden, M.J., Martin, A., and May, B.K. (1991). Human erythroid 5-aminolevulinate synthase: promoter analysis and identification of an iron-responsive element in the mRNA. EMBO J *10*, 1891-1902.

Crooks, D.R., Ghosh, M.C., Haller, R.G., Tong, W.H., and Rouault, T.A. (2010). Posttranslational stability of the heme biosynthetic enzyme ferrochelatase is dependent on iron availability and intact iron-sulfur cluster assembly machinery. Blood *115*, 860-869.

Dallman, P.R. (1986). Biochemical basis for the manifestations of iron deficiency. Annu Rev Nutr *6*, 13-40.

Dallman, P.R., and Goodman, J.R. (1970). Enlargement of mitochondrial compartment in iron and copper deficiency. Blood *35*, 496-505.

Dallman, P.R., and Goodman, J.R. (1971). The effects of iron deficiency on the hepatocyte: a biochemical and ultrastructural study. J Cell Biol *48*, 79-90.

Dallman, P.R., and Schwartz, H.C. (1965a). Distribution of Cytochrome C and Myoglobin in Rats with Dietary Iron Deficiency. Pediatrics *35*, 677-686.

Dallman, P.R., and Schwartz, H.C. (1965b). Myoglobin and cytochrome response during repair of iron deficiency in the rat. J Clin Invest *44*, 1631-1638.

Dandekar, T., Stripecke, R., Gray, N.K., Goossen, B., Constable, A., Johansson, H.E., and Hentze, M.W. (1991). Identification of a novel iron-responsive element in murine and human erythroid delta-aminolevulinic acid synthase mRNA. EMBO J *10*, 1903-1909.

Davies, K.J., Maguire, J.J., Brooks, G.A., Dallman, P.R., and Packer, L. (1982). Muscle mitochondrial bioenergetics, oxygen supply, and work capacity during dietary iron deficiency and repletion. Am J Physiol *242*, E418-427.

De Matteis, F., and Marks, G.S. (1983). The effect of N-methylprotoporphyrin and succinyl-acetone on the regulation of heme biosynthesis in chicken hepatocytes in culture. FEBS Lett *159*, 127-131.

DiMauro, S., and Davidzon, G. (2005). Mitochondrial DNA and disease. Ann Med *37*, 222-232.

DiMauro, S., and Schon, E.A. (2003). Mitochondrial respiratory-chain diseases. N Engl J Med *348*, 2656-2668.

DiMauro, S., Schon, E.A., Carelli, V., and Hirano, M. (2013). The clinical maze of mitochondrial neurology. Nat Rev Neurol *9*, 429-444.

Dominy, J.E., and Puigserver, P. (2013). Mitochondrial biogenesis through activation of nuclear signaling proteins. Cold Spring Harb Perspect Biol *5*.

Ebert, P.S., Hess, R.A., Frykholm, B.C., and Tschudy, D.P. (1979). Succinylacetone, a potent inhibitor of heme biosynthesis: effect on cell growth, heme content and delta-aminolevulinic acid dehydratase activity of malignant murine erythroleukemia cells. Biochem Biophys Res Commun *88*, 1382-1390.

Edgerton, V.R., Bryant, S.L., Gillespie, C.A., and Gardner, G.W. (1972). Iron deficiency anemia and physical performance and activity of rats. J Nutr *102*, 381-399.

Eisenstein, R.S., and Ross, K.L. (2003). Novel roles for iron regulatory proteins in the adaptive response to iron deficiency. J Nutr *133*, 1510S-1516S.

Ernster, L., and Schatz, G. (1981). Mitochondria: a historical review. J Cell Biol *91*, 227s-255s.

Finch, C.A., Miller, L.R., Inamdar, A.R., Person, R., Seiler, K., and Mackler, B. (1976). Iron deficiency in the rat. Physiological and biochemical studies of muscle dysfunction. J Clin Invest *58*, 447-453.

Foury, F. (1999). Low iron concentration and aconitase deficiency in a yeast frataxin homologue deficient strain. FEBS Lett *456*, 281-284.

Foury, F., and Cazzalini, O. (1997). Deletion of the yeast homologue of the human gene associated with Friedreich's ataxia elicits iron accumulation in mitochondria. FEBS Lett *411*, 373-377.

Fretham, S.J., Carlson, E.S., and Georgieff, M.K. (2011). The role of iron in learning and memory. Adv Nutr *2*, 112-121.

Friend, D.S., and Brassil, G.E. (1970). Osmium staining of endoplasmic reticulum and mitochondria in the rat adrenal cortex. J Cell Biol *46*, 252-266.

Fukuda, R., Zhang, H., Kim, J.W., Shimoda, L., Dang, C.V., and Semenza, G.L. (2007). HIF-1 regulates cytochrome oxidase subunits to optimize efficiency of respiration in hypoxic cells. Cell *129*, 111-122.

Furuyama, K., Kaneko, K., and Vargas, P.D. (2007). Heme as a magnificent molecule with multiple missions: heme determines its own fate and governs cellular homeostasis. Tohoku J Exp Med *213*, 1-16.

Galy, B., Ferring-Appel, D., Sauer, S.W., Kaden, S., Lyoumi, S., Puy, H., Kolker, S., Grone, H.J., and Hentze, M.W. (2010). Iron regulatory proteins secure mitochondrial iron sufficiency and function. Cell Metab *12*, 194-201.

Ganz, T., and Nemeth, E. (2015). Iron homeostasis in host defence and inflammation. Nat Rev Immunol *15*, 500-510.

Garland, S.A., Hoff, K., Vickery, L.E., and Culotta, V.C. (1999). Saccharomyces cerevisiae ISU1 and ISU2: members of a well-conserved gene family for iron-sulfur cluster assembly. J Mol Biol *294*, 897-907.

Giles, R.E., Blanc, H., Cann, H.M., and Wallace, D.C. (1980). Maternal inheritance of human mitochondrial DNA. Proc Natl Acad Sci U S A *77*, 6715-6719.

Goodman, J.R., Warshaw, J.B., and Dallman, P.R. (1970). Cardiac hypertrophy in rats with iron and copper deficiency: quantitative contribution of mitochondrial enlargement. Pediatr Res *4*, 244-256.

Gray, M.W. (2012). Mitochondrial evolution. Cold Spring Harb Perspect Biol *4*, a011403.

Gray, N.K., Pantopoulos, K., Dandekar, T., Ackrell, B.A., and Hentze, M.W. (1996). Translational regulation of mammalian and Drosophila citric acid cycle enzymes via iron-responsive elements. Proc Natl Acad Sci U S A *93*, 4925-4930.

Grimsrud, P.A., Carson, J.J., Hebert, A.S., Hubler, S.L., Niemi, N.M., Bailey, D.J., Jochem, A., Stapleton, D.S., Keller, M.P., Westphall, M.S.*, et al.* (2012). A quantitative map of the liver mitochondrial phosphoproteome reveals posttranslational control of ketogenesis. Cell Metab *16*, 672-683.

Hagler, L., Askew, E.W., Neville, J.R., Mellick, P.W., Coppes, R.I., Jr., and Lowder, J.F., Jr. (1981). Influence of dietary iron deficiency on hemoglobin, myoglobin, their respective reductases, and skeletal muscle mitochondrial respiration. Am J Clin Nutr *34*, 2169-2177.

Han, D.H., Hancock, C.R., Jung, S.R., Higashida, K., Kim, S.H., and Holloszy, J.O. (2011). Deficiency of the mitochondrial electron transport chain in muscle does not cause insulin resistance. PLoS One *6*, e19739.

Hausmann, A., Samans, B., Lill, R., and Muhlenhoff, U. (2008). Cellular and mitochondrial remodeling upon defects in iron-sulfur protein biogenesis. J Biol Chem *283*, 8318-8330.

Hebert, A.S., Dittenhafer-Reed, K.E., Yu, W., Bailey, D.J., Selen, E.S., Boersma, M.D., Carson, J.J., Tonelli, M., Balloon, A.J., Higbee, A.J.*, et al.* (2013). Calorie restriction and SIRT3 trigger global reprogramming of the mitochondrial protein acetylome. Mol Cell *49*, 186-199.

Hentze, M.W., Muckenthaler, M.U., Galy, B., and Camaschella, C. (2010). Two to tango: regulation of Mammalian iron metabolism. Cell *142*, 24-38.

Hock, M.B., and Kralli, A. (2009). Transcriptional control of mitochondrial biogenesis and function. Annu Rev Physiol *71*, 177-203.

Holt, I.J., Cooper, J.M., Morgan-Hughes, J.A., and Harding, A.E. (1988). Deletions of muscle mitochondrial DNA. Lancet *1*, 1462.

Hoppeler, H., Vogt, M., Weibel, E.R., and Fluck, M. (2003). Response of skeletal muscle mitochondria to hypoxia. Exp Physiol *88*, 109-119.

Hung, V., Zou, P., Rhee, H.W., Udeshi, N.D., Cracan, V., Svinkina, T., Carr, S.A., Mootha, V.K., and Ting, A.Y. (2014). Proteomic mapping of the human mitochondrial intermembrane space in live cells via ratiometric APEX tagging. Mol Cell *55*, 332-341.

Im, C.N., Lee, J.S., Zheng, Y., and Seo, J.S. (2007). Iron chelation study in a normal human hepatocyte cell line suggests that tumor necrosis factor receptor-associated protein 1 (TRAP1) regulates production of reactive oxygen species. J Cell Biochem *100*, 474-486.

Irrcher, I., Adhihetty, P.J., Joseph, A.M., Ljubicic, V., and Hood, D.A. (2003). Regulation of mitochondrial biogenesis in muscle by endurance exercise. Sports Med *33*, 783-793.

Ishii, K.A., Fumoto, T., Iwai, K., Takeshita, S., Ito, M., Shimohata, N., Aburatani, H., Taketani, S., Lelliott, C.J., Vidal-Puig, A.*, et al.* (2009). Coordination of PGC-1beta and iron uptake in mitochondrial biogenesis and osteoclast activation. Nat Med *15*, 259-266.

Jarvis, J.H., and Jacobs, A. (1974). Morphological abnormalities in lymphocyte mitochondria associated with iron-deficiency anaemia. J Clin Pathol *27*, 973-979.

Johnson, D.T., Harris, R.A., Blair, P.V., and Balaban, R.S. (2007a). Functional consequences of mitochondrial proteome heterogeneity. Am J Physiol Cell Physiol *292*, C698-707.

Johnson, D.T., Harris, R.A., French, S., Blair, P.V., You, J., Bemis, K.G., Wang, M., and Balaban, R.S. (2007b). Tissue heterogeneity of the mammalian mitochondrial proteome. Am J Physiol Cell Physiol *292*, C689-697.

Joshi, R.S., Morán, E., and Sánchez, M. (2012). Cellular Iron Metabolism – The IRP/IRE Regulatory Network. In Iron Metabolism, S. Arora, ed. (InTech), pp. 25-58.

Kalinowski, D.S., and Richardson, D.R. (2005). The evolution of iron chelators for the treatment of iron overload disease and cancer. Pharmacol Rev *57*, 547-583.

Kaplan, C.D., and Kaplan, J. (2009). Iron acquisition and transcriptional regulation. Chem Rev *109*, 4536-4552.

Kazak, L., Reyes, A., Duncan, A.L., Rorbach, J., Wood, S.R., Brea-Calvo, G., Gammage, P.A., Robinson, A.J., Minczuk, M., and Holt, I.J. (2013). Alternative translation initiation augments the human mitochondrial proteome. Nucleic Acids Res *41*, 2354-2369.

Keberle, H. (1964). The Biochemistry of Desferrioxamine and Its Relation to Iron Metabolism. Ann N Y Acad Sci *119*, 758-768.

Kidane, T.Z., Sauble, E., and Linder, M.C. (2006). Release of iron from ferritin requires lysosomal activity. Am J Physiol Cell Physiol *291*, C445-455.

Kim, H.Y., LaVaute, T., Iwai, K., Klausner, R.D., and Rouault, T.A. (1996). Identification of a conserved and functional iron-responsive element in the 5'-untranslated region of mammalian mitochondrial aconitase. J Biol Chem *271*, 24226-24230.

Kim, J.W., Tchernyshyov, I., Semenza, G.L., and Dang, C.V. (2006a). HIF-1-mediated expression of pyruvate dehydrogenase kinase: a metabolic switch required for cellular adaptation to hypoxia. Cell Metab *3*, 177-185.

Kim, R., Saxena, S., Gordon, D.M., Pain, D., and Dancis, A. (2001). J-domain protein, Jac1p, of yeast mitochondria required for iron homeostasis and activity of Fe-S cluster proteins. J Biol Chem *276*, 17524-17532.

Kim, S.C., Sprung, R., Chen, Y., Xu, Y., Ball, H., Pei, J., Cheng, T., Kho, Y., Xiao, H., Xiao, L.*, et al.* (2006b). Substrate and functional diversity of lysine acetylation revealed by a proteomics survey. Mol Cell *23*, 607-618.

Kirby, D.M., and Thorburn, D.R. (2008). Approaches to finding the molecular basis of mitochondrial oxidative phosphorylation disorders. Twin Res Hum Genet *11*, 395-411.

Kirienko, N.V., Ausubel, F.M., and Ruvkun, G. (2015). Mitophagy confers resistance to siderophore-mediated killing by Pseudomonas aeruginosa. Proc Natl Acad Sci U S A *112*, 1821-1826.

Kislinger, T., Cox, B., Kannan, A., Chung, C., Hu, P., Ignatchenko, A., Scott, M.S., Gramolini, A.O., Morris, Q., Hallett, M.T.*, et al.* (2006). Global survey of organ and organelle protein expression in mouse: combined proteomic and transcriptomic profiling. Cell *125*, 173-186.

Kispal, G., Csere, P., Prohl, C., and Lill, R. (1999). The mitochondrial proteins Atm1p and Nfs1p are essential for biogenesis of cytosolic Fe/S proteins. EMBO J *18*, 3981-3989.

Klimova, T., and Chandel, N.S. (2008). Mitochondrial complex III regulates hypoxic activation of HIF. Cell Death Differ *15*, 660-666.

Kohler, S.A., Henderson, B.R., and Kuhn, L.C. (1995). Succinate dehydrogenase b mRNA of Drosophila melanogaster has a functional iron-responsive element in its 5'-untranslated region. J Biol Chem *270*, 30781-30786.

Lander, E.S., Linton, L.M., Birren, B., Nusbaum, C., Zody, M.C., Baldwin, J., Devon, K., Dewar, K., Doyle, M., FitzHugh, W.*, et al.* (2001). Initial sequencing and analysis of the human genome. Nature *409*, 860-921.

Lane, N. (2005). Power, sex, suicide : mitochondria and the meaning of life (Oxford ; New York: Oxford University Press).

Lane, N., and Martin, W. (2010). The energetics of genome complexity. Nature *467*, 929-934.

Lange, H., Kaut, A., Kispal, G., and Lill, R. (2000). A mitochondrial ferredoxin is essential for biogenesis of cellular iron-sulfur proteins. Proc Natl Acad Sci U S A *97*, 1050-1055.

Lange, H., Muhlenhoff, U., Denzel, M., Kispal, G., and Lill, R. (2004). The heme synthesis defect of mutants impaired in mitochondrial iron-sulfur protein biogenesis is caused by reversible inhibition of ferrochelatase. J Biol Chem *279*, 29101-29108.

Laub, R., Schneider, Y.J., Octave, J.N., Trouet, A., and Crichton, R.R. (1985). Cellular pharmacology of deferrioxamine B and derivatives in cultured rat hepatocytes in relation to iron mobilization. Biochem Pharmacol *34*, 1175-1183.

Lesuisse, E., Santos, R., Matzanke, B.F., Knight, S.A., Camadro, J.M., and Dancis, A. (2003). Iron use for haeme synthesis is under control of the yeast frataxin homologue (Yfh1). Hum Mol Genet *12*, 879-889.

Li, J., Kogan, M., Knight, S.A., Pain, D., and Dancis, A. (1999). Yeast mitochondrial protein, Nfs1p, coordinately regulates iron-sulfur cluster proteins, cellular iron uptake, and iron distribution. J Biol Chem *274*, 33025-33034.

Li, J., Saxena, S., Pain, D., and Dancis, A. (2001). Adrenodoxin reductase homolog (Arh1p) of yeast mitochondria required for iron homeostasis. J Biol Chem *276*, 1503-1509.

Li, P., Jiao, J., Gao, G., and Prabhakar, B.S. (2011). Control of mitochondrial activity by miRNAs. J Cell Biochem.

Lill, R., Hoffmann, B., Molik, S., Pierik, A.J., Rietzschel, N., Stehling, O., Uzarska, M.A., Webert, H., Wilbrecht, C., and Muhlenhoff, U. (2012). The role of mitochondria in cellular iron-sulfur protein biogenesis and iron metabolism. Biochim Biophys Acta *1823*, 1491-1508.

Lin, E., Graziano, J.H., and Freyer, G.A. (2001). Regulation of the 75-kDa subunit of mitochondrial complex I by iron. J Biol Chem *276*, 27685-27692.

Ljubicic, V., Joseph, A.M., Saleem, A., Uguccioni, G., Collu-Marchese, M., Lai, R.Y., Nguyen, L.M., and Hood, D.A. (2010). Transcriptional and post-transcriptional regulation of mitochondrial biogenesis in skeletal muscle: effects of exercise and aging. Biochim Biophys Acta *1800*, 223-234.

Lloyd, J.B., Cable, H., and Rice-Evans, C. (1991). Evidence that desferrioxamine cannot enter cells by passive diffusion. Biochem Pharmacol *41*, 1361-1363.

Lowell, B.B., and Shulman, G.I. (2005). Mitochondrial dysfunction and type 2 diabetes. Science *307*, 384-387.

Lutz, T., Westermann, B., Neupert, W., and Herrmann, J.M. (2001). The mitochondrial proteins Ssq1 and Jac1 are required for the assembly of iron sulfur clusters in mitochondria. J Mol Biol *307*, 815-825.

MacAskill, A.F., and Kittler, J.T. (2010). Control of mitochondrial transport and localization in neurons. Trends Cell Biol *20*, 102-112.

Maguire, J.J., Davies, K.J., Dallman, P.R., and Packer, L. (1982). Effects of dietary iron deficiency of iron-sulfur proteins and bioenergetic functions of skeletal muscle mitochondria. Biochim Biophys Acta *679*, 210-220.

Maio, N., and Rouault, T.A. (2015). Iron-sulfur cluster biogenesis in mammalian cells: New insights into the molecular mechanisms of cluster delivery. Biochim Biophys Acta *1853*, 1493-1512.

Masini, A., Salvioli, G., Cremonesi, P., Botti, B., Gallesi, D., and Ceccarelli, D. (1994a). Dietary iron deficiency in the rat. I. Abnormalities in energy metabolism of the hepatic tissue. Biochim Biophys Acta *1188*, 46-52.

Masini, A., Trenti, T., Caramazza, I., Predieri, G., Gallesi, D., and Ceccarelli, D. (1994b). Dietary iron deficiency in the rat. II. Recovery from energy metabolism derangement of the hepatic tissue by iron therapy. Biochim Biophys Acta *1188*, 53-57.

McCann, J.C., and Ames, B.N. (2007). An overview of evidence for a causal relation between iron deficiency during development and deficits in cognitive or behavioral function. Am J Clin Nutr *85*, 931-945.

McLane, J.A., Fell, R.D., McKay, R.H., Winder, W.W., Brown, E.B., and Holloszy, J.O. (1981). Physiological and biochemical effects of iron deficiency on rat skeletal muscle. Am J Physiol *241*, C47-54.

McLean, E., Cogswell, M., Egli, I., Wojdyla, D., and de Benoist, B. (2009). Worldwide prevalence of anaemia, WHO Vitamin and Mineral Nutrition Information System, 1993-2005. Public Health Nutr *12*, 444-454.

Melefors, O. (1996). Translational regulation in vivo of the Drosophila melanogaster mRNA encoding succinate dehydrogenase iron protein via iron responsive elements. Biochem Biophys Res Commun *221*, 437-441.

Melefors, O., Goossen, B., Johansson, H.E., Stripecke, R., Gray, N.K., and Hentze, M.W. (1993). Translational control of 5-aminolevulinate synthase mRNA by iron-responsive elements in erythroid cells. J Biol Chem *268*, 5974-5978.

Mense, S.M., and Zhang, L. (2006). Heme: a versatile signaling molecule controlling the activities of diverse regulators ranging from transcription factors to MAP kinases. Cell Res *16*, 681-692.

Mick, D.U., Fox, T.D., and Rehling, P. (2011). Inventory control: cytochrome c oxidase assembly regulates mitochondrial translation. Nat Rev Mol Cell Biol *12*, 14-20.

Mootha, V.K., Bunkenborg, J., Olsen, J.V., Hjerrild, M., Wisniewski, J.R., Stahl, E., Bolouri, M.S., Ray, H.N., Sihag, S., Kamal, M.*, et al.* (2003). Integrated analysis of protein composition, tissue diversity, and gene regulation in mouse mitochondria. Cell *115*, 629-640.

Muhlenhoff, U., Richhardt, N., Ristow, M., Kispal, G., and Lill, R. (2002). The yeast frataxin homolog Yfh1p plays a specific role in the maturation of cellular Fe/S proteins. Hum Mol Genet *11*, 2025-2036.

Netz, D.J., Mascarenhas, J., Stehling, O., Pierik, A.J., and Lill, R. (2014). Maturation of cytosolic and nuclear iron-sulfur proteins. Trends Cell Biol *24*, 303-312.

Oexle, H., Gnaiger, E., and Weiss, G. (1999). Iron-dependent changes in cellular energy metabolism: influence on citric acid cycle and oxidative phosphorylation. Biochim Biophys Acta *1413*, 99-107.

Ohira, Y., Cartier, L.J., Chen, M., and Holloszy, J.O. (1987). Induction of an increase in mitochondrial matrix enzymes in muscle of iron-deficient rats. Am J Physiol *253*, C639-644.

Overmyer, K.A., Evans, C.R., Qi, N.R., Minogue, C.E., Carson, J.J., Chermside-Scabbo, C.J., Koch, L.G., Britton, S.L., Pagliarini, D.J., Coon, J.J.*, et al.* (2015). Maximal oxidative capacity during exercise is associated with skeletal muscle fuel selection and dynamic changes in mitochondrial protein acetylation. Cell Metab *21*, 468-478.

Pagliarini, D.J., Calvo, S.E., Chang, B., Sheth, S.A., Vafai, S.B., Ong, S.E., Walford, G.A., Sugiana, C., Boneh, A., Chen, W.K.*, et al.* (2008). A mitochondrial protein compendium elucidates complex I disease biology. Cell *134*, 112-123.

Pagliarini, D.J., and Rutter, J. (2013). Hallmarks of a new era in mitochondrial biochemistry. Genes Dev *27*, 2615-2627.

Palmfeldt, J., Vang, S., Stenbroen, V., Pedersen, C.B., Christensen, J.H., Bross, P., and Gregersen, N. (2009). Mitochondrial proteomics on human fibroblasts for identification of metabolic imbalance and cellular stress. Proteome Sci *7*, 20.

Pancrudo, J., Shanske, S., Coku, J., Lu, J., Mardach, R., Akman, O., Krishna, S., Bonilla, E., and DiMauro, S. (2007). Mitochondrial myopathy associated with a novel mutation in mtDNA. Neuromuscul Disord *17*, 651-654.

Puig, S., Askeland, E., and Thiele, D.J. (2005). Coordinated remodeling of cellular metabolism during iron deficiency through targeted mRNA degradation. Cell *120*, 99-110.

Puig, S., Vergara, S.V., and Thiele, D.J. (2008). Cooperation of two mRNA-binding proteins drives metabolic adaptation to iron deficiency. Cell Metab *7*, 555-564.

Quiros, P.M., Langer, T., and Lopez-Otin, C. (2015). New roles for mitochondrial proteases in health, ageing and disease. Nat Rev Mol Cell Biol *16*, 345-359.

Rensvold, J.W., Ong, S.E., Jeevananthan, A., Carr, S.A., Mootha, V.K., and Pagliarini, D.J. (2013). Complementary RNA and protein profiling identifies iron as a key regulator of mitochondrial biogenesis. Cell Rep *3*, 237-245.

Revel, J.P., Fawcett, D.W., and Philpott, C.W. (1963). Observations on mitochondrial structure angular configurations of the cristae. J Cell Biol *16*, 187-195.

Rhee, H.W., Zou, P., Udeshi, N.D., Martell, J.D., Mootha, V.K., Carr, S.A., and Ting, A.Y. (2013). Proteomic mapping of mitochondria in living cells via spatially restricted enzymatic tagging. Science *339*, 1328-1331.

Richardson, D., Ponka, P., and Baker, E. (1994). The effect of the iron(III) chelator, desferrioxamine, on iron and transferrin uptake by the human malignant melanoma cell. Cancer Res *54*, 685-689.

Richardson, D.R., Lane, D.J., Becker, E.M., Huang, M.L., Whitnall, M., Suryo Rahmanto, Y., Sheftel, A.D., and Ponka, P. (2010). Mitochondrial iron trafficking and the integration of iron metabolism between the mitochondrion and cytosol. Proc Natl Acad Sci U S A *107*, 10775-10782.

Rines, A.K., and Ardehali, H. (2013). Transition metals and mitochondrial metabolism in the heart. J Mol Cell Cardiol *55*, 50-57.

Rodriguez-Manzaneque, M.T., Tamarit, J., Belli, G., Ros, J., and Herrero, E. (2002). Grx5 is a mitochondrial glutaredoxin required for the activity of iron/sulfur enzymes. Mol Biol Cell *13*, 1109-1121.

Ross, K.L., and Eisenstein, R.S. (2002). Iron deficiency decreases mitochondrial aconitase abundance and citrate concentration without affecting tricarboxylic acid cycle capacity in rat liver. J Nutr *132*, 643-651.

Rotig, A., de Lonlay, P., Chretien, D., Foury, F., Koenig, M., Sidi, D., Munnich, A., and Rustin, P. (1997). Aconitase and mitochondrial iron-sulphur protein deficiency in Friedreich ataxia. Nat Genet *17*, 215-217.

Rouault, T.A. (2013). Iron metabolism in the CNS: implications for neurodegenerative diseases. Nat Rev Neurosci *14*, 551-564.

Rouault, T.A. (2015a). Iron-sulfur proteins hiding in plain sight. Nat Chem Biol *11*, 442-445.

Rouault, T.A. (2015b). Mammalian iron-sulphur proteins: novel insights into biogenesis and function. Nat Rev Mol Cell Biol *16*, 45-55.

Rouault, T.A., and Tong, W.H. (2005). Iron-sulphur cluster biogenesis and mitochondrial iron homeostasis. Nat Rev Mol Cell Biol *6*, 345-351.

Rouault, T.A., and Tong, W.H. (2008). Iron-sulfur cluster biogenesis and human disease. Trends Genet *24*, 398-407.

Rowland, T. (2012). Iron deficiency in athletes: an update. Am J Lifestyle Med *6*, 319-327.

Ruiz, J.C., Walker, S.D., Anderson, S.A., Eisenstein, R.S., and Bruick, R.K. (2013). F-box and leucine-rich repeat protein 5 (FBXL5) is required for maintenance of cellular and systemic iron homeostasis. J Biol Chem *288*, 552-560.

Ruiz-Pesini, E., Lott, M.T., Procaccio, V., Poole, J.C., Brandon, M.C., Mishmar, D., Yi, C., Kreuziger, J., Baldi, P., and Wallace, D.C. (2007). An enhanced MITOMAP with a global mtDNA mutational phylogeny. Nucleic Acids Res *35*, D823-828.

Salahudeen, A.A., Thompson, J.W., Ruiz, J.C., Ma, H.W., Kinch, L.N., Li, Q., Grishin, N.V., and Bruick, R.K. (2009). An E3 ligase possessing an iron-responsive hemerythrin domain is a regulator of iron homeostasis. Science *326*, 722-726.

Salmon, H.A. (1962). The cytochrome c content of the heart, kidney, liver and skeletal muscle of iron-deficient rats. J Physiol *164*, 17-30.

Sanchez, M., Galy, B., Schwanhaeusser, B., Blake, J., Bahr-Ivacevic, T., Benes, V., Selbach, M., Muckenthaler, M.U., and Hentze, M.W. (2011). Iron regulatory protein-1 and -2: transcriptome-wide definition of binding mRNAs and shaping of the cellular proteome by iron regulatory proteins. Blood *118*, e168-179.

Sanduja, S., Blanco, F.F., and Dixon, D.A. (2011). The roles of TTP and BRF proteins in regulated mRNA decay. Wiley Interdiscip Rev RNA *2*, 42-57.

Sato, M., and Sato, K. (2013). Maternal inheritance of mitochondrial DNA by diverse mechanisms to eliminate paternal mitochondrial DNA. Biochim Biophys Acta *1833*, 1979-1984.

Scarpulla, R.C. (2008). Transcriptional paradigms in mammalian mitochondrial biogenesis and function. Physiol Rev *88*, 611-638.

Scarpulla, R.C. (2011). Metabolic control of mitochondrial biogenesis through the PGC-1 family regulatory network. Biochim Biophys Acta *1813*, 1269-1278.

Scarpulla, R.C., Vega, R.B., and Kelly, D.P. (2012). Transcriptional integration of mitochondrial biogenesis. Trends Endocrinol Metab *23*, 459-466.

Schalinske, K.L., Chen, O.S., and Eisenstein, R.S. (1998). Iron differentially stimulates translation of mitochondrial aconitase and ferritin mRNAs in mammalian cells. Implications for iron regulatory proteins as regulators of mitochondrial citrate utilization. J Biol Chem *273*, 3740-3746.

Scharfe, C., Lu, H.H., Neuenburg, J.K., Allen, E.A., Li, G.C., Klopstock, T., Cowan, T.M., Enns, G.M., and Davis, R.W. (2009). Mapping gene associations in human mitochondria using clinical disease phenotypes. PLoS Comput Biol *5*, e1000374.

Scheffler, I.E. (2008). Mitochondria, 2nd edn (Hoboken, N.J.: Wiley-Liss).

Schiavi, A., Maglioni, S., Palikaras, K., Shaik, A., Strappazzon, F., Brinkmann, V., Torgovnick, A., Castelein, N., De Henau, S., Braeckman, B.P.*, et al.* (2015). Iron-Starvation-Induced Mitophagy Mediates Lifespan Extension upon Mitochondrial Stress in C. elegans. Curr Biol *25*, 1810-1822.

Schilke, B., Voisine, C., Beinert, H., and Craig, E. (1999). Evidence for a conserved system for iron metabolism in the mitochondria of Saccharomyces cerevisiae. Proc Natl Acad Sci U S A *96*, 10206-10211.

Schmidt, O., Pfanner, N., and Meisinger, C. (2010). Mitochondrial protein import: from proteomics to functional mechanisms. Nat Rev Mol Cell Biol *11*, 655-667.

Schofield, C.J., and Ratcliffe, P.J. (2004). Oxygen sensing by HIF hydroxylases. Nat Rev Mol Cell Biol *5*, 343-354.

Schultze, M.O. (1939). The effect of deficiencies in copper and iron on the cytochrome oxidase of rat tissues. J Biol Chem *129*, 729-737.

Schwanhausser, B., Gossen, M., Dittmar, G., and Selbach, M. (2009). Global analysis of cellular protein translation by pulsed SILAC. Proteomics *9*, 205-209.

Semenza, G.L. (2013). HIF-1 mediates metabolic responses to intratumoral hypoxia and oncogenic mutations. J Clin Invest *123*, 3664-3671.

Siekevitz, P. (1957). Powerhouse of the cell. Sci Am *197*, 131-144.

Simcox, J.A., and McClain, D.A. (2013). Iron and diabetes risk. Cell Metab *17*, 329-341.

Skladal, D., Halliday, J., and Thorburn, D.R. (2003). Minimum birth prevalence of mitochondrial respiratory chain disorders in children. Brain *126*, 1905-1912.

Spiegelman, B.M. (2007). Transcriptional control of mitochondrial energy metabolism through the PGC1 coactivators. Novartis Found Symp *287*, 60-63; discussion 63-69.

Stehling, O., and Lill, R. (2013). The role of mitochondria in cellular iron-sulfur protein biogenesis: mechanisms, connected processes, and diseases. Cold Spring Harb Perspect Med *3*, 1-17.

Still, A.J., Floyd, B.J., Hebert, A.S., Bingman, C.A., Carson, J.J., Gunderson, D.R., Dolan, B.K., Grimsrud, P.A., Dittenhafer-Reed, K.E., Stapleton, D.S.*, et al.* (2013). Quantification of mitochondrial acetylation dynamics highlights prominent sites of metabolic regulation. J Biol Chem *288*, 26209-26219.

Strain, J., Lorenz, C.R., Bode, J., Garland, S., Smolen, G.A., Ta, D.T., Vickery, L.E., and Culotta, V.C. (1998). Suppressors of superoxide dismutase (SOD1) deficiency in Saccharomyces cerevisiae. Identification of proteins predicted to mediate iron-sulfur cluster assembly. J Biol Chem *273*, 31138-31144.

Sun, X., Ge, R., Cai, Z., Sun, H., and He, Q.Y. (2009). Iron depletion decreases proliferation and induces apoptosis in a human colonic adenocarcinoma cell line, Caco2. J Inorg Biochem *103*, 1074-1081.

Taketani, S., Adachi, Y., and Nakahashi, Y. (2000). Regulation of the expression of human ferrochelatase by intracellular iron levels. Eur J Biochem *267*, 4685-4692.

Taylor, R.W., Schaefer, A.M., McDonnell, M.T., Petty, R.K., Thomas, A.M., Blakely, E.L., Hayes, C.M., McFarland, R., and Turnbull, D.M. (2004). Catastrophic presentation of mitochondrial disease due to a mutation in the tRNA(His) gene. Neurology *62*, 1420-1423.

Tian, Q., Li, T., Hou, W., Zheng, J., Schrum, L.W., and Bonkovsky, H.L. (2011). Lon peptidase 1 (LONP1)-dependent breakdown of mitochondrial 5-aminolevulinic acid synthase protein by heme in human liver cells. J Biol Chem *286*, 26424-26430.

Torti, S.V., and Torti, F.M. (2013). Iron and cancer: more ore to be mined. Nat Rev Cancer *13*, 342-355.

Uusimaa, J., Finnila, S., Remes, A.M., Rantala, H., Vainionpaa, L., Hassinen, I.E., and Majamaa, K. (2004). Molecular epidemiology of childhood mitochondrial encephalomyopathies in a Finnish population: sequence analysis of entire mtDNA of 17 children reveals heteroplasmic mutations in tRNAArg, tRNAGlu, and tRNALeu(UUR) genes. Pediatrics *114*, 443-450.

Vafai, S.B., and Mootha, V.K. (2012). Mitochondrial disorders as windows into an ancient organelle. Nature *491*, 374-383.

Vashisht, A.A., Zumbrennen, K.B., Huang, X., Powers, D.N., Durazo, A., Sun, D., Bhaskaran, N., Persson, A., Uhlen, M., Sangfelt, O.*, et al.* (2009). Control of iron homeostasis by an iron-regulated ubiquitin ligase. Science *326*, 718-721.

Vengellur, A., Phillips, J.M., Hogenesch, J.B., and LaPres, J.J. (2005). Gene expression profiling of hypoxia signaling in human hepatocellular carcinoma cells. Physiol Genomics *22*, 308-318.

Venter, J.C., Adams, M.D., Myers, E.W., Li, P.W., Mural, R.J., Sutton, G.G., Smith, H.O., Yandell, M., Evans, C.A., Holt, R.A.*, et al.* (2001). The sequence of the human genome. Science *291*, 1304-1351.

Voisine, C., Cheng, Y.C., Ohlson, M., Schilke, B., Hoff, K., Beinert, H., Marszalek, J., and Craig, E.A. (2001). Jac1, a mitochondrial J-type chaperone, is involved in the biogenesis of Fe/S clusters in Saccharomyces cerevisiae. Proc Natl Acad Sci U S A *98*, 1483-1488.

von Haehling, S., Jankowska, E.A., van Veldhuisen, D.J., Ponikowski, P., and Anker, S.D. (2015). Iron deficiency and cardiovascular disease. Nat Rev Cardiol.

Wallace, D.C. (2005). A mitochondrial paradigm of metabolic and degenerative diseases, aging, and cancer: a dawn for evolutionary medicine. Annu Rev Genet *39*, 359-407.

Wallace, D.C., Singh, G., Lott, M.T., Hodge, J.A., Schurr, T.G., Lezza, A.M., Elsas, L.J., 2nd, and Nikoskelainen, E.K. (1988). Mitochondrial DNA mutation associated with Leber's hereditary optic neuropathy. Science *242*, 1427-1430.

Walter, P.B., Knutson, M.D., Paler-Martinez, A., Lee, S., Xu, Y., Viteri, F.E., and Ames, B.N. (2002). Iron deficiency and iron excess damage mitochondria and mitochondrial DNA in rats. Proc Natl Acad Sci U S A *99*, 2264-2269.

Ward, R.J., Zucca, F.A., Duyn, J.H., Crichton, R.R., and Zecca, L. (2014). The role of iron in brain ageing and neurodegenerative disorders. Lancet Neurol *13*, 1045-1060.

Weinbach, E.C., and Ebert, P.S. (1985). Effects of succinylacetone on growth and respiration of L1210 leukemia cells. Cancer Lett *26*, 253-259.

Westermann, B. (2010). Mitochondrial fusion and fission in cell life and death. Nat Rev Mol Cell Biol *11*, 872-884.

Wiedemann, N., Urzica, E., Guiard, B., Muller, H., Lohaus, C., Meyer, H.E., Ryan, M.T., Meisinger, C., Muhlenhoff, U., Lill, R.*, et al.* (2006). Essential role of Isd11 in mitochondrial iron-sulfur cluster synthesis on Isu scaffold proteins. EMBO J *25*, 184-195.

Wingert, R.A., Galloway, J.L., Barut, B., Foott, H., Fraenkel, P., Axe, J.L., Weber, G.J., Dooley, K., Davidson, A.J., Schmid, B.*, et al.* (2005). Deficiency of glutaredoxin 5 reveals Fe-S clusters are required for vertebrate haem synthesis. Nature *436*, 1035-1039.

Wu, N., Yin, L., Hanniman, E.A., Joshi, S., and Lazar, M.A. (2009). Negative feedback maintenance of heme homeostasis by its receptor, Rev-erbalpha. Genes Dev *23*, 2201-2209.

Xu, W., Barrientos, T., and Andrews, N.C. (2013). Iron and copper in mitochondrial diseases. Cell Metab *17*, 319-328.

Yin, L., Wu, N., Curtin, J.C., Qatanani, M., Szwergold, N.R., Reid, R.A., Waitt, G.M., Parks, D.J., Pearce, K.H., Wisely, G.B.*, et al.* (2007). Rev-erbalpha, a heme sensor that coordinates metabolic and circadian pathways. Science *318*, 1786-1789.

Yoon, Y.S., Byun, H.O., Cho, H., Kim, B.K., and Yoon, G. (2003). Complex II defect via down-regulation of iron-sulfur subunit induces mitochondrial dysfunction and cell cycle delay in iron chelation-induced senescence-associated growth arrest. J Biol Chem *278*, 51577-51586.

Yoon, Y.S., Yoon, D.S., Lim, I.K., Yoon, S.H., Chung, H.Y., Rojo, M., Malka, F., Jou, M.J., Martinou, J.C., and Yoon, G. (2006). Formation of elongated giant mitochondria in DFO-induced cellular senescence: involvement of enhanced fusion process through modulation of Fis1. J Cell Physiol *209*, 468-480.

Youle, R.J., and Narendra, D.P. (2011). Mechanisms of mitophagy. Nat Rev Mol Cell Biol *12*, 9-14.

Youle, R.J., and van der Bliek, A.M. (2012). Mitochondrial fission, fusion, and stress. Science *337*, 1062-1065.

Yu, Y., Kovacevic, Z., and Richardson, D.R. (2007). Tuning cell cycle regulation with an iron key. Cell Cycle *6*, 1982-1994.

Zhang, H., Bosch-Marce, M., Shimoda, L.A., Tan, Y.S., Baek, J.H., Wesley, J.B., Gonzalez, F.J., and Semenza, G.L. (2008). Mitochondrial autophagy is an HIF-1-dependent adaptive metabolic response to hypoxia. J Biol Chem *283*, 10892-10903.

Zhang, H., Gao, P., Fukuda, R., Kumar, G., Krishnamachary, B., Zeller, K.I., Dang, C.V., and Semenza, G.L. (2007). HIF-1 inhibits mitochondrial biogenesis and cellular respiration in VHL-deficient renal cell carcinoma by repression of C-MYC activity. Cancer Cell *11*, 407-420.

Zhao, X., Leon, I.R., Bak, S., Mogensen, M., Wrzesinski, K., Hojlund, K., and Jensen, O.N. (2011). Phosphoproteome analysis of functional mitochondria isolated from resting human muscle reveals extensive phosphorylation of inner membrane protein complexes and enzymes. Mol Cell Proteomics *10*, M110 000299.

Zimmermann, M.B., and Hurrell, R.F. (2007). Nutritional iron deficiency. Lancet *370*, 511-520.

1.6 Figures

Figure 1: Key steps of heme and iron-sulfur cluster (Fe-S) biosynthesis occur in mitochondria. Heme and Fe-S clusters are used by the enzyme aconitase of the TCA cycle and within the electron transport chain (#X signifies the number of heme or Fe-S present, OMM is outer mitochondrial membrane, IMM is inner mitochondrial membrane, IMS is intermembrane space, CoQ is coenzyme Q, and Cyt *c* is cytochrome *c*). Each complex of OxPhos, with the exception of complex II, contains subunits encoded from nuclear and mitochondrial DNA. Electrons from NADH and $FADH_2$ are transferred through complexes I and II, respectively, to coenzyme Q, and then to complexes III and IV, and finally oxygen. Complexes I, III and IV use the energy from NADH and/or $FADH_2$ to pump protons from the matrix to the intermembrane space, thereby establishing an electrochemical proton gradient across the inner mitochondrial membrane. The energy from this gradient is used to generated ATP via the flow of protons back to the matrix through complex V.

Figure 1

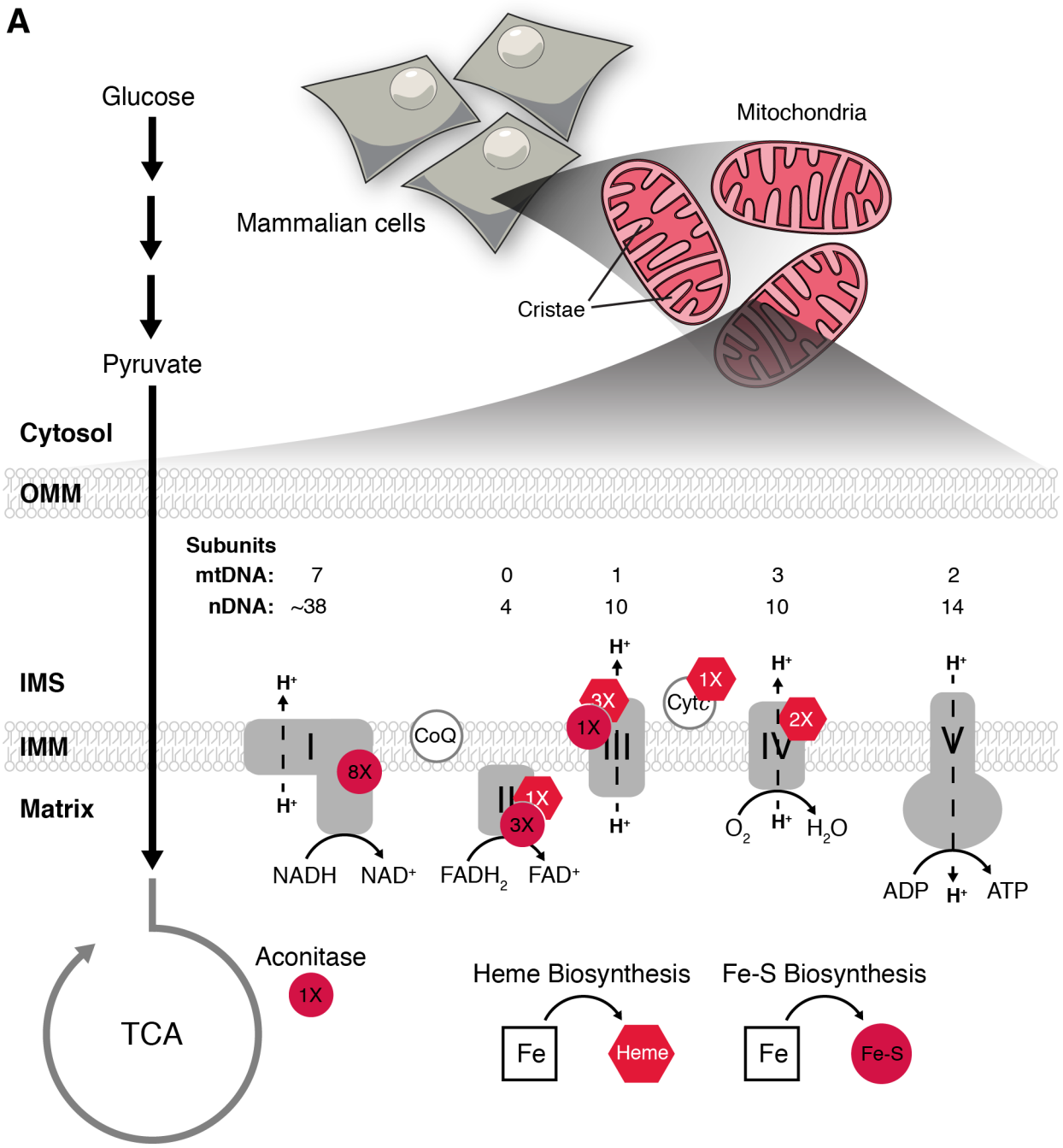
A
Glucose
Pyruvate
Mammalian cells
Mitochondria
Cristae
Cytosol
OMM
IMS
IMM
Matrix
Subunits
mtDNA: 7 0 1 3 2
nDNA: ~38 4 10 10 14
8X
CoQ
1X
3X
1X
3X
1X
2X
NADH
NAD+
FADH2
FAD+
O2
H2O
ADP
ATP
TCA
Aconitase
1X
Heme Biosynthesis
Fe
Heme
Fe-S Biosynthesis
Fe
Fe-S

CHAPTER TWO: Complementary RNA and Protein Profiling Identifies Iron as a Key Regulator of Mitochondrial Biogenesis

This chapter was originally published as the following journal article:

Rensvold, J.W., Ong, S.E., Jeevananthan, A., Carr, S.A., Mootha, V.K., Pagliarini, D.J. (2013). Complementary RNA and protein profiling identifies iron as a key regulator of mitochondrial biogenesis. Cell Reports *3*, 237-245.

2.1 Summary

Mitochondria are centers of metabolism and signaling whose content and function must adapt to changing cellular environments. The biological signals that initiate mitochondrial restructuring and the cellular processes that drive this adaptive response are largely obscure. To better define these systems, we performed matched quantitative genomic and proteomic analyses of mouse muscle cells as they performed mitochondrial biogenesis. We find that proteins involved in cellular iron homeostasis are highly coordinated with this process, and that depletion of cellular iron results in a rapid, dose-dependent decrease of select mitochondrial protein levels and oxidative capacity. We further show that this process is universal across a broad range of cell types and fully reversed when iron is reintroduced. Collectively, our work reveals that cellular iron is a key regulator of mitochondrial biogenesis, and provides quantitative datasets that can be leveraged to explore post-transcriptional and post-translational processes that are essential for mitochondrial adaptation.

2.2 Introduction

Mitochondria are ubiquitous organelles that are essential for cellular energy generation and a range of key metabolic pathways. The production of mitochondria—termed mitochondrial biogenesis—is a complex process involving the orchestrated transcription, translation and import of more than one thousand proteins encoded by two genomes (Mick et al., 2011; Pagliarini et al., 2008; Scarpulla, 2008; Schmidt et al., 2010). Moreover, these organelles vary considerably in composition across tissues (Mootha et al., 2003a; Pagliarini et al., 2008) and remodel to meet cellular needs (Baltzer et al., 2010; Hock and Kralli, 2009), indicating that the mitochondrial biogenesis program is customizable and responsive to environmental conditions. Defects in this

process are associated with a range of human disorders, including mitochondrial encephalomyopathy with ragged red fibers (MERRF), type 2 diabetes and various cancers (Calvo and Mootha, 2010; DiMauro and Schon, 2003; Lowell and Shulman, 2005; Wallace, 2005).

During the past two decades, major progress has been made in deciphering the transcriptional networks that drive mitochondrial biogenesis. Of particular importance was the identification of peroxisome proliferator-activated receptor gamma, coactivator 1 alpha (PGC-1α) (Puigserver et al., 1998). PGC-1α and related coactivators PGC-1β (Kressler et al., 2002; Lin et al., 2002) and PRC (PGC-1 related coactivator) (Andersson and Scarpulla, 2001) coordinate and activate the various transcription factors required for mitochondrial biogenesis (Scarpulla, 2008). Additionally, PGC-1α is activated by exercise, adaptive thermogenesis, changes in cellular redox state, and the availability of nutrients and growth factors (Hock and Kralli, 2009), helping to explain how mitochondrial content is responsive to changing cellular conditions.

Despite significant advancements in our understanding of PGC-1α and its corresponding transcription factors, important aspects of the cellular control of mitochondrial content remain unclear. These include post-transcriptional processes that control mitochondrial gene expression, mechanisms of active mitochondrial degradation and clearance, and extra-mitochondrial processes that help coordinate communication between mitochondria and the nucleus (Goldenthal and Marin-Garcia, 2004). Post-transcriptional control mechanisms, such as upstream open reading frames (uORFs) (Calvo et al., 2009), iron responsive elements (IREs) (Eisenstein and Ross, 2003) and microRNAs (Li et al., 2011) are already known to affect the expression of select mitochondrial genes, and the global discordance between cellular mRNA and protein levels suggests that these mechanisms are likely more widespread (Mootha et al., 2003a).

Additionally, macroautophagy (*i.e.,* mitophagy) is emerging as an important mechanism for eliminating damaged mitochondria (Youle and Narendra, 2011). However, identifying additional genes subject to post-transcriptional regulation, and spotlighting cellular processes that help synchronize the mitochondrial biogenesis program, would benefit from matched, cell-wide quantitative data of protein and mRNA abundance, which has largely been lacking.

Here, to produce such a resource, we performed parallel quantitative SILAC (stable isotope labeling by amino acids in cell culture)-based proteomics (Ong and Mann, 2006) and microarray analyses of PGC-1α-induced mitochondrial biogenesis in mouse muscle C2C12 cells. In doing so, we find that key proteins involved in maintaining cellular iron homeostasis are correlated with mitochondrial biogenesis. We further reveal that depriving various cell types of iron through chelation or active transport leads to a rapid and dose-dependent attenuation of mitochondrial transcript and protein levels that is fully reversible within 3-4 days. Together, our work demonstrates that iron deprivation results in an active and coordinated down-regulation of mitochondrial gene expression, suggesting that the bioavailability of iron is a key parameter for establishing a set point of cellular mitochondrial activity. As iron deficiency anemia is the most common nutritional disorder worldwide (McLean et al., 2009), this work has broad implications for understanding mitochondrial dysfunction in human health and disease. Additionally, our data serve as a resource for investigating genes subject to post-transcriptional regulation, and for identifying additional auxiliary pathways that might be important for calibrating or modulating the mitochondrial biogenesis program.

2.3 Results and Discussion

2.3.1 Complementary RNA and Protein Profiling of Mitochondrial Biogenesis

We sought to better define the mitochondrial biogenesis program in C2C12 mouse myotubes by performing complementary RNA and protein profiling. To maximize the transcriptional activation of mitochondrial genes, we overexpressed PGC-1α—the predominant transcriptional coactivator that drives mitochondrial biogenesis—more than 200-fold using an adenovirus-mediated delivery system. We chose C2C12 cells as a model because overexpression of PGC-1α in this cell line is sufficient to cause an approximate doubling of mitochondrial mass in three days (Wu et al., 1999). This approach allows us to assess the relative contribution of post-transcriptional mechanisms in regulating mitochondrial gene expression, and provides a more complete assessment of the cell-wide proteomic changes that accompany PGC-1α-induced mitochondrial production.

Following PGC-1α overexpression, we tracked changes in cellular mRNA and protein levels using microarrays and quantitative SILAC proteomics (Ong and Mann, 2006), respectively (Figure 1A). Consistent with previous studies, our microarray analyses showed that PGC-1α causes a robust increase in the transcript abundance of nuclear-encoded mitochondrial genes, especially those involved in oxidative phosphorylation (OxPhos) (Figure 1B). Our SILAC data revealed similar results for protein levels: of 442 mitochondrial proteins quantified using at least 2 unique peptides, 263 significantly increased in abundance (Figure 1C). As expected, PGC-1α-induced mRNA and protein fold changes were largely consistent in the direction of change (Figure S1A). However, the protein and mRNA abundances differed by as much as 9-fold for nuclear-encoded mitochondrial genes and, for 97 of these genes, mRNA abundance was increased while the corresponding protein abundance was decreased (Table S1, Figure S1B).

This mRNA:protein discordance reveals that regulation of protein stability or translation are likely to be important for titrating the expression level of select genes during PGC-1α-induced mitochondrial biogenesis. More broadly, these observations reveal the utility of our resource for spotlighting mitochondrial proteins whose expression may be subject to multiple levels of regulation.

2.3.2 Iron Chelation Causes a Pervasive Dampening of Mitochondrial Protein and Transcript Levels

Our experimental approach also enabled us to investigate peripheral genes and pathways that may be important for the mitochondrial biogenesis program. Interestingly, we noted that proteins involved in regulating cellular iron levels were among the most highly up- and down-regulated proteins in our SILAC analyses. The transferrin receptor, which is responsible for transporting transferrin-bound iron into cells, increased more than 4-fold with PGC-1α overexpression (Figure 1C). Reciprocally, the level of ferritin heavy chain, part of the ferritin complex that sequesters cellular iron, was decreased (Figure 1C). These results suggest that iron might be essential for the mitochondrial biogenesis program. Increased cellular iron availability during mitochondrial biogenesis might simply be necessary to accommodate the mitochondrial proteins that contain iron as a cofactor or may occur in anticipation of increased output from the mitochondrial iron-sulfur cluster biogenesis pathway (Lill, 2009; Richardson et al., 2010). However, the magnitude of these changes prompted us to explore whether cellular iron levels might impact the mitochondrial biogenesis program holistically.

To test whether loss of cellular iron is sufficient to induce a restructuring of cellular mitochondrial content, we modified the experimental approach outlined in Figure 1A. Here, *in*

lieu of PGC-1α overexpression, we treated the cells with deferoxamine (DFO), a clinically used cell-permeable iron chelator (Chaston and Richardson, 2003). Strikingly, the microarray results revealed that DFO treatment strongly diminished the abundance of mitochondrial transcripts (Figure 1D). Overall, the magnitude of the DFO effect was as robust as the powerful PGC-1α effect, and was also most prominent for genes encoding proteins involved in OxPhos (Figure 1E, S1C). Once again, our mRNA and protein measurements were largely consistent in direction and magnitude (Figure S1D), however there were notable differences in these measurements amongst the OxPhos complexes. Complexes I and II, each of which contain multiple iron-sulfur clusters, were most strongly affected, with protein levels more decreased than the corresponding mRNA levels (Figure 1F). Conversely, transcripts encoding complex V subunits were decreased while their corresponding protein levels were increased or unchanged (Figure 1F). A recent, large-scale study of protein dynamics found that mitochondrial proteins, including complex I and complex V, have largely similar turnover rates under normal conditions (Price et al., 2010), suggesting that the differences in complex I and complex V subunit levels following iron deprivation likely involves post-transcriptional regulation.

To assess whether cellular iron levels affect PGC-1α-induced mitochondrial biogenesis we repeated the experimental approach a third time with PGC-1α adenovirus added to cells simultaneously with DFO. Here, the presence of DFO had a pervasive dampening effect on the induction of mitochondrial transcripts by PGC-1α (Figure S1E, S1F). Notably, for many of the same OxPhos subunits highlighted in Figure 1F, transcript expression was increased under these conditions while the corresponding protein levels were decreased (Figure 1G, S1G). This again suggests that for select genes, iron chelation may lead to an active, post-transcriptional reduction of expression, as opposed to merely thwarting the effects of PGC-1α.

Our large-scale gene expression and proteomic data show that iron chelation has an approximately equal and opposite effect to that of PGC-1α, a powerful inducer of mitochondrial biogenesis. To validate these results, we performed immunoblots and quantitative PCR on the same samples used for our proteomics and microarray analyses. Consistent with our SILAC data, we found that OxPhos proteins were significantly decreased by the DFO treatment (Figure 2A). These results also validated that this effect was predominantly limited to mitochondrial proteins, as representative endoplasmic reticulum, nuclear and cytoplasmic markers were unaffected by this treatment (Figure 2A). For qPCR measurements, we chose two nuclear-encoded OxPhos genes (*Ndufb5,* which is part of iron-containing complex I, and *Atp5a1,* a subunit of iron-free complex V), and one mtDNA-encoded gene (*COX1*, which was not represented on the microarray or captured by mass spectrometry). All three genes were significantly upregulated with PGC-1α overexpression and diminished by DFO treatment (Figure 2B). These PCR results reveal that the iron chelation effect is not limited to nuclear-encoded mitochondrial genes or to genes encoding iron-dependent mitochondrial proteins. Furthermore, our microarray and SILAC data demonstrate that the expression of genes encoding *non*-mitochondrial iron-dependent proteins is not diminished by the iron chelation treatment (Figure S1H). Collectively, our data show that acute iron deprivation has a specific and dose-dependent dampening effect on mitochondrial protein expression that exceeds a mere cell-wide loss of iron-dependent proteins and processes.

2.3.3 Iron Chelation Causes a Rapid, Universal and Dose-Dependent Decrease in Mitochondrial Protein Abundance

The results above suggest that cells might possess the ability to calibrate their mitochondrial protein levels to the concentration of available iron. To further test this hypothesis, we grew myotubes in the presence of increasing concentrations of DFO. The results show that even 20 μM DFO has a marked effect on cytochrome *c* and complex I levels, and that the effect is directly proportional to the concentration of DFO (Figure 2C). To begin to assess the universality of the iron deprivation effect, we treated myotubes alongside their undifferentiated myoblast counterparts. Surprisingly, the response in myoblasts was even more robust: after just 24 hours of treatment with DFO, the 8 kDa-complex I subunit was nearly completely lost, whereas the level of this protein continued to gradually vanish from myotubes up through 72 hours (Figure S2A). This effect was also evident in a panel of cell lines differing in species and tissue of origin (Figure 2D), suggesting that iron availability might be a universal gauge that cells use to calibrate mitochondrial activity.

To further define the effect of DFO on OxPhos protein abundance in undifferentiated myoblasts, we examined individual subunits from each OxPhos complex using standard SDS-PAGE and fully assembled, native OxPhos complexes using blue native PAGE (BN-PAGE). SDS-PAGE revealed that DFO causes a decrease in the abundance of complex I, complex II and complex IV subunits (Figure 2E). Consistent with our proteomic analysis of differentiated myotubes (Figure 1F), BN-PAGE revealed that DFO most strongly affects the abundance of fully assembled complex I and complex II (Figure 2F). Moreover, iron chelation also seems to affect supercomplex formation (Figure 2F). A distinguishing feature of complexes I and II among the OxPhos machinery is that they each possess multiple iron-sulfur cluster centers. As

such, although many mitochondrial proteins are affected by iron deprivation, this suggests that iron-sulfur clusters might be particularly important for the cellular response to this perturbation.

Our data demonstrate that iron deprivation causes a pervasive, but not complete, reduction in the expression of mitochondrial proteins. This result is consistent with a calibrated remodeling of the mitochondrial proteome, as opposed to total mitochondrial turnover. To further test this, we measured changes in mitochondrial mass from C2C12 myoblasts using MitoTracker and nonyl acridine orange (NAO) following treatment with 100 μM DFO. Consistent with a similar recent study (Yoon et al., 2006), our results revealed either no change or a slight *increase* in mitochondrial mass after DFO treatment (Figure 2G). Additionally, fluorescence microscopy with MitoTracker staining revealed no obvious changes in mitochondrial mass or morphology after administration of DFO (Figure S2B). Together with the observation that select mitochondrial proteins are not diminished with DFO treatment, including VDAC (voltage dependent anion channel) (Figure 2A, 2C), these results strongly suggests that the iron chelation effect does not involve complete mitochondrial turnover, as would be expected for a mitophagy process.

2.3.4 Iron-Dependent Mitochondrial Restructuring is Distinct from Prominent Regulators of Mitochondrial Biogenesis

Through large-scale and targeted measurements of mRNA and protein abundance, we have found that iron chelation causes a powerful downregulation of mitochondrial protein expression. DFO is a well-characterized and clinically used iron chelator (Chaston and Richardson, 2003); nonetheless, to ensure that our observed effects are not an off-target effect of this drug, we deprived cells of iron through two additional mechanisms. First, we depleted cellular iron stores by overexpressing the iron exporter ferroportin (Nemeth et al., 2004) in

human embryonic kidney (HEK) 293 cells (one of the lines tested in Figure 2D). Similar to DFO, ferroportin expression resulted in a loss of cytochrome *c*, the complex IV COXIV subunit and the complex I 8 kDa subunit (Figure 3A). Both treatments also lead to a decrease in ferritin, indicating a reduction in cellular iron levels (Figure S3A). Second, we demonstrated that a comparable effect was achieved with 2,2'-dipyridyl (DP), a structurally and functionally distinct iron chelator (Figure 3H). Moreover, because the iron chelation effect is robust in the post-mitotic myotubes used in our microarray and proteomics experiments, it is likely independent of the known effect that DFO has on cell proliferation (Yu et al., 2007).

We next sought to determine whether established regulators of mitochondrial biogenesis could explain this response. First, because of the largely reciprocal effects of DFO and PGC-1α treatments (Figure 1E), we hypothesized that DFO might simply cause a decrease in the expression of PGC-1α or its associated transcription factors. From a detailed time course, we found that the abundance of mitochondrial transcripts (Figure 3B, 3C) and proteins (Figure S3B) begins to decrease around 12 hours and reaches a minimum approximately 24 hours after DFO treatment. As a control, we measured the transcript levels of *Tfrc*, whose expression is regulated by iron levels (Figure S3C). We found that DFO had little effect on the transcript levels of *Esrra, Nrf1* or *Gabpa* (the primary PGC-1α-associated transcription factors) (Figure S3C) and caused a marked *increase* in the levels of *Ppargc1a* mRNA (Figure 3D). Furthermore, PGC-1$\alpha^{-/-}$ cells (Uldry et al., 2006) responded comparably to wild type cells when deprived of iron (Figure 3E), together indicating that iron deprivation does not affect mitochondrial gene expression by opposing the function of this coactivator. Interestingly, the levels of PGC-1β mRNA (*Ppargc1b*) (Figure 3F) and protein (Figure S3B) were decreased following DFO treatment. However, similar to PGC-1$\alpha^{-/-}$ cells, depletion of PGC-1β expression in primary satellite cells isolated

from soleus muscle of PGC-1β$^{f/f/MLC\text{-}Cre}$ mice (Zechner et al., 2010) did not cause diminished levels mitochondrial markers, nor did it alter the cellular response to DFO treatment (Figure 3G). Together these results suggest the observed effects of iron deprivation are independent of PGC-1α and PGC-1β.

Iron chelation is also known to activate the hypoxia response by inhibiting the iron-dependent hydroxylases that constitutively target the transcription factor HIF-1α (hypoxia inducible factor 1 alpha) for degradation (Schofield and Ratcliffe, 2004), and HIF-1α activation has recently been shown to initiate a loss of mitochondrial mass in renal clear cell carcinoma cells (Zhang et al., 2007). To determine if the loss of mitochondrial proteins observed here is also due to HIF-1α stabilization, we treated C2C12 myoblasts with the 2-oxoglutarate analog dimethyloxalylglycine (DMOG). The same HIF-1α hydroxylases that require iron also require 2-oxoglutarate as a cofactor, and can therefore be inhibited by 2-oxoglutarate analogs even when iron levels are normal (Jaakkola et al., 2001). As seen in Figure 3H, C2C12 cells treated with the iron chelators DFO or DP responded comparably in their ability to stabilize HIF-1α. Cells treated with DMOG also stabilized HIF-1α but did not affect the OxPhos proteins, suggesting that HIF-1α activation is not sufficient for the iron chelation response. To test whether HIF-1α is necessary for this response, we treated wild type and HIF-1α$^{-/-}$ cells with DFO for 24 hours. These cells showed the same response as all other cell types tested, regardless of the HIF-1α genotype (Figure 3I). Coupled with the fact that HIF-2α is not expressed in this cell line (data not shown), these experiments reveal that the widespread loss of mitochondrial proteins following iron chelation is a distinct, HIF-independent process. Overall, our data reveals that mere deprivation of iron elicits an effect comparable in magnitude to, but independent of, the most well-established drivers of the mitochondrial biogenesis program.

2.3.5 The Mitochondrial Response to Iron Deprivation is Reversible

As noted above, depletion of cellular iron has various known side effects on cellular functions, including inhibition of cell division, initiation of apoptosis and induction of autophagy (De Domenico et al., 2009; Yu et al., 2007). Therefore, we next sought to determine whether our observed mitochondrial effect represents a true acute metabolic adaptation or merely irreversible cellular damage. To do so, we treated C2C12 mouse myoblasts +/− DFO and, after 24 hours, passaged the cells into fresh, DFO-free media (Figure 4A). We continued to passage the cells every 24 hours and took samples at each time point (Figure 4A). Once again, 24 hours of DFO treatment resulted in the selective loss of mitochondrial markers (Figure 4B, S4A). However, 72 to 96 hours following the removal of DFO, protein (Figure 4B) and transcript (Figure S4A) levels were comparable to those found in their untreated counterparts. To determine whether the recovery of mitochondrial proteins also represents a recovery of mitochondrial function, we profiled mitochondrial respiration using a Seahorse XF Analyzer (Figure 4C). As shown in Figure 4D (and Figure S4B), iron chelation lead to a strong decrease in basal oxygen consumption rate (OCR) and spare respiratory capacity (Figure 4E). As DFO is known to suppress cell proliferation (Yu et al., 2007), we normalized the basal OCR of untreated and DFO treated cells to cell number. Remarkably, the basal OCR of DFO treated cells recovered within 48 hours following their passage into DFO free media (Figure 4D). Interestingly, after this recovery of basal OCR, the DFO treated cells continued to recover their spare respiratory capacity, which reached untreated levels by day five (Figure 4E). Coupling efficiency remained unchanged in the iron-depleted cells, indicating that DFO likely does not damage the integrity of the mitochondrial inner membrane (Figure 4F). Altogether, our results reveal that iron

deprivation initiates a reversible and adaptive cellular response that involves remodeling of the mitochondrial proteome and a reduction in mitochondrial respiratory function.

2.3.6 Conclusions

Mitochondria are vital metabolic organelles that must continually adapt to changing external environments and cellular needs. To better define this adaptive process, we performed extensive, matched microarray and quantitative proteomic analyses of mouse muscle cells under a variety of conditions. In doing so, we created a robust resource that can be mined to discover proteins whose expression levels are affected by post-transcriptional regulation, and auxiliary cellular processes that both sense the need for and drive mitochondrial restructuring. We leveraged this resource to find that proteins involved in cellular iron homeostasis are coordinated with mitochondrial biogenesis, and have shown that depriving cells of iron through a variety of mechanisms results in a rapid down-regulation of mitochondrial protein levels and oxidative capacity. We further demonstrated that this drastic effect occurs in a wide range of cell types and that it is fully reversible within 2-3 days following reintroduction of iron. Last, we have shown that this process is independent of the well established PGC-1α-, PGC-1β- and HIF-1α-driven mitochondrial biogenesis programs. As iron deficiency is the world's number one nutritional deficiency, affecting approximately 25% of the population (McLean et al., 2009), our work could have significant implications for human health and disease. Our extensive, freely available mRNA and protein profiling datasets will serve as a rich resource for further exploring the cellular response to acute metabolic stress and the roles of transcriptional and post-transcriptional processes important for mitochondrial biogenesis.

2.4 Experimental Procedures

2.4.1 Cell Culture

Brown preadipocytes were maintained in high glucose DMEM with 20% FBS and 1 × PS (Invitrogen) at 37°C and 5% CO_2. Primary soleus muscle satellite cells were maintained on rat tail collagen (Invitrogen) coated plates in Ham's F-10 media (as detailed in the Extended Experimental Procedures). All other cell lines were maintained in high glucose DMEM with 10% FBS and 1 × PS (Invitrogen). Deferoxamine mesylate salt (DFO), dimethyloxalylglycine (DMOG) and 2,2'-dipyridyl (DP) were obtained from Sigma-Aldrich. For ferroportin (Fpn-GFP) expression, HEK 293FT cells were transfected with 1 μg Fpn-GFP (Nemeth et al., 2004) using Lipofectamine LTX (Invitrogen). Myotube differentiation, metabolic labeling and adenoviral infection were performed using standard procedures (as detailed in the Extended Experimental Procedures).

2.4.2 Microarray and Mass Spectrometry

RNA purification, cRNA preparation and hybridization to Affymetrix 430 2.0 arrays were performed according to established methods (Mootha et al., 2003b). Unique Entrez Gene identifiers from the mapped data where selected and sorted by the average GFP probe intensity from the two metabolic labeling experiments. Data corresponding to these brightest probes that gave present call (P) across all samples were used for analysis (8313 probes total).
Mass spectrometry was performed using standard procedures (as detailed in the Extended Experimental Procedures). For comparison of mRNA and protein abundance, all data were mapped to Entrez Gene identifiers. Gene products were identified as mitochondrial using the

MitoCarta inventory (Pagliarini et al., 2008). OxPhos and iron-containing proteins were manually curated from Gene Ontology annotations.

2.4.3 Relative Quantification Real Time-qPCR

Total RNA was purified using an RNeasy Kit (QIAGEN). First-strand cDNA was synthesized from 500 ng RNA using SuperScript III (Invitrogen). Real-time qPCR was performed using predesigned TaqMan Assays or SYBR green-based detection (ABI) with *Actb* (microarray samples) or *Rplp0* as the endogenous control (see the Extended Experimental Procedures for primer sequences).

2.4.4 Immunoblotting and ELISA

For immunoblot analysis, 15 μg of cleared whole-cell lysate, as determined by BCA assay (Pierce), was separated on a 4-12% Bis-Tris Mini Gel (Invitrogen), transferred to PVDF and probed with primary antibodies (listed in the Extended Experimental Procedures). For BN-PAGE, 12 μg of mitochondrial protein, prepared as previously described (Pello et al., 2008), was separated on a 3-12% NativePAGE Bis-Tris Mini-Gel (Invitrogen), transferred to PVDF and probed with an OxPhos Blue Native Antibody Cocktail (MitoSciences). For ferritin measurement, 15-35 μg of cleared whole-cell lysate was analyzed by ELISA (Ramco Laboratories) and normalized to total protein concentration, as determined by BCA assay (Pierce).

2.4.5 Analysis of Mitochondrial Mass

For determination of mitochondrial mass, C2C12 myoblasts were seeded at 4,500 cells/well in 96-well microplates and incubated for 24 hrs. Following DFO treatment,

mitochondria were stained with 100 nM MitoTracker Green FM or nonyl acridine orange (NAO) (Invitrogen) for 30 min. The cells were then washed 2 × with PBS and fluorescence was measured using a BioTek Synergy 2 Microplate Reader with a 485/20 excitation, 528/20 emission filter set. Fluorescence was normalized to cell number (as described in the Extended Experimental Procedures).

2.4.6 Oxygen Consumption Measurements

Oxygen consumption rate (OCR) measurements were performed using a Seahorse Biosciences XF96 Extracellular Flux Analyzer as previously described (Nicholls et al., 2010). Briefly, C2C12 myoblasts were seeded at 12,000 cells/well in XF96 microplates (Seahorse Biosciences). After a 24-hr incubation, the growth media was exchanged for XF Assay Medium (Seahorse Biosciences) supplemented with 25 mM glucose (Sigma-Aldrich). OCR measurements were 5-min periods following 3-min mix periods. Myoblasts were treated by sequential addition of 1 μg/mL oligomycin (Sigma-Aldrich), 300 nM FCCP (Sigma-Aldrich) and 2 μM rotenone (MP Biomedicals). Spare respiratory capacity and coupling efficiency were calculated using Seahorse Bioscience instructions (see Figure S4B for details). Basal OCR was normalized to cell number (as described in the Extended Experimental Procedures).

2.4.7 Statistics

p Values were calculated by Student's two-tailed t test, one-way ANOVA with Tukey's post-hoc analysis, Spearman's rank correlation test or χ^2 contingency test as indicated in the figure legends.

2.5 Accession Numbers

The Gene Expression Omnibus accession number for the microarray data reported in this paper is GSE42299. The processed microarray and quantitative proteomic data are also available for download from http://www.pagliarinilab.org/datasets.

2.6 Acknowledgements

We would like to thank the members of the Eisenstein, Kaplan and V.K.M. and D.J.P. laboratories for helpful discussions and assistance regarding this project. We specifically thank Sarah Calvo and Dan Arlow of the V.K.M. lab for assistance with microarray analyses, Jerry Kaplan and Ivana De Domenico (University of Utah) for providing the ferroportin expression vector, Bruce Spiegelman (Harvard Medical School) for providing the PGC-1a$^{-/-}$ cells, Daniel Kelly (Sanford-Burnham) for providing the PGC-1β$^{f/f/MLC\text{-}Cre}$ cells, Randall Johnson and Alex Weidemann (UCSD) for providing the HIF-1a$^{-/-}$ cells, Eric Shoubridge (McGill) for providing the MCH58 cells, and Kelly Werner of the D.J.P. lab for critical reading of the manuscript. This work was supported by a Searle Scholars Award, a Shaw Scientist Award and USDA Hatch Award WIS01671 (to D.J.P.), NIH R01GM077465 (to V.K.M.), and NIH Molecular Biosciences Training Grant 5T32GM007215-37 (to J.W.R.).

2.7 References

Andersson, U., and Scarpulla, R.C. (2001). Pgc-1-related coactivator, a novel, serum-inducible coactivator of nuclear respiratory factor 1-dependent transcription in mammalian cells. Mol Cell Biol *21*, 3738-3749.

Baltzer, C., Tiefenbock, S.K., and Frei, C. (2010). Mitochondria in response to nutrients and nutrient-sensitive pathways. Mitochondrion *10*, 589-597.

Calvo, S.E., and Mootha, V.K. (2010). The mitochondrial proteome and human disease. Annu Rev Genomics Hum Genet *11*, 25-44.

Calvo, S.E., Pagliarini, D.J., and Mootha, V.K. (2009). Upstream open reading frames cause widespread reduction of protein expression and are polymorphic among humans. Proc Natl Acad Sci U S A *106*, 7507-7512.

Chaston, T.B., and Richardson, D.R. (2003). Iron chelators for the treatment of iron overload disease: relationship between structure, redox activity, and toxicity. Am J Hematol *73*, 200-210.

De Domenico, I., Ward, D.M., and Kaplan, J. (2009). Specific iron chelators determine the route of ferritin degradation. Blood *114*, 4546-4551.

DiMauro, S., and Schon, E.A. (2003). Mitochondrial respiratory-chain diseases. N Engl J Med *348*, 2656-2668.

Eisenstein, R.S., and Ross, K.L. (2003). Novel roles for iron regulatory proteins in the adaptive response to iron deficiency. J Nutr *133*, 1510S-1516S.

Goldenthal, M.J., and Marin-Garcia, J. (2004). Mitochondrial signaling pathways: a receiver/integrator organelle. Mol Cell Biochem *262*, 1-16.

Hock, M.B., and Kralli, A. (2009). Transcriptional control of mitochondrial biogenesis and function. Annu Rev Physiol *71*, 177-203.

Jaakkola, P., Mole, D.R., Tian, Y.M., Wilson, M.I., Gielbert, J., Gaskell, S.J., von Kriegsheim, A., Hebestreit, H.F., Mukherji, M., Schofield, C.J., et al. (2001). Targeting of HIF-alpha to the von Hippel-Lindau ubiquitylation complex by O2-regulated prolyl hydroxylation. Science *292*, 468-472.

Kressler, D., Schreiber, S.N., Knutti, D., and Kralli, A. (2002). The PGC-1-related protein PERC is a selective coactivator of estrogen receptor alpha. J Biol Chem *277*, 13918-13925.

Li, P., Jiao, J., Gao, G., and Prabhakar, B.S. (2012). Control of mitochondrial activity by miRNAs. J Cell Biochem *113*, 1104-1110.

Lill, R. (2009). Function and biogenesis of iron-sulphur proteins. Nature *460*, 831-838.

Lin, J., Puigserver, P., Donovan, J., Tarr, P., and Spiegelman, B.M. (2002). Peroxisome proliferator-activated receptor gamma coactivator 1beta (PGC-1beta), a novel PGC-1-related transcription coactivator associated with host cell factor. J Biol Chem *277*, 1645-1648.

Lowell, B.B., and Shulman, G.I. (2005). Mitochondrial dysfunction and type 2 diabetes. Science *307*, 384-387.

McLean, E., Cogswell, M., Egli, I., Wojdyla, D., and de Benoist, B. (2009). Worldwide prevalence of anaemia, WHO Vitamin and Mineral Nutrition Information System, 1993-2005. Public Health Nutr *12*, 444-454.

Mick, D.U., Fox, T.D., and Rehling, P. (2011). Inventory control: cytochrome c oxidase assembly regulates mitochondrial translation. Nat Rev Mol Cell Biol *12*, 14-20.

Mootha, V.K., Bunkenborg, J., Olsen, J.V., Hjerrild, M., Wisniewski, J.R., Stahl, E., Bolouri, M.S., Ray, H.N., Sihag, S., Kamal, M.*, et al.* (2003a). Integrated analysis of protein composition, tissue diversity, and gene regulation in mouse mitochondria. Cell *115*, 629-640.

Mootha, V.K., Lindgren, C.M., Eriksson, K.F., Subramanian, A., Sihag, S., Lehar, J., Puigserver, P., Carlsson, E., Ridderstrale, M., Laurila, E., et al. (2003b). PGC-1alpha-responsive genes involved in oxidative phosphorylation are coordinately downregulated in human diabetes. Nat Genet *34*, 267-273.

Nemeth, E., Tuttle, M.S., Powelson, J., Vaughn, M.B., Donovan, A., Ward, D.M., Ganz, T., and Kaplan, J. (2004). Hepcidin regulates cellular iron efflux by binding to ferroportin and inducing its internalization. Science *306*, 2090-2093.

Nicholls, D.G., Darley-Usmar, V.M., Wu, M., Jensen, P.B., Rogers, G.W., and Ferrick, D.A. (2010). Bioenergetic profile experiment using C2C12 myoblast cells. J Vis Exp *46*, 2511.

Ong, S.E., and Mann, M. (2006). A practical recipe for stable isotope labeling by amino acids in cell culture (SILAC). Nat Protoc *1*, 2650-2660.

Pagliarini, D.J., Calvo, S.E., Chang, B., Sheth, S.A., Vafai, S.B., Ong, S.E., Walford, G.A., Sugiana, C., Boneh, A., Chen, W.K.*, et al.* (2008). A mitochondrial protein compendium elucidates complex I disease biology. Cell *134*, 112-123.

Pello, R., Martin, M.A., Carelli, V., Nijtmans, L.G., Achilli, A., Pala, M., Torroni, A., Gomez-Duran, A., Ruiz-Pesini, E., Martinuzzi, A.*, et al.* (2008). Mitochondrial DNA background modulates the assembly kinetics of OXPHOS complexes in a cellular model of mitochondrial disease. Hum Mol Genet *17*, 4001-4011.

Price, J.C., Guan, S., Burlingame, A., Prusiner, S.B., and Ghaemmaghami, S. (2010). Analysis of proteome dynamics in the mouse brain. Proc Natl Acad Sci U S A *107*, 14508-14513.

Puigserver, P., Wu, Z., Park, C.W., Graves, R., Wright, M., and Spiegelman, B.M. (1998). A cold-inducible coactivator of nuclear receptors linked to adaptive thermogenesis. Cell *92*, 829–839.

Richardson, D.R., Lane, D.J., Becker, E.M., Huang, M.L., Whitnall, M., Suryo Rahmanto, Y., Sheftel, A.D., and Ponka, P. (2010). Mitochondrial iron trafficking and the integration of iron metabolism between the mitochondrion and cytosol. Proc Natl Acad Sci U S A *107*, 10775-10782.

Scarpulla, R.C. (2008). Transcriptional paradigms in mammalian mitochondrial biogenesis and function. Physiol Rev *88*, 611-638.

Schmidt, O., Pfanner, N., and Meisinger, C. (2010). Mitochondrial protein import: from proteomics to functional mechanisms. Nat Rev Mol Cell Biol *11*, 655-667.

Schofield, C.J., and Ratcliffe, P.J. (2004). Oxygen sensing by HIF hydroxylases. Nat Rev Mol Cell Biol *5*, 343-354.

Uldry, M., Yang, W., St-Pierre, J., Lin, J., Seale, P., and Spiegelman, B.M. (2006). Complementary action of the PGC-1 coactivators in mitochondrial biogenesis and brown fat differentiation. Cell Metab *3*, 333-341.

Wallace, D.C. (2005). A mitochondrial paradigm of metabolic and degenerative diseases, aging, and cancer: a dawn for evolutionary medicine. Annu Rev Genet *39*, 359-407.

Wu, Z., Puigserver, P., Andersson, U., Zhang, C., Adelmant, G., Mootha, V., Troy, A., Cinti, S., Lowell, B., Scarpulla, R.C., and Spiegelman, B.M. (1999). Mechanisms controlling mitochondrial biogenesis and respiration through the thermogenic coactivator PGC-1. Cell *98*, 115-124.

Yoon, Y.S., Yoon, D.S., Lim, I.K., Yoon, S.H., Chung, H.Y., Rojo, M., Malka, F., Jou, M.J., Martinou, J.C., and Yoon, G. (2006). Formation of elongated giant mitochondria in DFO-induced cellular senescence: involvement of enhanced fusion process through modulation of Fis1. J Cell Physiol *209*, 468-480.

Youle, R.J., and Narendra, D.P. (2011). Mechanisms of mitophagy. Nat Rev Mol Cell Biol *12*, 9-14.

Yu, Y., Kovacevic, Z., and Richardson, D.R. (2007). Tuning cell cycle regulation with an iron key. Cell Cycle *6*, 1982-1994.

Zechner, C., Lai, L., Zechner, J.F., Geng, T., Yan, Z., Rumsey, J.W., Collia, D., Chen, Z., Wozniak, D.F., Leone, T.C., and Kelly, D.P. (2010). Total skeletal muscle PGC-1 deficiency uncouples mitochondrial derangements from fiber type determination and insulin sensitivity. Cell Metab *12*, 633-642.

Zhang, H., Gao, P., Fukuda, R., Kumar, G., Krishnamachary, B., Zeller, K.I., Dang, C.V., and Semenza, G.L. (2007). HIF-1 inhibits mitochondrial biogenesis and cellular respiration in VHL-deficient renal cell carcinoma by repression of C-MYC activity. Cancer Cell *11*, 407-420.

2.8 Figures

Figure 1. Complementary RNA and Protein Profiling of PGC-1α-Induced Mitochondrial Biogenesis

(A) Experimental workflow for proteomic and microarray analysis of differentiated C2C12 mouse myotubes overexpressing PGC-1α and/or treated with 100 μM DFO.

(B) Comparison of mRNA expression in GFP treated cells and PGC-1α treated cells (AU, arbitrary units).

(C) Changes in protein expression during PGC-1α overexpression. Proteins are ordered from least to greatest fold change.

(D) Comparison of mRNA expression in GFP treated cells and DFO treated cells (AU, arbitrary units).

(E) Comparison of PGC-1α and DFO induced changes in mRNA expression (59% of mitochondrial genes versus 18% of all genes are in the lower right quadrant, $p = 9.1 \times 10^{-222}$, χ^2 contingency test).

(F) Comparison of OxPhos mRNA and protein expression during DFO treatment.

(G) Mitochondrial mRNA and protein expression that show discordance during PGC-1α+DFO treatment.

See also Figure S1 and Table S1.

Figure 1

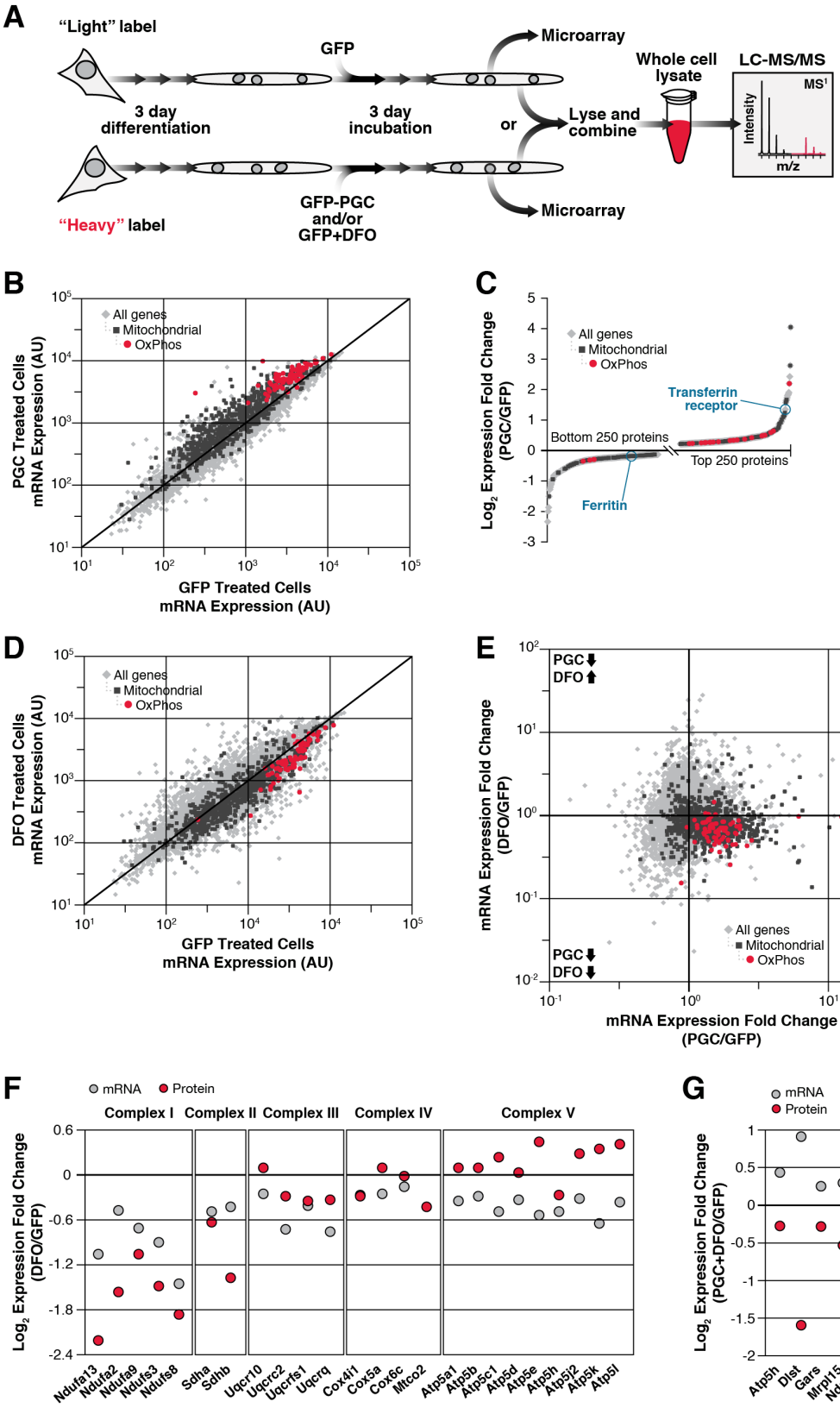
A
"Light" label
GFP
Microarray
Whole cell lysate
LC-MS/MS
3 day differentiation
3 day incubation
or
Lyse and combine
MS1
Intensity
m/z
"Heavy" label
GFP-PGC and/or GFP+DFO
Microarray
B
All genes
Mitochondrial
OxPhos
PGC Treated Cells mRNA Expression (AU)
GFP Treated Cells mRNA Expression (AU)
C
All genes
Mitochondrial
OxPhos
Transferrin receptor
Bottom 250 proteins
Top 250 proteins
Ferritin
Log2 Expression Fold Change (PGC/GFP)
D
All genes
Mitochondrial
OxPhos
DFO Treated Cells mRNA Expression (AU)
GFP Treated Cells mRNA Expression (AU)
E
PGC⬇ DFO⬆
PGC⬆ DFO⬆
PGC⬇ DFO⬇
PGC⬆ DFO⬇
All genes
Mitochondrial
OxPhos
mRNA Expression Fold Change (DFO/GFP)
mRNA Expression Fold Change (PGC/GFP)
F
mRNA
Protein
Complex I
Complex II
Complex III
Complex IV
Complex V
Log2 Expression Fold Change (DFO/GFP)
Ndufa13 Ndufa2 Ndufa9 Ndufs3 Ndufs8
Sdha Sdhb
Uqcr10 Uqcrc2 Uqcrfs1 Uqcrq
Cox4i1 Cox5a Cox6c Mtco2
Atp5a1 Atp5b Atp5c1 Atp5d Atp5e Atp5h Atp5j2 Atp5k Atp5l
G
mRNA
Protein
Log2 Expression Fold Change (PGC+DFO/GFP)
Atp5h Dlst Gars Mrpl15 Ndufa9 Ndufs3 Ndufs8 Sdhb Uqcrfs1

Figure 2. Effect of Iron Deprivation on Nuclear and mtDNA Encoded Gene Expression

(A) Level of the indicated proteins from samples used in the proteomic analyses as assessed by immunoblotting.

(B) Abundance of the indicated transcripts from samples used in the microarray analyses as detected by real-time qPCR. Data are displayed as mean ± SD of triplicate measurements (*$p < 0.05$, ANOVA with Tukey's test).

(C) Level of the indicated proteins in C2C12 myotubes after treatment with a range of DFO concentrations for 3 days as assessed by immunoblotting.

(D) Level of the indicated proteins after DFO treatment for 24 hrs in the indicated cell lines as assessed by immunoblotting.

(E) Level of the indicated proteins after DFO treatment for 24 hrs in C2C12 myoblasts as assessed by SDS-PAGE and immunoblotting.

(F) Level of the indicated proteins after DFO treatment for 24 hrs in myoblasts as assessed by blue native PAGE (BN-PAGE) and immunoblotting (SC, respiratory supercomplex; NS, non-specific band).

(G) Mitochondrial mass in myoblasts after DFO treatment for 24 hrs as assessed by plate reader based quantitation of MitoTracker Green FM or nonyl acridine orange (NAO) fluorescence/cell number. Data are displayed as mean ± SD of triplicate measurements (NS signifies $p \geq 0.05$, Student's t test).

See also Figure S2.

Figure 2

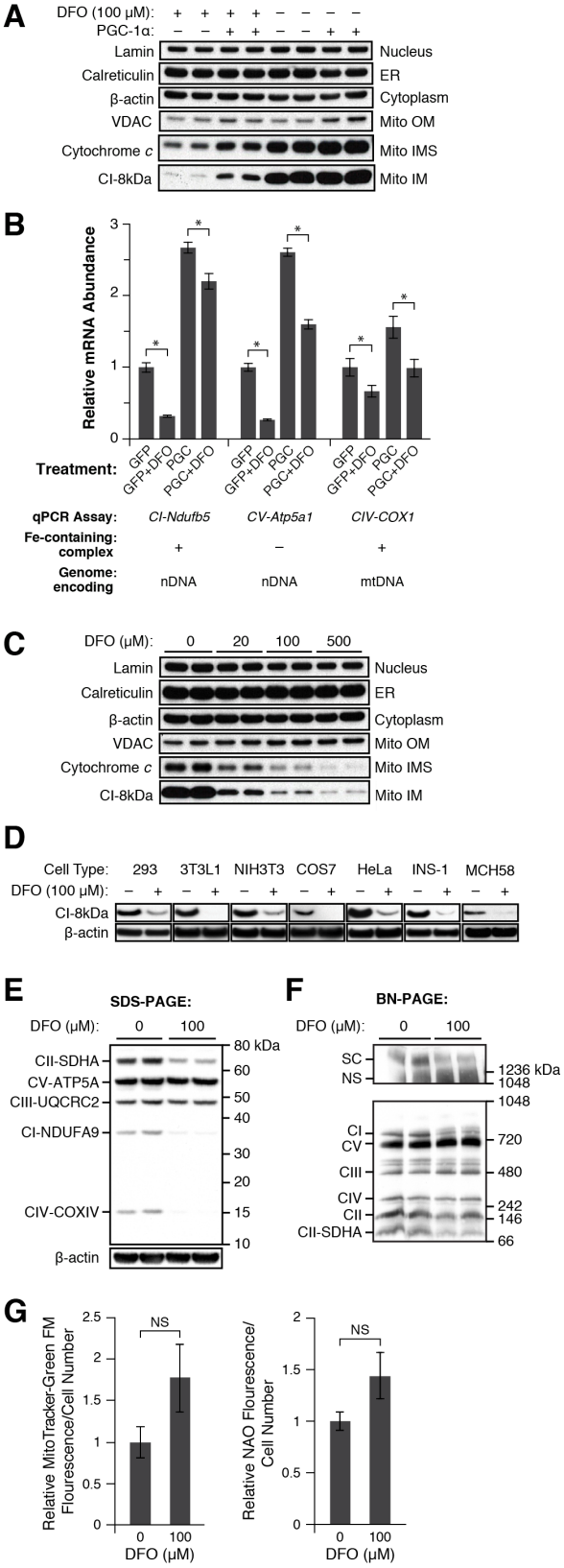
A
DFO (100 μM):
PGC-1α:
Lamin
Calreticulin
β-actin
VDAC
Cytochrome c
CI-8kDa
Nucleus
ER
Cytoplasm
Mito OM
Mito IMS
Mito IM
B
Relative mRNA Abundance
Treatment:
GFP
GFP+DFO
PGC
PGC+DFO
qPCR Assay:
CI-Ndufb5
CV-Atp5a1
CIV-COX1
Fe-containing complex
Genome encoding
nDNA
mtDNA
C
DFO (μM):
0
20
100
500
D
Cell Type:
293
3T3L1
NIH3T3
COS7
HeLa
INS-1
MCH58
E
SDS-PAGE:
CII-SDHA
CV-ATP5A
CIII-UQCRC2
CI-NDUFA9
CIV-COXIV
80 kDa
F
BN-PAGE:
SC
NS
1236 kDa
1048
CI
CV
CIII
CIV
CII
CII-SDHA
720
480
242
146
66
G
Relative MitoTracker-Green FM Flouresscence/Cell Number
Relative NAO Flouresscence/ Cell Number
NS
DFO (μM)

Figure 3. The Mitochondrial Response to Iron Deprivation is Independent of PGC-1α, PGC-1β and HIF-1α

(A-I) Immunoblotting was used to assess protein abundance and real-time qPCR was used to assess mRNA abundance. Data are displayed as mean ± SD of triplicate measurements (*$p < 0.05$, Student's t test).

(A) Protein levels in HEK 293 cells after 100 μM DFO treatment or ferroportin (Fpn-GFP) overexpression for 48 hrs. Abundance of **(B)** *Ndufs8*, **(C)** *Uqcrc1* and **(D)** *Ppargc1a* in C2C12 myoblasts following DFO treatment for the indicated times.

(E) Level of the indicated proteins in wild type or PGC-1$\alpha^{-/-}$ brown preadipocytes after 100 μM DFO treatment for 24 hrs.

(F) Abundance of *Ppargc1b* in myoblasts following DFO treatment for the indicated times.

(G) Level of the indicated proteins in wild type or PGC-1$\beta^{f/f/MLC\text{-}Cre}$ soleus muscle primary satellite cells after 100 μM DFO treatment for 24 hrs.

(H) Level of the indicated proteins after 100 μM DFO, 100 μM DP or 500 μM DMOG treatment for 24 hrs in myoblasts.

(I) Level of the indicated proteins in wild type or HIF-1$\alpha^{-/-}$ MEFs after 100 μM DFO treatment for 24 hrs.

See also Figure S3.

Figure 3

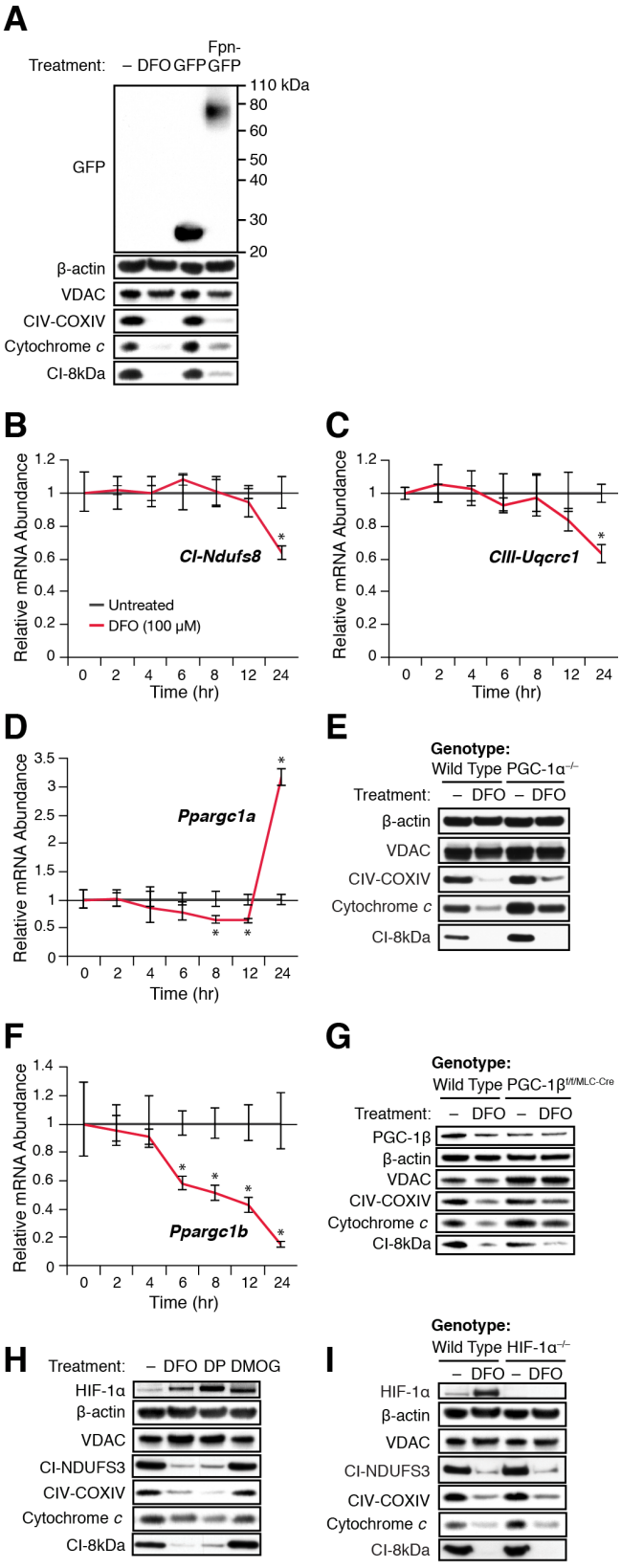
A
Treatment: – DFO GFP Fpn-GFP
110 kDa
80
60
50
40
30
20
GFP
β-actin
VDAC
CIV-COXIV
Cytochrome c
CI-8kDa
B
Relative mRNA Abundance
CI-Ndufs8
Untreated
DFO (100 μM)
Time (hr)
C
Relative mRNA Abundance
CIII-Uqcrc1
Time (hr)
D
Relative mRNA Abundance
Ppargc1a
Time (hr)
E
Genotype:
Wild Type PGC-1α−/−
Treatment: – DFO – DFO
β-actin
VDAC
CIV-COXIV
Cytochrome c
CI-8kDa
F
Relative mRNA Abundance
Ppargc1b
Time (hr)
G
Genotype:
Wild Type PGC-1βfl/fl;MLC-Cre
Treatment: – DFO – DFO
PGC-1β
β-actin
VDAC
CIV-COXIV
Cytochrome c
CI-8kDa
H
Treatment: – DFO DP DMOG
HIF-1α
β-actin
VDAC
CI-NDUFS3
CIV-COXIV
Cytochrome c
CI-8kDa
I
Genotype:
Wild Type HIF-1α−/−
– DFO – DFO
HIF-1α
β-actin
VDAC
CI-NDUFS3
CIV-COXIV
Cytochrome c
CI-8kDa

Figure 4. Mitochondrial Gene Expression and Respiratory Function during Iron Deprivation and Recovery

(A) Experimental workflow for the analysis of mitochondrial gene expression and respiration during DFO response and recovery.

(B) Level of the indicated proteins in C2C12 myoblasts treated with 100 μM DFO for 24 hrs then passaged every 24 hrs in DFO free media as assessed by immunoblotting.

(C) Mitochondrial respiratory profile of untreated myoblasts at day 1 of analysis. Data are displayed as mean ± SD of 14-16 replicates.

(D-F) Basal OCR (pMol/min)/cell number **(D)**, spare respiratory capacity **(E)** and coupling efficiency **(F)** of myoblasts treated with 100 μM DFO for 24 hrs then passaged every 24 hrs in DFO free media. Data are displayed as mean ± SD of 14-16 replicates (*$p < 0.05$, Student's t test in D, ANOVA with Tukey's test in E and F).

See also Figure S4.

Figure 4

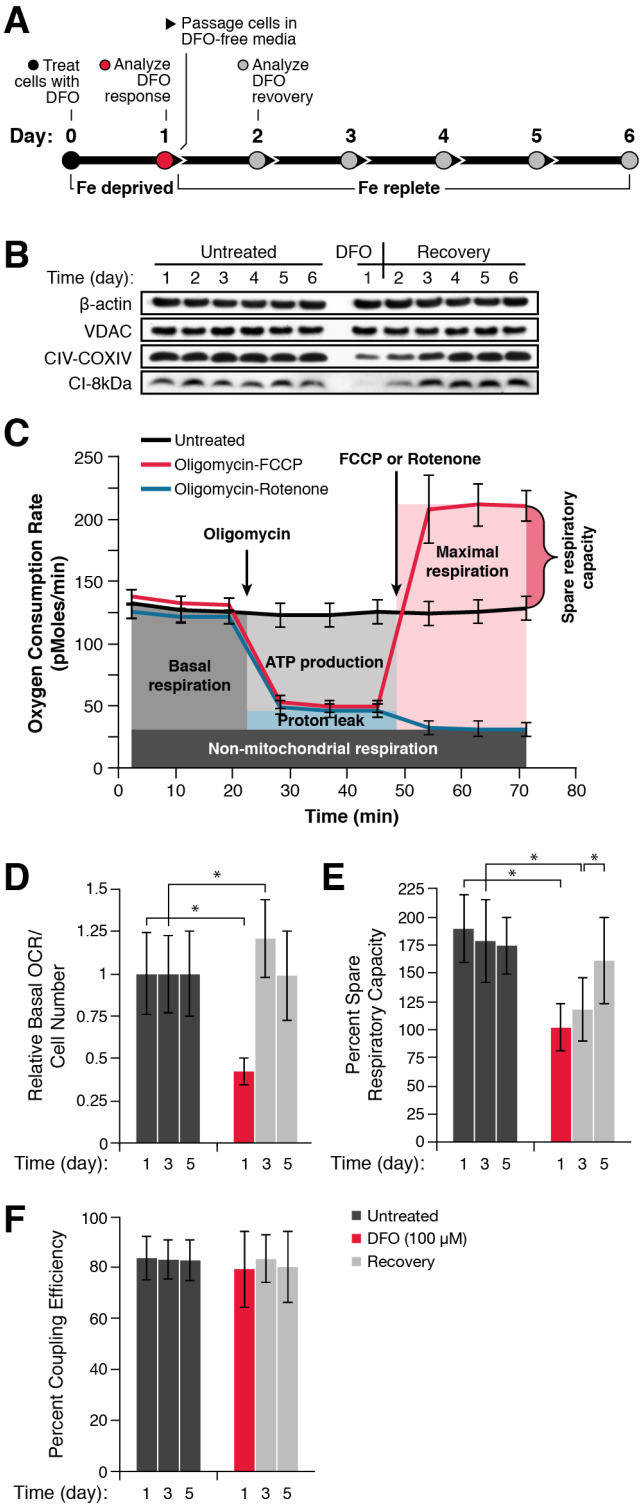
A
Passage cells in DFO-free media
Treat cells with DFO
Analyze DFO response
Analyze DFO revovery
Day: 0 1 2 3 4 5 6
Fe deprived
Fe replete
B
Untreated
DFO
Recovery
Time (day): 1 2 3 4 5 6 1 2 3 4 5 6
β-actin
VDAC
CIV-COXIV
CI-8kDa
C
Untreated
Oligomycin-FCCP
Oligomycin-Rotenone
FCCP or Rotenone
Oligomycin
Maximal respiration
Spare respiratory capacity
Basal respiration
ATP production
Proton leak
Non-mitochondrial respiration
Oxygen Consumption Rate (pMoles/min)
Time (min)
D
Relative Basal OCR/ Cell Number
Time (day): 1 3 5 1 3 5
E
Percent Spare Respiratory Capacity
Time (day): 1 3 5 1 3 5
F
Percent Coupling Efficiency
Time (day): 1 3 5 1 3 5
Untreated
DFO (100 μM)
Recovery

2.9 Supplemental Figures

Figure S1. Large-Scale Analyses of mRNA and Protein Abundance Reveal a Widespread Role for Iron in Mitochondrial Biogenesis, Related to Figure 1

(A-H) Differentiated C2C12 mouse myotubes were analyzed after 3 days of PGC-1α overexpression and/or 100 μM DFO treatment.

(A) Relationship between PGC-1α induced changes in protein and mRNA expression (all genes, $r_s = 0.41$, $p = 5.7 \times 10^{-52}$; mitochondrial genes, $r_s = 0.53$, $p = 1.9 \times 10^{-30}$; Spearman's rank correlation test). **(B)** Changes in OxPhos mRNAs and proteins showing discordance in expression during PGC-1α overexpression.

(C) Comparison of PGC-1α and DFO induced changes in protein expression (50% of mitochondrial proteins versus 27% of all proteins are in the lower right quadrant, $p = 2.2 \times 10^{-6}$, χ^2 contingency test). **(D)** Relationship between DFO induced changes in protein and mRNA expression (all genes, $r_s = 0.58$, $p = 8.8 \times 10^{-35}$; mitochondrial genes, $r_s = 0.58$, $p = 2.5 \times 10^{-9}$; Spearman's rank correlation test). **(E)** Comparison of mRNA expression in GFP treated cells and PGC-1α+DFO treated cells (AU, arbitrary units).

(F) Comparison of the average PGC-1α, PGC-1α+DFO and DFO induced changes in transcript levels for the indicated groups. Data are displayed as mean ± SEM. **(G)** Relationship between PGC-1α+DFO induced changes in protein and mRNA expression (all genes, $r_s = 0.54$, $p = 6.8 \times 10^{-29}$; mitochondrial genes, $r_s = 0.60$, $p = 4.4 \times 10^{-10}$; Spearman's rank correlation test).

(H) Comparison of average DFO induced changes to transcript and protein levels for the indicated groups. The sample size (n) is indicated. Data are displayed as mean ± SEM.

Figure S1

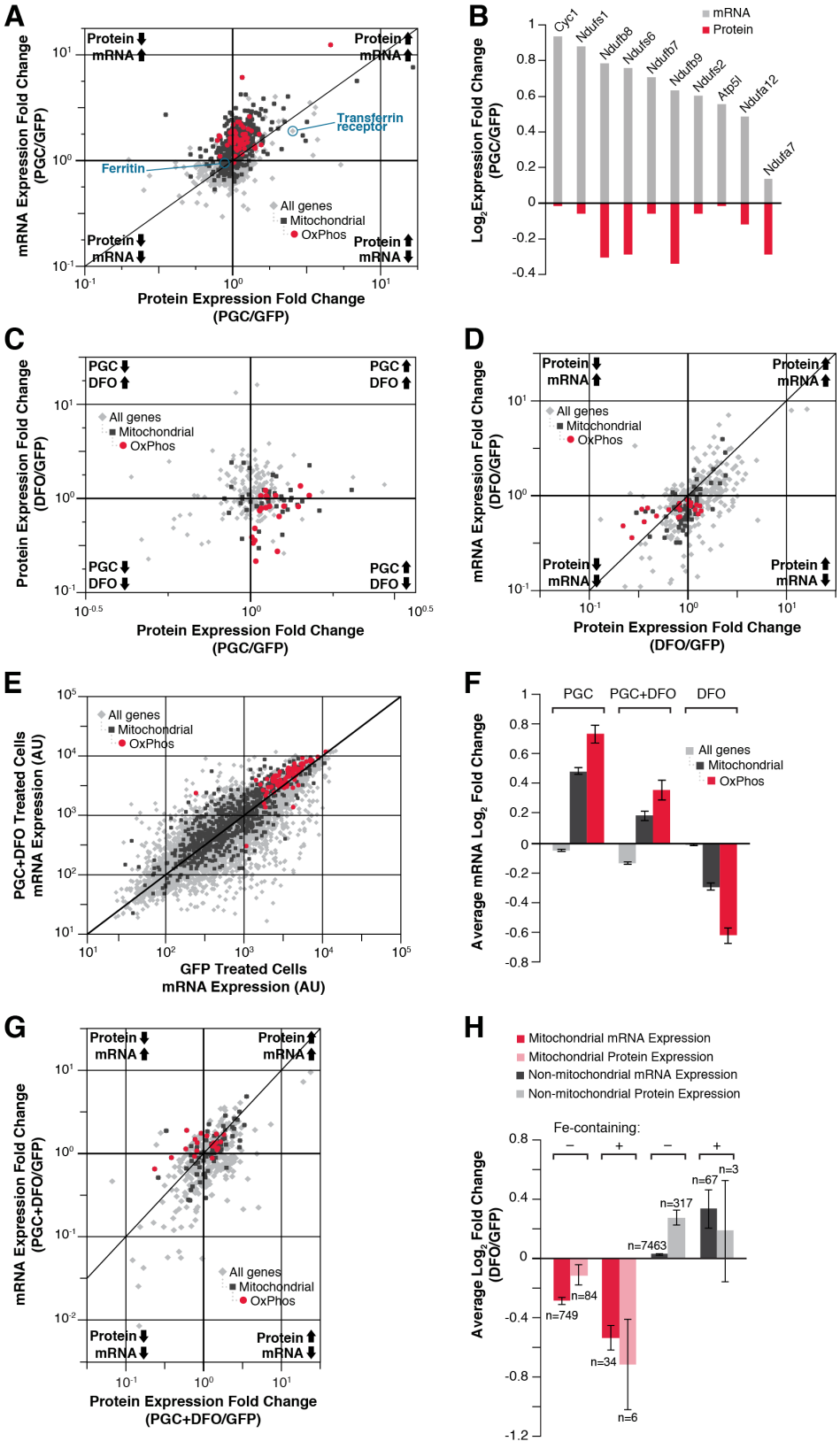
A
Protein ⬇ mRNA ⬆
Protein ⬆ mRNA ⬆
Protein ⬇ mRNA ⬇
Protein ⬆ mRNA ⬇
Transferrin receptor
Ferritin
All genes
Mitochondrial
OxPhos
mRNA Expression Fold Change (PGC/GFP)
Protein Expression Fold Change (PGC/GFP)
B
mRNA
Protein
Cyc1
Ndufs1
Ndufb8
Ndufs6
Ndufb7
Ndufb9
Ndufs2
Atp5l
Ndufa12
Ndufa7
Log2Expression Fold Change (PGC/GFP)
C
PGC ⬇ DFO ⬆
PGC ⬆ DFO ⬆
PGC ⬇ DFO ⬇
PGC ⬆ DFO ⬇
All genes
Mitochondrial
OxPhos
Protein Expression Fold Change (DFO/GFP)
Protein Expression Fold Change (PGC/GFP)
D
Protein ⬇ mRNA ⬆
Protein ⬆ mRNA ⬆
Protein ⬇ mRNA ⬇
Protein ⬆ mRNA ⬇
All genes
Mitochondrial
OxPhos
mRNA Expression Fold Change (DFO/GFP)
Protein Expression Fold Change (DFO/GFP)
E
All genes
Mitochondrial
OxPhos
PGC+DFO Treated Cells mRNA Expression (AU)
GFP Treated Cells mRNA Expression (AU)
F
PGC
PGC+DFO
DFO
All genes
Mitochondrial
OxPhos
Average mRNA Log2 Fold Change
G
Protein ⬇ mRNA ⬆
Protein ⬆ mRNA ⬆
Protein ⬇ mRNA ⬇
Protein ⬆ mRNA ⬇
All genes
Mitochondrial
OxPhos
mRNA Expression Fold Change (PGC+DFO/GFP)
Protein Expression Fold Change (PGC+DFO/GFP)
H
Mitochondrial mRNA Expression
Mitochondrial Protein Expression
Non-mitochondrial mRNA Expression
Non-mitochondrial Protein Expression
Fe-containing:
n=749
n=84
n=34
n=6
n=7463
n=317
n=67
n=3
Average Log2 Fold Change (DFO/GFP)

Figure S2. Iron Chelation Causes a Specific Remodeling of Mitochondrial Content, Related to Figure 2

(A) Level of the indicated proteins after DFO treatment for the indicated times in C2C12 myotubes and myoblasts as assessed by immunoblotting.

(B) MitoTracker Red CMXRos staining of live MCH58 cells treated with the indicated concentrations of DFO for 24 hrs (three replicates per DFO concentration are shown).

Figure S2

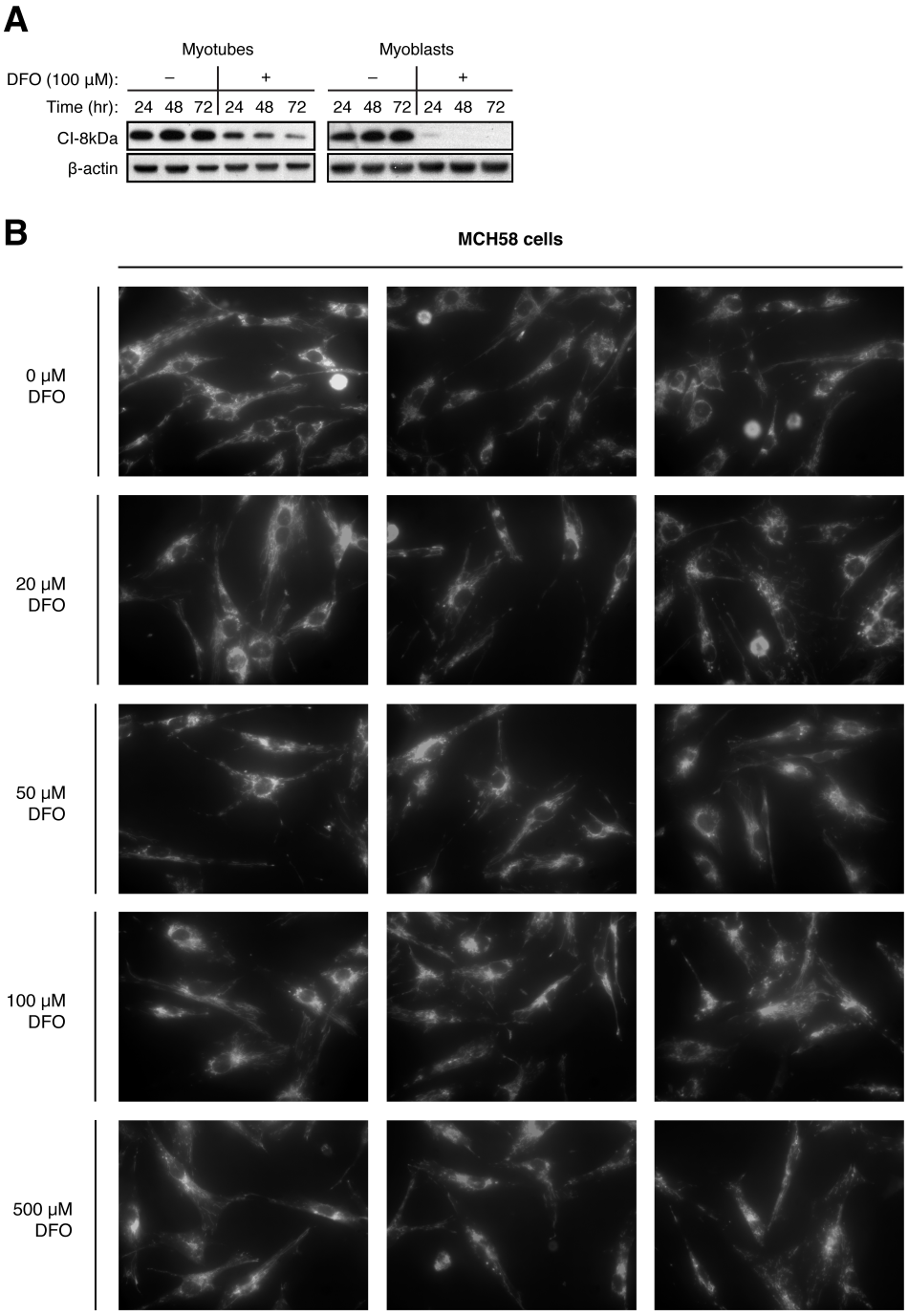
A
Myotubes
Myoblasts
DFO (100 μM):
–
+
–
+
Time (hr):
24 48 72 24 48 72 24 48 72 24 48 72
CI-8kDa
β-actin
B
MCH58 cells
0 μM DFO
20 μM DFO
50 μM DFO
100 μM DFO
500 μM DFO

Figure S3. Time Course Expression Analysis of Mitochondrial Genes, Mitochondrial Biogenesis-Related Transcription Factors and Coactivators during Iron Deprivation, Related to Figure 3

(A) Ferritin protein abundance/total protein abundance in HEK 293 cells after 100 μM DFO treatment or ferroportin (Fpn-GFP) overexpression for 48 hrs as determined by ELISA. Data are displayed as mean ± SD of triplicate measurements (*$p < 0.05$, ANOVA with Tukey's test).

(B) Level of the indicated proteins in C2C12 myoblasts following DFO treatment for the indicated times as assessed by immunoblotting.

(C) Abundance of *Tfrc*, *Esrra*, *Nrf1,* and *Gabpa* in myoblasts following DFO treatment for the indicated times as assessed by real-time qPCR. Data are displayed as mean ± SD of triplicate measurements (*$p < 0.05$, Student's t test).

Figure S3

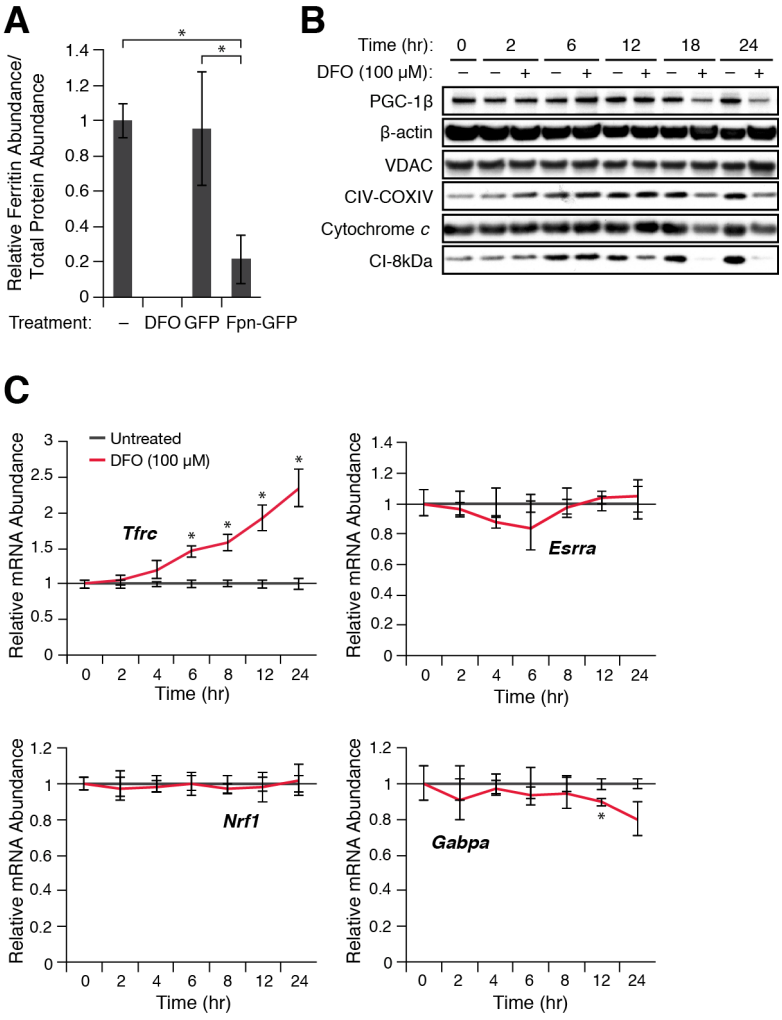
A
Relative Ferritin Abundance/ Total Protein Abundance
Treatment: – DFO GFP Fpn-GFP
B
Time (hr): 0 2 6 12 18 24
DFO (100 μM): – – + – + – + – + – +
PGC-1β
β-actin
VDAC
CIV-COXIV
Cytochrome c
CI-8kDa
C
Untreated
DFO (100 μM)
Tfrc
Esrra
Nrf1
Gabpa
Relative mRNA Abundance
Time (hr)

Figure S4. Iron Deprivation Causes a Universal and Reversible Reduction in Mitochondrial Protein Levels and Respiratory Function, Related to Figure 4

(A) Abundance of *Ndufs8* and *Tfrc* in C2C12 myoblasts during DFO response and recovery as assessed by real-time qPCR. Data are displayed as mean ± SD of triplicate measurements (*$p < 0.05$, Student's t test).

(B) Mitochondrial respiratory profiles of myoblasts treated with DFO for 24 hrs then passaged every 24 hrs in DFO free media. OCR was measured after 24 hrs of DFO treatment (day 1), then 48 hrs (day 3) and 96 hrs (day 5) following the passage of DFO treated myoblasts into DFO-free media. Data are displayed as mean ± SD of 14-16 replicates. Spare respiratory capacity was calculated by dividing the maximal rate after FCCP injection by the basal rate (third basal measurement before the first injection) with the minimal rate after the rotenone injection subtracted from each of these rates. Coupling efficiency was calculated as 1 minus the quotient of the minimal rate after oligomycin injection divided by the basal rate with the minimal rate after the rotenone injection subtracted from each of these rates.

Figure S4

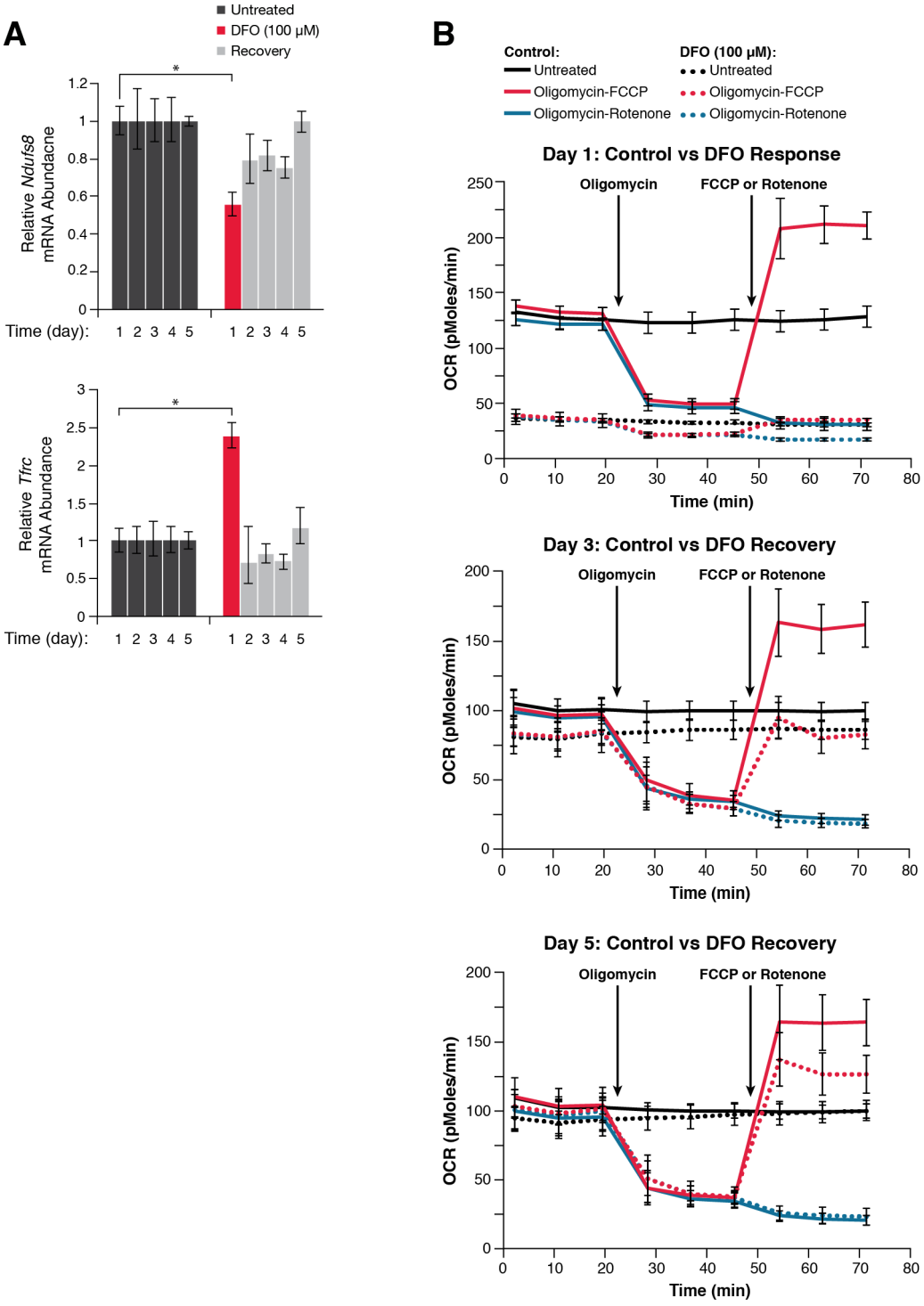
A
Untreated
DFO (100 μM)
Recovery
Relative Ndufs8 mRNA Abundance
Time (day): 1 2 3 4 5 1 2 3 4 5
Relative Tfrc mRNA Abundance
Time (day): 1 2 3 4 5 1 2 3 4 5
B
Control:
Untreated
Oligomycin-FCCP
Oligomycin-Rotenone
DFO (100 μM):
Untreated
Oligomycin-FCCP
Oligomycin-Rotenone
Day 1: Control vs DFO Response
Day 3: Control vs DFO Recovery
Day 5: Control vs DFO Recovery
Oligomycin
FCCP or Rotenone
OCR (pMoles/min)
Time (min)

2.10 Supplemental Tables

Table S1. Top 58 nuclear-Encoded Mitochondrial mRNAs/Proteins Showing Discordance during PGC-1α Overexpression in C2C12 Mouse Myotubes, Related to Figure 1

Entrez Gene	Gene Symbol	SILAC PGC/GFP	Microarray PGC/GFP	Mircoarray/ SILAC	OxPhos	Iron-Binding
73724	Mcee	0.35	2.72	7.71	0	0
67308	Mrpl46	0.96	2.84	2.96	0	0
217707	Coq6	0.89	2.56	2.87	0	0
232536	Mrps35	0.99	2.72	2.76	0	0
108841	Rdh13	0.93	2.38	2.54	0	0
118451	Mrps2	0.99	2.44	2.47	0	0
27395	Mrpl15	0.91	2.22	2.43	0	0
213012	Abhd10	0.88	2.14	2.42	0	0
20917	Suclg2	0.52	1.15	2.21	0	0
68971	1500001M20Rik	0.72	1.58	2.19	0	0
57312	Mrps31	0.60	1.30	2.16	0	0
67264	Ndufb8	0.81	1.72	2.14	1	0
407785	Ndufs6	0.82	1.69	2.06	1	0
228026	Pdk1	0.94	1.92	2.04	0	0
66821	Bcs1l	0.96	1.94	2.03	0	0
319518	4930402E16Rik	0.99	2.01	2.03	0	0
66525	Timm50	0.90	1.81	2.00	0	0
66218	Ndufb9	0.79	1.55	1.98	1	0
66445	Cyc1	0.99	1.91	1.93	1	1
79464	Lias	0.83	1.59	1.93	0	1
66163	Mrpl4	1.00	1.92	1.93	0	0
12894	Cpt1a	0.98	1.88	1.91	0	0
227197	Ndufs1	0.96	1.84	1.91	1	1
59054	Mrps30	0.99	1.89	1.91	0	0
73694	2410091C18Rik	0.66	1.24	1.89	0	0
56280	Mrpl37	0.93	1.72	1.85	0	0
110821	Pcca	0.74	1.36	1.85	0	0
60441	Mrpl38	0.98	1.82	1.84	0	0
104776	Aldh6a1	0.61	1.09	1.80	0	0
66399	Tsfm	0.95	1.67	1.76	0	0
68537	Mrpl13	0.98	1.70	1.74	0	0
94061	Mrpl1	1.00	1.74	1.74	0	0
12896	Cpt2	0.98	1.68	1.72	0	0
12257	Bzrp	0.85	1.46	1.71	0	0
66916	Ndufb7	0.96	1.63	1.70	1	0

229211	Acad9	0.85	1.45	1.69	0	0
216821	Tmem11	0.90	1.52	1.69	0	0
230935	Dnajc11	0.93	1.55	1.66	0	0
217830	9030617O03Rik	0.80	1.32	1.64	0	0
70047	Trnt1	0.99	1.58	1.60	0	0
52538	Acaa2	0.94	1.51	1.60	0	0
76784	Mtif2	0.99	1.56	1.58	0	0
226646	Ndufs2	0.96	1.52	1.58	1	1
66701	Spryd4	0.91	1.43	1.57	0	0
72039	Mccc1	0.79	1.24	1.57	0	0
99045	Mrps26	0.84	1.29	1.54	0	0
68572	Ict1	0.97	1.49	1.54	0	0
69029	1500032L24Rik	0.86	1.32	1.54	0	0
94063	Mrpl16	0.78	1.19	1.53	0	0
66414	Ndufa12	0.92	1.40	1.52	1	0
69527	Mrps9	0.98	1.49	1.51	0	0
68165	B230118G17Rik	0.88	1.33	1.51	0	1
108147	Atic	1.03	0.69	0.67	0	0
28200	Dhrs4	1.08	0.72	0.67	0	0
216188	Aldh1l2	1.06	0.70	0.66	0	0
14467	Gbas	1.15	0.74	0.64	0	0
56748	Hirip5	1.32	0.83	0.63	0	1
20655	Sod1	1.03	0.63	0.62	0	0

Differentiated myotubes were analyzed after 3 days of PGC-1α overexpression. Nuclear-encoded mitochondrial mRNAs/proteins showing discordance in expression fold change (PGC-1α/GFP) are displayed. Oxidative phosphorylation (OxPhos) and iron-binding proteins are indicated. SILAC, stable isotope labeling by amino acids in cell culture; PGC, peroxisome proliferator-activated receptor gamma, coactivator 1 alpha; GFP, green fluorescent protein.

2.11 Extended Experimental Procedures

2.11.1 Myotube Differentiation and Metabolic Labeling

C2C12 mouse myoblasts were grown to near confluence then switched to media containing 2% dialyzed FBS (Invitrogen). During differentiation, cells were metabolically labeled using established methods (Ong et al., 2002; Ong and Mann, 2006). Briefly, cells were grown in Lys and Arg dropout medium supplemented with $^{12}C_6$-Lys and $^{12}C_6$-Arg or $^{13}C_6$-Lys and $^{13}C_6$-Arg, and after 3 days of differentiation, cells were infected with an adenovirus expressing either green fluorescent protein (GFP) or GFP tagged PGC-1α (GFP-PGC-1α) as previously described (Wu et al., 1999). Alternatively, cells were labeled with $^{12}C_6$-Lys and $^{12}C_6$,$^{14}N_4$-Arg, $^{12}C_6$-Lys and $^{13}C_6$,$^{14}N_4$-Arg or $^{12}C_6$-Lys and $^{13}C_6$,$^{15}N_4$-Arg, and after 3 days were infected with an adenovirus expressing GFP or GFP-PGC-1α ± DFO treatment as indicated. Three days following infection, cells were washed with PBS and processed for microarray or protein mass spectrometry. Experiments were performed in biological duplicate.

2.11.2 Primary Mouse Satellite Cell Media Formulation

80% Ham's F-10 Nutrient Mix (Invitrogen)

20% FBS (Invitrogen)

1 × GlutaMAX (Invitrogen)

2.5 ng/mL FGF-basic, human (added fresh to 50 mL aliquot) (Sigma-Aldrich)

10 ng/mL EGF, human (Sigma-Aldrich)

1 μg/mL insulin (Sigma-Aldrich)

0.5 mg/mL fetuin (added fresh to 50 mL aliquot) (Sigma-Aldrich)

0.4 μg/mL dexamethasone (Sigma-Aldrich)

1 × Antibiotic/Antimycotic (Invitrogen)

2.11.3 Mass Spectrometry

100 μg of protein lysate from each SILAC state was combined and resolved on 1D-SDS-PAGE (Nupage, Invitrogen). Gel lanes were cut into nine (GFP vs. GFP-PGC-1a) or ten (triple encoding SILAC GPF vs. GFP-PGC-1α ± DFO) slices. The gel slices from the latter group were acetylated in-gel (Thevis et al., 2003) before trypsin digestion to minimize trypsin digestion after lysine residues and improve SILAC-Arg quantification. Proteins were digested with a standard in-gel trypsin digestion protocol (Ong and Mann, 2006). Peptides were desalted off-line with C18 StageTips (Rappsilber et al., 2007) and analyzed with nanoESI-LC-MS using an Agilent 1100 (Santa Clara, CA) nanoflow pump and LTQ-Orbitrap (Thermo, Bremen). Peptides were separated on a C18 reversed phase column measuring 75 μm by 10 cm column with a 15 μ tip pulled in-house with a P2000 laser puller (Sutter, Novato CA) and packed with 3 μm Reprosil C18-aq beads (Dr. Maisch, Germany). Solvents A and B were 0.1% formic acid (Fluka, Germany) in water (HPLC grade, J.T. Baker) and 0.1% formic acid in 90% acetonitrile and 10%

water, respectively. Peptides were eluted with a 90 min gradient of increasing acetonitrile (5% to 40% B) and analyzed with a data-dependent experiment selecting Top 3 most intense precursors for a CID MS/MS experiment in the linear ion trap. Raw files were processed for protein identification and SILAC quantification using MaxQuant ver. 1.2.0.18 with the appropriate SILAC mass modifications. The IPI mouse FASTA ver. 3.68 database plus common contaminants (MaxQuant) was used for database search with fixed modifications of carbamidomethylated cysteines and variable modifications of oxidized methionines, acetylated protein N-termini and lysines. Peptides containing up to two missed cleavages and a maximum of three SILAC labels per peptide were considered. Peptide mass tolerances were 20 ppm at the MS precursor level and 0.5 Da for MS/MS peptide data. Protein and peptide FDR rates were 1% and a minimum of 2 quantified peptides for each protein ratio was required.

2.11.4 Analysis of Mitochondrial Morphology

Following DFO treatment, mitochondrial morphology was analyzed in live MCH58 cells stained with 100 nM MitoTracker Red CMXRos (Invitrogen) for 30 min at 37°C and 5% CO_2. The stained cells were observed at 60× magnification with an Olympus IX81 microscope and fluorescent images were captured with a Hamamatsu C4742-95-12G04 digital camera.

2.11.5 Primers used for SYBR Green Real-Time qPCR

SYBR green primers were designed using the Roche Universal ProbeLibrary Assay Design Center tool.

Rplp0:

Left: actggtctaggacccgagaag Right: tcccaccttgtctccagtct

Tfrc:

Left: tcctttccttgcatattctgg Right: ccaaataaggatagtctgcatcc

Ppargc1b:

Left: gacgtggacgagctttcact Right: gagcgtcagagcttgctgtt

Ppargc1a:

Left: gaaagggccaaacagagaga Right: gtaaatcacacggcgctctt

Ndufs8:

Left: ttgcctgcaaactctgtgag Right: catcggctcttggctcag

2.11.6 Lysis Buffer Compositions

For immunoblotting, protein lysates were prepared in RIPA buffer composed of 150 mM NaCl, 1% IGEPAL CA-630, 0.5% sodium deoxycholate, 0.1% SDS, 50 mM Tris (pH 8.0), 0.4 mM EDTA (pH 8.0), 10% glycerol and a protease inhibitor cocktail (Roche Diagnostics).
For ferroportin experiments, the lysis buffer consisted of 150 mM NaCl, 1% Triton X-100, 10 mM Tris (pH 7.4), 10 mM EDTA (pH 8.0) and a protease inhibitor cocktail (Roche Diagnostics).

2.11.7 Primary Antibodies used for Immunoblotting

Antigen	**Host**	**Dilution**	**Supplier**
β-actin	Mouse	1:10,000	Sigma-Aldrich
Calreticulin	Rabbit	1:1,000	Cell Signaling Technology
CI subunit 8kDa	Mouse	1:1,000	MitoSciences
COXIV	Mouse	1:2,000	MitoSciences
Cytochrome c	Mouse	1:8,000	MitoSciences

GFP	Mouse	1:1,000	Santa Cruz Biotechnology
Lamin A	Mouse	1:500	Abcam
NDUFS3	Mouse	1:1,000	MitoSciences
PGC-1β	Rabbit	1:500	Sigma-Aldrich
TFRC	Mouse	1:1,000	Invitrogen
VDAC	Rabbit	1:8,000	Abcam

2.11.8 Post Assay Cell Quantitation

Cell number was quantified post-MitoTracker quantitation and XF analysis by crystal violet staining as previously described. (Kueng et al., 1989). Briefly, cells were fixed with 10 µL of 11% glutaraldehyde added to 100 µL of medium. Following a 15-min incubation, the plates were washed by submersion in diH_2O, air-dried and stained with 100 µL of 0.1% crystal violet. After a 20-min incubation, the plates were washed to remove excess dye and were air-dried. Bound dye was solubilized with 100 µL of 10% acetic acid and the absorbance was measured at 590 nm using a BioTek Synergy 2 Microplate Reader.

2.12 Supplemental References

Kueng, W., Silber, E., and Eppenberger, U. (1989). Quantification of cells cultured on 96-well plates. Anal Biochem *182*, 16-19.

Ong, S.E., Blagoev, B., Kratchmarova, I., Kristensen, D.B., Steen, H., Pandey, A., and Mann, M. (2002). Stable isotope labeling by amino acids in cell culture, SILAC, as a simple and accurate approach to expression proteomics. Mol Cell Proteomics *1*, 376-386.

Rappsilber, J., Mann, M., and Ishihama, Y. (2007). Protocol for micro-purification, enrichment, pre-fractionation and storage of peptides for proteomics using StageTips. Nat Protoc *2*, 1896-1906.

Thevis, M., Ogorzalek Loo, R.R., and Loo, J.A. (2003). In-gel derivatization of proteins for cysteine-specific cleavages and their analysis by mass spectrometry. J Proteome Res *2*, 163-172.

CHAPTER THREE: Iron Deprivation Induces Epigenetic Regulation of Mitochondrial Biogenesis

The following people contributed to this chapter:

Jarred W. Rensvold, Kimberly A. Krautkramer, James A. Dowell, Sheila A. Anderson, Richard S. Eisenstein, John M. Denu and David J. Pagliarini

Sections of this chapter are in preparation for publication.

3.1 Summary

Mitochondrial biogenesis responds to changes in cellular metabolism and nutrient availability. We recently described an adaptive mitochondrial biogenesis response to cellular iron deprivation. To determine the mechanism of this response, we used a combination of unbiased, large-scale approaches and hypothesis-driven experiments. Utilizing an RNA labeling approach we determined that the decrease in transcripts encoding mitochondrial proteins is due to a decrease in transcription and not due to increased transcript degradation. We also find that the decrease in mitochondrial proteins precedes this transcriptional dampening. Additionally, we explored the role of the major mitochondrial quality control proteases and mTOR in this response. Moreover, we show that iron deprivation-induced transcriptional changes are accompanied by changes in histone acetylation and methylation, and that the effect of iron deprivation on histone acetylation and nuclear-encoded mitochondrial transcript levels is blocked with HDAC inhibition, consistent with histone PTM regulation of gene expression. Finally, we show that the effect of iron deprivation on mitochondrial transcripts and proteins is mostly conserved in a mouse model of iron deficiency. Altogether, our investigations provide a system for understanding how nutrient deprivation can induce epigenetic control of mitochondrial biogenesis.

3.2 Introduction

Cells must adapt to varying environmental conditions, including changes in the availability of nutrients. In particular, mechanisms controlling mitochondrial content and function, including mitochondrial biogenesis, dynamics and quality control, are essential for maintaining cellular homeostasis (Chan, 2012; Friedman and Nunnari, 2014; MacAskill and

Kittler, 2010; Quiros et al., 2015; Scarpulla, 2012; Stotland and Gottlieb, 2015; Vega et al., 2015; Youle and Narendra, 2011). Mitochondrial biogenesis involves the coordinated expression of approximately 1200 proteins encoded from two genomes—nuclear and mitochondrial DNA (Dominy and Puigserver, 2013; Harbauer et al., 2014; Mick et al., 2011; Pagliarini et al., 2008; Scarpulla, 2008; Schmidt et al., 2010). Dysfunctions in mitochondrial biogenesis are associated with a broad range of human diseases, including a number of mitochondrial myopathies (characterized by a proliferation of abnormal mitochondria in muscle resulting in ragged-red fibers), diabetes, cancer and age-related disorder as well as the aging process itself (Calvo and Mootha, 2010; DiMauro and Schon, 2003; Lowell and Shulman, 2005; Nunnari and Suomalainen, 2012; Vafai and Mootha, 2012; Wallace, 1999, 2005). Although important advances have been made in understanding the signals and transcriptional networks that induce mitochondrial biogenesis, many basic features of this process remain obscure. These include epigenetic and post-transcriptional mechanisms that control mitochondrial biogenesis, signals that coordinate gene expression between mitochondria and the nucleus, and states that result in decreased mitochondrial production (Goldenthal and Marin-Garcia, 2004; Hock and Kralli, 2009; Mouchiroud et al., 2014; Wallace and Fan, 2010). Importantly, connecting the disease states and nutritional signals that cause mitochondrial dysfunction to mechanisms of mitochondrial adaptation will offer insight into possible therapeutic interventions and treatments.

Iron is among the most prevalent elements in nature (Frey and Reed, 2012; Sheftel et al., 2012). Its ubiquity is especially apparent in mitochondria, where it can be stored or transformed into cofactors such as heme and iron-sulfur (Fe-S) clusters for use in oxidation-reduction reactions within mitochondria (Lane et al., 2015; Richardson et al., 2010; Rouault and Tong, 2005), including the tricarboxylic acid (TCA) cycle and oxidative phosphorylation (OxPhos),

and throughout the cell (Netz et al., 2014; Rouault, 2015a). Throughout the past 60+ years, studies using rat models of iron deficiency have shown that iron deprivation causes a decrease in select mitochondrial proteins, mitochondrial oxygen consumption and activity of the respiratory complexes as well as changes in mitochondrial morphology in a variety of tissues (Cartier et al., 1986; Dallman, 1986; Dallman and Goodman, 1970). Iron deficiency is the #1 nutritional disorder worldwide and iron deficiency contributes to many common diseases (McLean et al., 2009), however, apart from several reports of increased mitochondrial specific autophagy (mitophagy) in cultured mammalian cells under high concentrations of iron chelator (Allen et al., 2013) or during long term iron deprivation in the nematode *Caenorhabditis elegans* (Kirienko et al., 2015; Schiavi et al., 2015), regulation of select mitochondrial transcripts via iron responsive elements (IREs) (Eisenstein and Ross, 2003), and possible regulation of mitochondrial dynamics (Yoon et al., 2006), little is known about the molecular mechanisms that drive these well-known mitochondrial adaptations to iron depletion.

Through a combination of large-scale microarray and mass spectrometry-based proteomic analyses, we recently discovered that iron deprivation initiates a global, adaptive mitochondrial biogenesis response in mammalian cells (Rensvold et al., 2013). Specifically, iron depletion, through chelation or active transport, caused a rapid and reversible decrease in the abundance of nuclear DNA- and mitochondrial DNA-encoded mitochondrial transcripts and proteins, that was equal and opposite to the transcriptional coactivator PGC-1α, a well-described and potent activator of mitochondrial biogenesis. This response to iron deprivation was dose-dependent, universal across a broad range of cell types and independent of well-established regulators of mitochondrial biogenesis, including PGC-1α and HIF-1α.

Here, we employ biochemical, proteomic and pharmacological approaches to investigate the mechanism by which iron deprivation causes the rapid and coordinate loss of mitochondrial gene expression in skeletal muscle cells. Utilizing an RNA labeling approach we determine that the decrease in transcripts is due to a decrease in the synthesis of new transcripts and not due to increased transcript turnover. We also find that the decrease in mitochondrial function and proteins precedes this transcriptional dampening, perhaps suggesting a mitochondrial retrograde response. Further, we show that iron chelation causes a decrease in histone acetylation at nuclear DNA-encoded mitochondrial genes and that the effect of iron chelation on transcript levels is fully reversed with histone deacetylase (HDAC) inhibition, consistent with epigenetic regulation of mitochondrial biogenesis.

3.3 Results and Discussion

3.3.1 Matched Timecourse Analyses Reveal Discordance in Mitochondrial Transcript and Protein Levels in Response to Iron Deprivation

Iron deprivation initiates an adaptive cellular response involving a decrease in mitochondrial transcript and protein levels. Our previous large-scale, complementary mRNA and protein profiling analyses revealed that subunits of the OxPhos complexes were strongly affected by iron deprivation with mRNA and protein measurements being generally similar in direction and magnitude of change (Rensvold et al., 2013). However, we noted some differences. Complex I and complex II had protein levels that were more decreased than their mRNA levels. Conversely, complex V proteins were increased or unchanged whereas their transcripts were decreased.

To investigate these differences more extensively, we performed detailed timecourse measurements of nuclear-encoded OxPhos proteins and their corresponding transcripts using real-time quantitative PCR (qPCR) and immunoblotting, respectively, as well as measurements of cellular metabolic activity, including cellular oxygen consumption rate (OCR), an indicator of mitochondrial respiration, and extracellular acidification rate (ECAR), an indicator of glycolytic activity (Figure 1, S1). We tracked the abundance of at least one subunit from each complex starting at 8-10 hours through 24 hours following treatment with the iron chelator deferoxamine (DFO). From these timecourse analyses, we find that for some subunits, including those from both complex I and complex II, that protein levels dropped before their matching transcript (Figure 1A, S1A, S1B). For other subunits, including complex III and complex V, we observed no change in protein abundance while their transcripts were decreased (Figure 1B, S1A). Conversely, for complex IV, protein levels were drastically decreased but transcripts were unchanged (Figure 1C, S1A). Interestingly, the OCR/ECAR ratio, a measure of cellular reliance on respiration compared to glycolysis, changes before both transcripts and proteins following iron chelation (Figure 1D, S1C). For the complexes that had decreases in protein levels that preceded their transcripts or that had no change in transcripts, regulation of translation or protein degradation is likely contributing to the observed changes. Altogether, the discordance in the levels and timing of the changes in mitochondrial transcripts, proteins and cellular metabolic activity suggests either that iron deprivation has independent effects on transcripts and on proteins *or* that iron deprivation affects mitochondrial function and proteins first, and this results in the transcript changes, which could occur through mitochondrial to nuclear (retrograde) signaling.

3.3.2 Iron Deprivation Decreases Transcription of Nuclear DNA-Encoded Mitochondrial Genes

Iron depletion results in a rapid loss of nuclear DNA-encoded mitochondrial transcripts, proteins and oxidative capacity. Our timecourse analyses show that the decrease in mitochondrial proteins precedes the decrease in their corresponding transcripts, suggesting that this effect involves regulation of gene expression at multiple levels. To determine whether the decrease in mitochondrial transcripts was due to a decrease in transcript synthesis or an increase in transcript degradation we performed detailed RNA pulse-chase and pulse labeling timecourse analyses (Figure 2, S2). For the RNA label, we chose the uridine analog 5-ethynyluridine (EU) (Jao and Salic, 2008), a non-toxic, widely used, rapid and specific ribonucleotide label that is incorporated into cellular RNA (but not DNA) and has virtually no effect on the global transcriptome. EU contains an alkyne group that following isolation of total cellular RNA is reacted with a biotin azide via click-chemistry and is then captured using strepavidin coated magnetic beads. Complementary DNA (cDNA) synthesized from the captured RNA is detected using real-time qPCR. For our pulse-chase analysis, we first labeled cellular RNA for 18 hours then after replacing the EU-containing cell culture media with EU-free media, treated the cells +/−DFO and collected several time points following treatment (Figure 2A, S2A). We found that DFO did not increase the decay rate of the labeled mRNA for any of our mitochondrial markers but did increase the half-life of transferrin receptor mRNA (*Tfrc*) (Figure 2B), a transcript that is known to be stabilized during iron deprivation (Anderson et al., 2012; Ponka and Lok, 1999). DFO also did not change the decay rate of *Rplp0* (Figure S2A), the endogenous control used in our relative quantitation (RQ) real-time qPCR analyses. Importantly, the half-lives of OxPhos transcripts determined from our analyses are similar to those from a global analysis of transcript turnover (Figure S2B) (Schwanhausser et al., 2011).

To test if iron deprivation causes a decrease in the synthesis of mitochondrial transcripts, we treated cells +/−DFO, then 2 hours prior to collecting each time point, we added the EU label so that it is incorporated only into new transcripts made during that time and so that degradation has little to no effect on transcript abundance (Figure 2C). From this analysis, we discovered that iron deprivation decreases the incorporation of the EU label into all of the nuclear-encoded OxPhos mRNAs measured (Figure 2D, S2C), suggesting a decrease in the synthesis of those transcripts. The synthesis of *Tfrc* was increased or unchanged (Figure 2D) as its expression is also transcriptionally regulated during iron deprivation (Lok and Ponka, 1999; Ponka and Lok, 1999). Interestingly, the change in synthesis of the complex IV-encoding mRNA, *Cox4i1*, and our RQ endogenous control *Rplp0*, were similar to the other transcripts but their half-lives were much greater, potentially explaining why there is no overall change in their total levels (Figure 1C, S2C). Overall, our evidence indicates that the decrease in nDNA-encoded mitochondrial transcripts is not due to an increase in transcript degradation but rather, due to a decrease in the synthesis of new transcripts.

3.3.3 The Mitochondrial Responses to Iron Deprivation are Independent of Well-Established Transcriptional and Post-Transcriptional Regulators of Mitochondria

Iron deprivation causes a pervasive downregulation of mitochondrial gene expression in mammalian cells. In our previous analysis, we found that the effect of iron deprivation on mitochondrial *proteins* is independent of the potent regulators of mitochondrial biogenesis, PGC-1α and HIF-1α (Rensvold et al., 2013). However, considering the discordance in the levels and timing of the mitochondrial transcript and protein response to iron deprivation, we re-examined the role of PGC-1α and HIF-1α in regulating mitochondrial *transcripts* in response to iron

deprivation. The level of transcripts from PGC-1α$^{-/-}$ cells (Uldry et al., 2006) responded comparably to wild-type cells when deprived of iron (Figure 3A), indicating that iron deprivation does not affect mitochondrial transcripts by opposing this important transcriptional coactivator. Similarly, HIF-1α$^{-/-}$ cells showed the same decrease in mitochondrial transcripts as wild-type cells when treated with DFO for 24 hours (Figure 3B). Together, these results suggest that the observed effects of iron deprivation are independent of the transcriptional regulators PGC-1α and HIF-1α.

The mechanistic/mammalian target of rapamycin (mTOR) is a protein kinase that controls cell growth and survival in response to changes in cellular nutrients, energy and stress (Laplante and Sabatini, 2012; Shimobayashi and Hall, 2014). mTOR also regulates mitochondrial biogenesis and through multiple mechanisms (Bentzinger et al., 2008; Blattler et al., 2012; Chen et al., 2008; Cunningham et al., 2007; Larsson et al., 2012; Morita et al., 2013; Ramanathan and Schreiber, 2009) and has recently been shown to regulate cellular iron homeostasis with rapamycin inhibition of mTOR causing a reduction in cellular iron uptake (Bayeva et al., 2012). Therefore, we hypothesized that mTOR inhibition and iron chelation could be regulating mitochondrial biogenesis through similar mechanisms. Specifically, mTOR inhibition has been shown to inhibit the interaction between the transcription factor yin-yang 1 (YY1) and PGC-1α, and loss of this interaction leads to a decrease in mitochondrial gene expression (Blattler et al., 2012; Cunningham et al., 2007). We have already shown that the mitochondrial response to iron deprivation is independent of PGC-1α (Figure 3A) (Rensvold et al., 2013). However, mTOR also controls mitochondrial biogenesis through translational regulation of nuclear-encoded mitochondrial transcripts (Morita et al., 2013). This mTOR translational regulation occurs through inhibition of the eukaryotic translation initiation factor 4E

(eIF4E)-binding proteins (4E-BPs) and was shown to be specific for a subset of mitochondrial transcripts, including mRNAs encoding for complex V subunits but not the complex IV subunit COX4I1. The translation of transcripts encoding complex I subunits and assembly factors were also identified as being affected by mTOR inhibitors in an earlier genome wide screen (Larsson et al., 2012), but those changes were not investigated in greater detail (Morita et al., 2013). As the OxPhos complexes affected by iron chelation (complexes I, II and COX4I1 but not complex V) are somewhat dissimilar to those affected by mTOR inhibition (complex V and possibly complex I but not COX4I1), we directly compared the iron chelation- and mTOR inhibition-induced changes in OxPhos subunits via immunoblotting (Figure 4). Surprisingly, treatment of cells with rapamycin (Figure 4A) or the active-site mTOR inhibitor PP242 (Figure 4B) did not cause decreases in OxPhos proteins, with the possible exception of a slight decrease in COX4I1 with PP242, while the inhibitors did cause selective decreases in phosphorylation of known mTOR substrates (Feldman et al., 2009), including 4E-BP1 (for PP242) and S6 ribosomal protein (for both inhibitors), indicating that mTOR activity was inhibited. DFO treatment did not cause any changes in phosphorylation of the mTOR targets. Moreover, when cells were treated simultaneously with DFO and mTOR inhibitors, DFO caused the same decreases in OxPhos proteins, suggesting that the effect of iron deprivation on mitochondrial proteins is independent of mTOR activity and its downstream regulatory processes.

Next, we sought to determine whether the iron deprivation induced decreases in mitochondrial proteins could be explained by an increase in mitochondrial quality control (QC) proteolysis. Mitochondria contain multiple QC proteases specific to each of its subcompartments that degrade damaged, misfolded or non-assembled proteins (Baker and Haynes, 2011; Baker et al., 2011; Goard and Schimmer, 2014; Quiros et al., 2015). The matrix contains two major QC

proteases, the AAA (ATPases associated with diverse cellular activities) serine proteases LONP1 and CLPP (which forms a complex with its chaperone CLPX). Two QC metalloproteases are located in the inner membrance, the *m*-AAA (composed of SPG7/paraplegin, AFG3L2 and in mice, AFG3L1), whose proteolytic domain faces the matrix, and the *i*-AAA (YME1L1), whose proteolytic domain faces the intermembrane space. The intermembrane space contains the ATP-independent serine protease HTRA2. Interestingly, LONP1 and CLPP levels and activity are increased, and mitochondrial Fe–S proteins are decreased (with no change in their transcript levels) during dysregulation of cellular iron metabolism in a mouse heart specific knockout of the Fe-S cluster biogenesis protein frataxin (Guillon et al., 2009).

To investigate if these major QC proteases are involved in the mitochondrial response to iron deprivation, we first profiled their expression following iron deprivation (Figure S3A). We found that the transcript levels of *Htra2*, *Afg3l1* and *Afg3l2* were significantly decreased, making their role in regulating mitochondrial protein levels in response to iron deprivation less probable. The transcript levels of *Lonp1* were significantly increased, however HIF-1 activation has been shown to increase *Lonp1* expression and we have shown that the effects of iron deprivation are independent of HIF-1α (Figure 3B) (Rensvold et al., 2013). Importantly, we still observe a slight *Lonp1* increase in HIF-1$\alpha^{-/-}$ cells (Figure 3B), suggesting that iron-deprivation might induce *Lonp1* in a HIF-1α independent mechanism to regulate mitochondrial protein levels. To determine whether LONP1 is necessary for the response, we knocked down expression of this protease using RNAi (Figure 5A, 5B). Additionally, regardless of their expression profile, we knocked down each of the other major QC proteases discussed above (Figure S3B, S3C). We found that when *LONP1* levels are reduced to less than 20% of the control, even for up to 5 days, the cells show the same response to DFO for both mitochondrial proteins (Figure 5A) and

transcripts (Figure 5B). We also found similar results for the other proteases (Figure S3B, S3C). Together, these results suggest that the iron deprivation-induced decrease in mitochondrial proteins is independent of these major mitochondrial QC proteases on an individual protease basis. However, many of these proteases have overlapping targets, for example, LONP1, *m*-AAA and *i*-AAA have all been shown to regulate levels of complex I and complex IV subunits (Fukuda et al., 2007; Hornig-Do et al., 2012; Quiros et al., 2014; Stiburek et al., 2012; Zurita Rendon and Shoubridge, 2012), and one protease could potentially compensate for a reduction in the levels of another. In addition to QC, many of these proteases are also important for mitochondrial biogenesis (see reductions in COX4I1 and complex I subunits in the 5 day LONP1 knockdown, Figure 5A) (Quiros et al., 2015), further complicating these analyses. Therefore, we cannot conclude that the effect of iron deprivation on mitochondrial proteins is completely independent of mitochondrial QC proteolysis.

3.3.4 Dynamic Changes in Histone Tail Acetylation and Methylation Accompany Cellular Iron Deprivation

We previously found that the mitochondrial transcriptional response to iron deprivation is independent of several important regulators of mitochondrial biogeneis, including HIF-1α and PGC-1α (Figure 3A, 3B) (Rensvold et al., 2013). In addition to transcription factors and transcriptional co-regulators, changes in the epigenome—an additional layer of information that functions above the genome—can regulate transcription through multiple mechanisms (Venkatesh and Workman, 2015; Zentner and Henikoff, 2013). The "epigenetic code" is comprised of DNA methylation, histone post-translational modifications (PTMs) and histone variant proteins, all of which function to regulate processes that require physical access to DNA,

including transcription and DNA replication (Jenuwein and Allis, 2001). Histones are small, highly basic proteins with flexible and heavily modified N-terminal tails. Although a myriad of histone PTMs have been identified, the most common are lysine acetylation and mono-, di-, and trimethylation (Bannister and Kouzarides, 2011; Britton et al., 2011; Huang et al., 2014). Histone PTMs function not only to regulate chromatin structure (i.e. "open" vs. "closed" chromatin states), but also serve as a signal integration platform and binding site for other non-histone chromatin complexes (Fan et al., 2015; Johnson and Dent, 2013). To assess a potential role for histone PTMs in the mitochondrial response to iron deprivation, we performed a large-scale, quantitative mass spectrometry-based analysis of histone tail acetylation and methylation during DFO response and recovery (Figure 6A). Using a data independent acquisition (DIA) mass spectrometry workflow (Krautkramer et al., 2015), we quantified peptides from histone H3 and H4 proteins across multiple time points (Figure S4A).

Overall, we found that changes in histone acetylation and methylation are coordinated with changes in mitochondrial gene expression during DFO treatment and recovery (Figure 6B-E, S4A). For example, histone H3 lysine 27 trimethylation (H3K27me3) increased in DFO-treated cells relative to controls as early as day 0.5 of treatment (Figure 6D). This PTM increased even further at day 1 of DFO treatment prior to returning to an unchanged state relative to control cells during the recovery period (days 3 and 5 of the time course; Figure 6D). Similar patterns across the response and recovery timecourse were observed for acetylation of Histone H3 (K18 and K23) and Histone H4 (singly to quadruply acetylated H4 peptides) (Figure 6C, E). Interestingly, decreased abundance of the doubly acetylated H3K9ac+K14ac and H3K27ac peptides is maintained throughout the response and recovery phases (Figure 6B, D). Thus, while some of the epigenetic effects of iron deprivation appear to be more transient, others are

maintained across multiple cell cycles. This suggests that iron deprivation may have lasting effects on gene regulatory programs and offers potential mechanistic insight into observations that iron deprivation leads to a lasting developmental delay, which has been demonstrated to persist beyond iron repletion (Lozoff et al., 1991).

Given that the Jumonji C (JmjC) domain protein family members catalyze histone demethylation in an Fe^{2+} and α-ketoglutarate dependent manner (Cloos et al., 2008), we expected iron deprivation to decrease the activity of these enzymes. Indeed, we observed increased di- and trimethylation of H3K27 at both 0.5 and 1 day of DFO treatment (1.4-1.6 fold, $p < 0.001$-0.05; Figure 6D). We also observed trends toward increased di- and trimethylation of H3K9 (Figure 6B). Notably, decreases in monomethylated H3K9, K27 and K36 and unmodified forms of these histone H3 peptides are likely due to the fact that highly methylated forms are maintained at the expense of other possible histone PTM states due to lack of JmjC family histone demethylase activity.

Surprisingly, DFO also induced global decreases in acetylation of histones H3 (Figure 6B-C). The singly acetylated peptide containing H3K9ac/K14ac trended toward a 1.4-1.7 fold decrease during days 0.5-1 of DFO treatment, and the doubly acetylated H3K9ac+K14ac peptide decreased more than 35-fold during DFO treatment ($p < 0.01$-0.05, Figure 6B). Trimethylation of H3K27 has been reported to antagonistically prevent acetylation at the same site by preventing acetyltransferases from binding, thus maintaining a repressed transcriptional state over target genes (Pasini et al., 2010). In the setting of iron deprivation, it is likely that inhibition of JmjC family histone demethylases maintains a high degree of histone methylation on target lysine residues. Of the more than 25 known JmjC histone demethylases, KDM4A-D and KDM6A-B, which target histone H3 K9me3 and K27me3, respectively, appear to be most affected by iron

deprivation (Cloos et al., 2008). Ultimately, maintenance of a high degree of histone methylation at K9 and K27 at the expense of acetylation creates a more "closed" chromatin state and silence transcription of target genes.

Histone H4 acetylation is also decreased in response to iron deprivation. Lysines 5, 8, 12, and 16 on the N-terminal tail of histone H4 can all be acetylated. Here, peptides are reported by the number of acetylated lysines contained on the histone H4 peptide spanning residues 4-17. Thus, a peptide containing a single acetylated lysine is denoted as 1ac, whereas a peptide wherein all 4 lysines are acetylated is denoted as 4ac. Similar to observations on histone H3, DFO induces global decreases on histone H4, ranging from 1.2-1.7 fold ($p < 0.001$-0.05, Figure 6E). These decreases in acetylation trend back toward a relatively unchanged state during the recovery phase. Thus, decreased acetylation on histone H4 also supports the establishment of a more "closed" chromatin state and transcriptional repression in response to iron deprivation.

Next, we validated these changes in histone tail acetylation and methylation with immunoblotting. Iron deprivation caused decreases in total lysine acetylation on histone H3 and H4 and specifically for H3K9ac (Figure 6F). While we were unable to detect histone H4 K20 peptides since these small peptides were below the m/z range scanned in our mass spectrometry workflow, we also found that levels of H4K20me3 and H3K27me3 are increased following iron relative to overall histone levels (Figure 6F). Altogether, we observe dynamic changes in histone PTMs that can provide key insights into the epigenetic mechanisms involved in the response to iron deprivation.

3.3.5 Iron Deprivation Decreases Histone Acetylation at Nuclear DNA-Encoded Mitochondrial Genes

Our data demonstrates that acute iron depletion leads to profound effects on mitochondrial gene expression and the nuclear epigenome. Changes in histone acetylation and methylation can affect transcription through different mechanisms (Bannister and Kouzarides, 2011; Kouzarides, 2007; Zentner and Henikoff, 2013). For example, acetylation neutralizes the positive charge of lysine, thereby weakening the interaction between histones and negatively charged DNA. This results in an open chromatin state (euchromatin) and greater access to DNA for transcription. For example, acetylation of a single histone H4 lysine residue (K16) is sufficient to "open" the compacted 30nm chromatin fiber and affects interactions with non-histone proteins (Robinson et al., 2008; Shogren-Knaak et al., 2006). Both acetylation and methylation can affect the recruitment of different protein complexes with reader domains that specifically recognize these modifications and activate or repress gene expression. Moreover, different types of modifications on different histone lysine residues are correlated with either transcriptional activation or repression. For example, H3K9ac is strongly associated with transcriptional activation and H3K27me3 with repression (Berger, 2007; Kooistra and Helin, 2012). In both our quantitative MS-based analysis and immunoblot analysis we found an overall decrease in H3K9ac and an increase in H3K27me3 (Figure 6, S4A). To determine if changes in these modifications are found at nuclear-encoded mitochondrial genes whose expression is affected by iron deprivation, we performed chromatin immunoprecipitation (ChIP)-qPCR analyses. From these experiments, we find reduced levels of H3K9ac at all mitochondrial genes analyzed (Figure 7A), indicating a direct regulatory link between a decrease in histone acetylation and mitochondrial gene expression in response to iron deprivation. Unexpectedly, we

did not observe an increase in H3K27me3, but instead found that this mark was slightly decreased or unchanged at mitochondrial genes, suggesting that changes in H3K27me3 are not directly affecting their expression (Figure 7A). However, it is possible that H3K27me3 affects the expression of those genes through changes in long-range chromatin interactions or regulation of higher-order chromatin structure (Kouzarides, 2007; Zhou et al., 2011).

3.3.6 Histone Deacetylase Inhibition Blocks the Mitochondrial Biogenesis Iron Deprivation Response

Our results show that the iron deprivation-induced transcriptional changes are accompanied by decreases in histone acetylation at mitochondrial genes. The enzymes that regulate acetylation include acetyl-CoA-dependent lysine acetyltransferases (HATs), and the NAD^+- or iron/zinc- dependent deacetylases (HDACs) (Smith and Denu, 2009). To determine whether the effect of iron deprivation on mitochondrial biogenesis is dependent on histone acetylation levels, we treated iron-deprived cells with the clinically relevant HDAC inhibitor suberoylanilide hydroxamic acid (SAHA, also known as vorinostat) which chelates zinc in the active site of Class I, II, and IV HDACs but does not inhibit Class III HDACs (Falkenberg and Johnstone, 2014; Kazantsev and Thompson, 2008; Marks and Breslow, 2007; Xu et al., 2007). Strikingly, we found that HDAC inhibition completely blocked the effect of iron deprivation on mitochondrial transcripts (Figure 8A, S5A) and histone acetylation levels (Figure 8B), and attenuated the effect on mitochondrial protein levels (Figure 8C, S5B), consistent with histone PTM regulation of gene expression. We also discovered similar effects on mitochondrial transcripts and proteins when we treated cells with the HDAC inhibitor, trichostatin A (TSA),

which also acts by chelating zinc in the active site of HDACs and has been demonstrated to have anti-tumor effects (Figure S5C, S5D) (Finnin et al., 1999).

3.3.7 Mitochondrial Gene Expression is Dampened in Iron Deficient Mice

Our analyses show that iron deprivation of tissue culture cells leads to a global decrease in mitochondrial gene expression at both the mRNA and protein level. These results motivated us to determine if the iron deprivation-induced mitochondrial remodeling effect seen in cultured mouse cells is also seen in iron deficient mice. We analyzed mitochondrial gene expression in three tissues, including liver, soleus muscle and heart, collected from mice fed an iron sufficient diet (50 ppm iron) or iron-deficient diet (less than 5 ppm iron) for three weeks (Figure 9A). The average hematocrits of the iron sufficient and iron deficient groups were 37 ± 4 and 19 ± 3, respectively, indicating iron-deficient anemia in the iron deprived mice.

To assess the effect of iron deficiency on mitochondrial gene expression in these mice, we measured the transcript expression of three mitochondrial genes: *Ndufs8* and *Uqcrc1*, which are subunits of the iron containing complexes I and III, respectively, and *Atp5a1*, a subunit of iron-free complex V. In all three tissues analyzed, we observed a significant decrease in transcripts for at least one of these mitochondrial genes, with the greatest decreases occurring in liver (Figure 9B). As expected, expression of the transferrin receptor (*Tfrc*) was significantly increased in all tissues of the iron-deficient mice (Figure 9B). In heart tissue from iron-deprived mice, we also observed a decrease in protein abundance of the complex I-8 kDa subunit and a slight decrease in the complex I NDUFB3 subunit (Figure 9C), although no clear change in these proteins in the other tissues was observed (Figure 9C). The differences in the response of mitochondrial transcripts and proteins between the different tissues could be due to differences in

translational activity or mitochondrial transcript and protein turnover rates. Overall, the discordance we observe between the levels of transcripts (decreased in all 3 tissues) and proteins (decreased in only 1 tissue) is consistent with what we observed in cell culture, and these differences imply that iron deprivation could have independent effects on mitochondrial transcripts and proteins, or that the transcript changes are in response mitochondrial dysfunction (that may or may not result in decreased protein levels). Previous studies of iron deficiency in rats have reported various effects of iron deficiency on mitochondria, with decreases in the activity of respiratory complexes, spectroscopic cytochrome content and morphological changes (Cartier et al., 1986; Dallman, 1986; Dallman and Goodman, 1970). However, there have been no reports on iron deficiency affecting the level of mitochondrial gene expression. Altogether, these results suggest that iron deficiency in mice results in a similar decrease in mitochondrial gene expression as seen in iron-deprived cell lines, and that the effect on mitochondrial transcripts and proteins are especially prominent in liver and heart tissue, respectively.

3.3.8 Conclusions

Mitochondria are essential organelles that adjust to changes in environment and nutrients. We recently discovered that cellular iron deprivation initiates a powerful mitochondrial biogenesis response. To elucidate the molecular basis of this response, we used a combination of unbiased, large-scale mass spectrometry-based approaches and hypothesis-driven experiments. From detailed timecourse analyses we find that the decrease in mitochondrial proteins precedes the decrease in their corresponding transcripts, and for the mitochondrial proteins unaffected by iron chelation, their transcripts are nonetheless reduced, suggesting that iron deprivation may have independent effects on mitochondrial transcripts and proteins (Figure 10A), *or* that the

decrease in transcripts is in response to the changes in mitochondrial function and proteins, perhaps through a mitochondrial to nuclear retrograde signaling response (Figure 10B). Importantly, these two scenarios are not mutually exclusive, and both mechanisms could be contributing to the mitochondrial biogenesis response. Using an RNA labeling approach we determined that the decrease in transcripts encoding mitochondrial proteins is due to a decrease in transcription and not due to increased transcript degradation (Figure 10). We show that iron deprivation-induced transcriptional changes are accompanied by dynamic changes in histone acetylation and methylation, decreases in acetylated histones at mitochondrial genes and that the effect of iron deprivation on transcript levels is blocked with HDAC inhibition, consistent with histone PTM regulation of gene expression (Figure 10). Last, we show that the effects of iron deprivation on mitochondrial gene expression are largely preserved in a mouse model of iron deficiency. Collectively, our work provides a model for how nutrient deprivation can drive epigenetic regulation of mitochondrial biogenesis.

3.4 Experimental Procedures

3.4.1 Cell Culture

Brown preadipocytes were maintained in high glucose DMEM with 20% FBS and 1 × PS (Gibco) at 37°C and 5% CO_2. All other cell lines were maintained in high glucose DMEM with 10% FBS and 1 × PS (Invitrogen). Deferoxamine mesylate salt (DFO), trichostatin A (TSA), rapamycin and PP242 hydrate were obtained from Sigma-Aldrich. Suberoylanilide hydroxamic acid (SAHA) was obtained from Tocris Bioscience.

3.4.2 Relative Quantification Real Time-qPCR

Total RNA was purified from liver using RNA STAT-60 (Tel-Test), and from heart, soleus muscle and cultured cells using the RNeasy Mini Kit (QIAGEN). First-strand cDNA was synthesized from purified RNA (500 ng) using the SuperScript III Synthesis System for RT-PCR (Invitrogen). Real time-quantitative PCR was performed using TaqMan- or SYBR green-based detection (Applied Biosystems) with *Hprt1* as the endogenous control for analysis of mouse tissue and *Rplp0/RPLP0* as the endogenous control for analysis of cultured cells. Primer sequences are listed below (predesigned probes were used for the TaqMan assays).

3.4.3 Primers used for SYBR Green Real-Time qPCR

SYBR green primers were designed using the Roche Universal ProbeLibrary Assay Design Center tool or the Integrated DNA Technologies (IDT) RealTime qPCR Assay tool.

Mouse:

Afg3l1:

Left: gcccaggaaattcagtacctc Right: cctttccctcctctgttgc

Afg3l2:

Left: ggtttatattgctgagagcgatg Right: atgagtacggtgggcaacat

Atp5a1:

Left: tccatgcctctaacactcgac Right: gacgtgtcagctcccagaa

Clpp:

Left: gcaacaagaagcccattcat Right: gtactgcattgtgtcgtagatgg

Clpx:

Left: tggtgcctttaatggcttaga Right: ggtgttccaaagccgagata

Cox4i1:

Left: tcactgcgctcgttctgat Right: cgatcgaaagtatgagggatg

Cycs:

Left: aacgttcgtggtgttgacc Right: ttatgcttgcctccctttc

Hif1a:

Left: ttacgtgtgagaaaacttctggat Right: gccatctagggctttcagataa

Htra2:

Left: ttggagtgatgatgctgacc Right: ttggctcacggagctgtagt

Lonp1:

Left: tggcgtcttcctaaagagagat Right: tcccgtatggtagatttcatcc

Ndufa9:

Left: ttagagcgcttccaatgtca Right: atggtgaagctggcgatg

Ndufs3:

Left: cggcagaaccgttttgag Right: tcaatgggtgtcagctcatc

Ndufs7:

Left: gtggtgaccaagctggatg Right: cgaaggtcataggccacag

Ndufs8:

Left: ttgcctgcaaactctgtgag Right: catcggctcttggctcag

Ppargc1a:

Left: cttcctccatgcctgacg Right: tggctggtgccagtaagag

Rplp0:

Left: actggtctaggacccgagaag Right: tcccaccttgtctccagtct

Sdha:

Left: tgttcagttccaccccaca Right: tctccacgacacccttctg

Spg7:

Left: tgatggaccatgaagcaaag Right: tttccagaagggcattcg

Tfrc:

Left: tcctttccttgcatattctgg Right: ccaaataaggatagtctgcatcc

Uqcrc2:

Left: gcaactgctagagccatgaa Right: caactttgagggaataaaatctcg

Yme1l1:

Left: cggtagaccctgtccagatg Right: ttcaaccacttcctgtaactcttg

Human:

AFG3L2:

Left: ttcgagtgacctttacaccag Right: cccgattttctccttctatgcc

CLPP:

Left: ccttgttatcgcacagctcc Right: gatcgggttgaggatgtactg

HTRA2:

Left: cggagtcagtacaacttcatcg Right: gaatcctgagccgttcgag

LONP1:

Left: caactacctagactggctcac Right: tggctaacggcaatgaactc

NDUFB3:

Left: gggacaccattagaaactatcca Right: ccacccatgtatctccaagc

RPLP0:

Left: tctacaaccctgaagtgcttgat Right: caatctgcagacagacactgg

YME1L1:

Left: gtgtccctgttacctgagaatg Right: caaaatcactggaagcacctg

3.4.4 Immunoblotting

For immunoblot analysis, 15 μg of cleared whole-cell or mouse tissue lysate or 2 μg of purified histones, as determined by BCA assay (Thermo Scientific), was separated on a Novex NuPAGE 4-12% Bis-Tris Mini Gel (Invitrogen), transferred to PVDF and probed with primary antibodies (listed below). Whole-cell lysates were prepared in RIPA buffer composed of 150 mM NaCl, 1% IGEPAL CA-630, 0.5% sodium deoxycholate, 0.1% SDS, 50 mM Tris (pH 8.0), 0.4 mM EDTA (pH 8.0), 10% glycerol and a protease inhibitor cocktail (Roche Diagnostics). Frozen mouse tissues were pulverized in liquid nitogen, homogenized in RIPA buffer using a Tissue-Terror (BioCold Scientific) and stored at -80°C until analysis. Histones were purified from 2×10^6 cells per condition via acid extraction as previously described (Shechter et al., 2007).

3.4.5 Mass Spectrometry

Cell fractionation and sample preparation: Roughly 20×10^6 cells were trypsinized and pelleted prior to washing twice with ice-cold PBS. Cells were then resuspended in 800 μL ice-cold buffer A (10 mM Tris-HCl, 10 mM NaCl, 3 mM $MgCl_2$, 0.1% NP-40 alternative, pH 7.4)

with histone deacetylase and protease inhibitors (1 mM sodium butyrate, 4 μM trichostatin A, 100 μM phenylmethylsulfonyl fluoride, 10 μg/mL leupeptin, and 10 μg/mL aprotinin). Cells were vortexed at medium speed for 5 seconds prior to being transferred to a pre-chilled 1 mL dounce homogenizer. Cells were homogenized with 60 strokes with the tight pestle and centrifuged at 800 × *g*. The crude nuclear pellet was then washed twice with ice-cold PBS prior to acid extraction. Histones were acid extracted, followed by two rounds of chemical derivatization using propionic anhydride and trypsinized as described (Lin and Garcia, 2012). After chemical derivatization all N-termini and unmodified or monomethylated lysine residues were propionylated. This labeling method protects all lysine residues from cleavage by trypsin, which cleaves C-terminally to unmodified lysine and arginine residues, enabling consistent generation of histone peptides amenable to analysis by mass spectrometry.

Nano-liquid chromatography and electrospray ionization tandem mass spectrometry: Samples were injected twice, once using data dependent acquisition (DDA) and a second time with data independent acquisition (DIA). For both DDA and DIA, 1 μg of propionylated histone peptides was injected onto a Dionex Ultimate3000 nanoflow HPLC with a Waters NanoEase C18 column (100 μm × 15 cm, 3 μm) coupled to a Thermo Fisher Q-Exactive mass spectrometer at 700 nL/min. Mobile phase consisted of water + 0.1% formic acid (A) and acetonitrile + 0.1% formic acid (B). Histone peptides were resolved with a linear gradient of 2% to 35% mobile phase B over 65 minutes. The mass spectrometer was operated in DDA mode with dynamic exclusion enabled (exclusion duration = 8 seconds), MS1 resolution = 70,000, MS1 automatic gain control target = 1×10^6, MS1 maximum fill time = 100 ms, MS2 resolution = 17,500, MS2 automatic gain control target = 2×10^5, MS2 maximum fill time = 500 ms, and MS2 normalized collision energy = 30. For each cycle, one full MS1 scan range = 300-1100 m/z, was followed by

10 MS2 scans using an isolation window size of 2.0 m/z. An inclusion list was employed to increase the detection efficiency of histone peptides of interest. In data-independent mode (DIA) the mass spectrometer was operated with a MS1 scan at resolution = 35,000, automatic gain control target = 1×10^6, and scan range = 295-1105 m/z, followed by a DIA scan with a loop count of 10. DIA settings were as follows: window size = 20 m/z, resolution = 17,500, automatic gain control target = 1×10^6, DIA maximum fill time = AUTO, and normalized collision energy = 30. For each cycle, one full MS1 was followed by 10 MS2 scans using an isolation window size of 20 m/z. Total cycle time for a complete scan across the whole scan range was 2.0 seconds.

Database search and spectral library construction: Database searches were performed for each DDA sample using Mascot (v 2.2.07). Spectra were searched against the human Uniprot database (Download: November, 2014; containing 134,172 sequences). Peak lists were generated by converting Thermo.raw files from DDA experiments to .mgf files for Mascot database search using MSConvert, a tool in the ProteoWizard Library (Kessner et al., 2008). Mascot parameters were as follows: fixed modifications = N-terminal propionylation and lysine propionylation; variable modifications = lysine acetylation, lysine butyrylation (an equivalent mass shift to monomethylation + propionylation, since both unmodified and monomethylated lysine residues are propionylated during chemical derivatization), lysine dimethylation, and lysine trimethylation; peptide mass tolerance = 10 ppm; fragment mass tolerance = 0.01 Da; the enzyme was set to ArgC since trypsin will only cleave after arginine due to chemical derivatization and a maximum of one missed cleavage was allowed. A probability based Mowse score of 26 or higher indicated identity with $p < 0.05$. Spectral libraries were generated using Skyline (v 2.5.0.6157) using Mascot search results.

Histone PTM Quantitation: The DIA files were imported into Skyline for quantitative analysis (MacLean, et al., 2010). All MS1 and MS2 peaks were matched to a spectral library upon import based on retention times and presence of appropriate transitions. All imported histone peptide MS1 peaks and their integration bounds were also manually verified using XCalibur Qual Browser (v2.2). Peak areas for all selected transitions were exported and precursor ion peak areas were combined for quantitation. Three precursor ions were used for quantitation and minimum of 4 MS2 ions were used to validate peak picking. This ensured accurate, unbiased measurement.

To quantify the percent of total for each peptide species, all peptide areas belonging to a peptide "family" were summed to obtain the total area for that "family." A peptide "family" is defined as a group of peptides spanning the same residues within a histone protein, e.g. H3 residues 18-26 (KQLATKAAR), which contains lysines 18 and 23 is a family of peptides with 5 members: K18ac+K23un, K18un+K23ac, K18ac+K23ac, K18me1+K23un, and K18un+K23un. The proportion of the total for each peptide member of the family was then obtained by dividing the individual peptide area by the summed family area. Isobaric and co-eluting histone H3 and H4 peptides were not deconvoluted, and are denoted as such (eg: K18ac+K23un and K18un+K23ac are isobaric and co-eluting and are denoated as a single value for K18ac/K23ac since the MS1 ions for these two species are identical).

Data normalization and statistics: Exported area values from Skyline were normalized within peptide families to the total area prior to calculations of fold changes and statistics. All p-values were generated using a Welch's t-test (biological replicates, $n = 3$). Statistical significance was determined by $p < 0.05$.

3.4.6 Primary Antibodies used for Immunoblotting

Antigen	**Supplier**	**Product Number**
4E-BP1	Cell Signaling Technology	9644P
β-actin	Abcam	ab8224
CI subunit 8 kDa	Abcam	ab110245
H3K9ac	Active Motif	61252
H3K27ac	Active Motif	39134
H3K27me3	Active Motif	39157
H4K20me3	Active Motif	39672
NDUFB3	Proteintech Group	12358-1-AP
NDUFS3	Abcam	ab14711
OxPhos Antibody Cocktail	Abcam	ab110412
(ATP5A1, SDHA, UQCRC2, NDUFA9, COXIV)		
pan-acK	Cell Signaling Technology	9814S
p4E-BP1 (T37/46)	Cell Signaling Technology	2855P
pS6 (S235/236)	Cell Signaling Technology	4858P
TFRC	Invitrogen	136800
VDAC	Abcam	ab18988

3.4.7 Extracellular Flux Measurements

Oxygen consumption rate (OCR, pMoles/min) and extracellular acidification rate (ECAR, mpH/min) measurements were performed using a Seahorse Biosciences XF96 Extracellular Flux Analyzer as previously described (Nicholls et al., 2010). Briefly, C2C12 myoblasts were seeded

at 1.2×10^4 cells/well in XF96 microplates (Seahorse Biosciences). After a 24-hr incubation, the growth media was exchanged for XF Assay Medium (Seahorse Biosciences) supplemented with 25 mM glucose (Sigma-Aldrich). OCR and ECAR measurements were 5-min periods following 3-min mix periods. For run 1 (main figure), DFO was injected after 3 mix-measure cycles. Measurements following DFO injection consisted of 2 mix-measure cycles punctuated by 14 min wait periods (only data from the second measurement are displayed, 34 total measurements). For run 2 (supplemental figure), DFO was injected after 2 mix-measure cycles punctuated by 22 min wait periods. Measurements following DFO injection consisted of 1 mix-measure cycle punctuated by 22 min wait periods (33 total measurements). All measurements were baselined to the measurement prior to injection and measurements at each timepoint were normalized to the corresponding untreated (control) values.

3.4.8 EU Labeling

RNA labeling was performed using the Click-iT Nascent RNA Capture Kit (Invitrogen) following the manufacturer's protocol. Briefly, C2C12 myoblasts were seeded at 1.5×10^5 cells/well in 6 well plates. For the pulse-chase experiment, 5-ethynyl uridine (EU) was added at 0.2 mM, and after 18 hours, the media was replaced with fresh growth media without EU, and then DFO was added. For the pulse-labeling experiments, 0.2 mM EU was added to cells for 2 hours prior to collection. Total RNA was purified using the RNeasy Mini Kit (QIAGEN). Biotinylation of RNA was performed using 4 μg of total RNA and 0.5 mM biotin azide per reaction (for each sample). Binding of biotinylated RNA to magnetic beads was performed using 100 ng RNA and 300 μL of beads per reaction with 25 μL of Click-iT RNA binding buffer and 2 μL of RNAseOUT. Complementary DNA synthesis was performed using the SuperScript VILO

cDNA Synthesis Kit (Invitrogen) using 4 µL of 5× VILO Reaction Mix, 2 µL of 10× SuperScript and 10 µL of RNA based on the manufacturer's recommendations. The cDNA was analyzed via real-time qPCR.

3.4.9 RNAi

HEK 293FT cells were seeded at 2×10^5 cells/well in 6 well plates and the following day were transfected with 10 nM of Dharmacon siGENOME SMARTpools targeting individual mitochondrial proteases or the Non-Targeting siRNA Control Pool #2 using 5 µL/well of DharmaFECT 1 Transfection Reagent (GE Healthcare) based on the manufacturer's protocol. The next day the cells were treated with DFO, and after 24 hrs were collected for real-time qPCR and immunoblot analyses.

3.4.10 ChIP-qPCR

Chromatin immunoprecipitation (ChIP) was performed using 1×10^6 cells per condition with the Pierce Magnetic ChIP Kit (Thermo Scientific) following the manufacturer's protocol. After cross-linking, cell lysis and nuclei isolation, DNA was digested using 3 µL of micrococcal nuclease (1 U/µL) and nuclei were broken using a Sonic Dismembrator Model 100 micro-tip probe sonicator (Fisher Scientific). Immunoprecipitations were performed overnight using 5 µg of primary antibody (listed below) per ChIP reaction. Real time-quantitative PCR was performed using SYBR green-based detection (Applied Biosystems). Primer sequences are listed below. ChIP-qPCR data was normalized using the percent input method (with 10% of the digested chromatin was used as input for each sample).

3.4.11 Primary Antibodies and Primers used for ChIP-qPCR

Antigen	**Supplier**	**Product Number**
H3K9ac	Millipore	06-942
H3K27me3	Cell Signaling Technology	9733S
Rabbit IgG Control	Cell Signaling Technology	3900S

Primers were designed using the Integrated DNA Technologies (IDT) PrimerQuest tool.

Atp5a1 (set 1):

Forward: cttgcattgtgggatggtttac Reverse: ccatcgtcgtccacagttt

Atp5a1 (set 2):

Forward: ggacgacgatggcgtattt Reverse: tggacaactcaagggcaaa

Ndufa9 (set 1):

Forward: gacgggaacatgacctttct Reverse: ccacaatccacgcactatct

Ndufa9 (set 2):

Forward: catgtcagaccacgtagaagag Reverse: caaagaagtggtgatggctttag

Sdha (set 1):

Forward: cgtcttggtctagcgaagtt Reverse: cccagactaccaacggattac

Sdha (set 2):

Forward: gggttagttggcagctattct Reverse: gaggtggaagtaggagtttgtg

Uqcrc2 (set 1):

Forward: ctgttgagagagtgcttctagc Reverse: gcatttccgcgttgtaactg

Uqcrc2 (set 2):

Forward: tagttgtcacttgcggtgag Reverse: gctcccattctcatctcttgaa

3.4.12 Mice

Mice were C57Bl/6J from Jackson Laboratories, weaned at 18 days onto either iron deficient (<5ppm Fe) or iron sufficient (50 ppm Fe) powdered synthetic diet, fed ad libitum. Water was ddH2O and all glassware and feeding dishes were acid washed and rinsed with ddH2O to remove Fe. We started with 6 pups/group but lost one of the iron deficient pups the first week. Body weight and food intake were measured daily. Mice eating the iron sufficient diet were given only the average amount of food consumed the previous day by the iron-deficient group so that caloric intake was matched between the two groups. The mice were maintained on this diet for 3 weeks. Other husbandry was standard and performed according to RARC guidelines and protocols. At the end of 3 weeks the mice were anesthetized with isoflurane. Blood was removed by cardiac puncture under anesthesia for hematocrit measurement and plasma collection. The liver, heart and soleus muscles were then removed and snap frozen in liquid nitrogen until analysis.

3.4.13 Statistics

p Values were calculated by Student's two-tailed t test as indicated in the figure legends.

3.5 Acknowledgements

We would like to thank the members of the R.S.E., J.M.D. and D.J.P. laboratories for helpful discussions and assistance regarding this project. We specifically thank Hillary St. John (UW-Madison) for help with ChIP methods and Christopher Nizzi (UW-Madison) for assistance with mouse tissue preparation methods. Thank you to Bruce Spiegelman (Harvard Medical School) for providing the PGC-1a$^{-/-}$ cells, and Randall Johnson and Alex Weidemann (UCSD) for providing the HIF-1a$^{-/-}$ cells. This work was supported by a Searle Scholars Award, a Shaw

Scientist Award and USDA Hatch Award WIS01671 (to D.J.P.), and NIH Molecular Biosciences Training Grant 5T32GM007215-40 and a Louis and Elsa Thomsen Wisconsin Distinguished Graduate Fellowship (to J.W.R.).

3.6 References

Allen, G.F., Toth, R., James, J., and Ganley, I.G. (2013). Loss of iron triggers PINK1/Parkin-independent mitophagy. EMBO Rep *14*, 1127-1135.

Anderson, C.P., Shen, M., Eisenstein, R.S., and Leibold, E.A. (2012). Mammalian iron metabolism and its control by iron regulatory proteins. Biochim Biophys Acta *1823*, 1468-1483.

Baker, B.M., and Haynes, C.M. (2011). Mitochondrial protein quality control during biogenesis and aging. Trends Biochem Sci *36*, 254-261.

Baker, M.J., Tatsuta, T., and Langer, T. (2011). Quality control of mitochondrial proteostasis. Cold Spring Harb Perspect Biol *3*.

Bannister, A.J., and Kouzarides, T. (2011). Regulation of chromatin by histone modifications. Cell Res *21*, 381-395.

Bayeva, M., Khechaduri, A., Puig, S., Chang, H.C., Patial, S., Blackshear, P.J., and Ardehali, H. (2012). mTOR regulates cellular iron homeostasis through tristetraprolin. Cell Metab *16*, 645-657.

Bentzinger, C.F., Romanino, K., Cloetta, D., Lin, S., Mascarenhas, J.B., Oliveri, F., Xia, J., Casanova, E., Costa, C.F., Brink, M.*, et al.* (2008). Skeletal muscle-specific ablation of raptor, but not of rictor, causes metabolic changes and results in muscle dystrophy. Cell Metab *8*, 411-424.

Berger, S.L. (2007). The complex language of chromatin regulation during transcription. Nature *447*, 407-412.

Blattler, S.M., Verdeguer, F., Liesa, M., Cunningham, J.T., Vogel, R.O., Chim, H., Liu, H., Romanino, K., Shirihai, O.S., Vazquez, F.*, et al.* (2012). Defective mitochondrial morphology and bioenergetic function in mice lacking the transcription factor Yin Yang 1 in skeletal muscle. Mol Cell Biol *32*, 3333-3346.

Britton, L.M., Gonzales-Cope, M., Zee, B.M., and Garcia, B.A. (2011). Breaking the histone code with quantitative mass spectrometry. Expert Rev Proteomics *8*, 631-643.

Calvo, S.E., and Mootha, V.K. (2010). The mitochondrial proteome and human disease. Annu Rev Genomics Hum Genet *11*, 25-44.

Cartier, L.J., Ohira, Y., Chen, M., Cuddihee, R.W., and Holloszy, J.O. (1986). Perturbation of mitochondrial composition in muscle by iron deficiency. Implications regarding regulation of mitochondrial assembly. J Biol Chem *261*, 13827-13832.

Chan, D.C. (2012). Fusion and fission: interlinked processes critical for mitochondrial health. Annu Rev Genet *46*, 265-287.

Chen, C., Liu, Y., Liu, R., Ikenoue, T., Guan, K.L., Liu, Y., and Zheng, P. (2008). TSC-mTOR maintains quiescence and function of hematopoietic stem cells by repressing mitochondrial biogenesis and reactive oxygen species. J Exp Med *205*, 2397-2408.

Cloos, P.A., Christensen, J., Agger, K., and Helin, K. (2008). Erasing the methyl mark: histone demethylases at the center of cellular differentiation and disease. Genes Dev *22*, 1115-1140.

Cunningham, J.T., Rodgers, J.T., Arlow, D.H., Vazquez, F., Mootha, V.K., and Puigserver, P. (2007). mTOR controls mitochondrial oxidative function through a YY1-PGC-1alpha transcriptional complex. Nature *450*, 736-740.

Dallman, P.R. (1986). Biochemical basis for the manifestations of iron deficiency. Annu Rev Nutr *6*, 13-40.

Dallman, P.R., and Goodman, J.R. (1970). Enlargement of mitochondrial compartment in iron and copper deficiency. Blood *35*, 496-505.

DiMauro, S., and Schon, E.A. (2003). Mitochondrial respiratory-chain diseases. N Engl J Med *348*, 2656-2668.

Dominy, J.E., and Puigserver, P. (2013). Mitochondrial biogenesis through activation of nuclear signaling proteins. Cold Spring Harb Perspect Biol *5*.

Eisenstein, R.S., and Ross, K.L. (2003). Novel roles for iron regulatory proteins in the adaptive response to iron deficiency. J Nutr *133*, 1510S-1516S.

Falkenberg, K.J., and Johnstone, R.W. (2014). Histone deacetylases and their inhibitors in cancer, neurological diseases and immune disorders. Nat Rev Drug Discov *13*, 673-691.

Fan, J., Krautkramer, K.A., Feldman, J.L., and Denu, J.M. (2015). Metabolic regulation of histone post-translational modifications. ACS Chem Biol *10*, 95-108.

Feldman, M.E., Apsel, B., Uotila, A., Loewith, R., Knight, Z.A., Ruggero, D., and Shokat, K.M. (2009). Active-site inhibitors of mTOR target rapamycin-resistant outputs of mTORC1 and mTORC2. PLoS Biol *7*, e38.

Finnin, M.S., Donigian, J.R., Cohen, A., Richon, V.M., Rifkind, R.A., Marks, P.A., Breslow, R., and Pavletich, N.P. (1999). Structures of a histone deacetylase homologue bound to the TSA and SAHA inhibitors. Nature *401*, 188-193.

Frey, P.A., and Reed, G.H. (2012). The ubiquity of iron. ACS Chem Biol *7*, 1477-1481.

Friedman, J.R., and Nunnari, J. (2014). Mitochondrial form and function. Nature *505*, 335-343.

Fukuda, R., Zhang, H., Kim, J.W., Shimoda, L., Dang, C.V., and Semenza, G.L. (2007). HIF-1 regulates cytochrome oxidase subunits to optimize efficiency of respiration in hypoxic cells. Cell *129*, 111-122.

Goard, C.A., and Schimmer, A.D. (2014). Mitochondrial matrix proteases as novel therapeutic targets in malignancy. Oncogene *33*, 2690-2699.

Goldenthal, M.J., and Marin-Garcia, J. (2004). Mitochondrial signaling pathways: a receiver/integrator organelle. Mol Cell Biochem *262*, 1-16.

Guillon, B., Bulteau, A.L., Wattenhofer-Donze, M., Schmucker, S., Friguet, B., Puccio, H., Drapier, J.C., and Bouton, C. (2009). Frataxin deficiency causes upregulation of mitochondrial Lon and ClpP proteases and severe loss of mitochondrial Fe-S proteins. FEBS J *276*, 1036-1047.

Harbauer, A.B., Zahedi, R.P., Sickmann, A., Pfanner, N., and Meisinger, C. (2014). The protein import machinery of mitochondria-a regulatory hub in metabolism, stress, and disease. Cell Metab *19*, 357-372.

Hock, M.B., and Kralli, A. (2009). Transcriptional control of mitochondrial biogenesis and function. Annu Rev Physiol *71*, 177-203.

Hornig-Do, H.T., Tatsuta, T., Buckermann, A., Bust, M., Kollberg, G., Rotig, A., Hellmich, M., Nijtmans, L., and Wiesner, R.J. (2012). Nonsense mutations in the COX1 subunit impair the stability of respiratory chain complexes rather than their assembly. EMBO J *31*, 1293-1307.

Huang, H., Sabari, B.R., Garcia, B.A., Allis, C.D., and Zhao, Y. (2014). SnapShot: histone modifications. Cell *159*, 458-458 e451.

Jao, C.Y., and Salic, A. (2008). Exploring RNA transcription and turnover in vivo by using click chemistry. Proc Natl Acad Sci U S A *105*, 15779-15784.

Jenuwein, T., and Allis, C.D. (2001). Translating the histone code. Science *293*, 1074-1080.

Johnson, D.G., and Dent, S.Y. (2013). Chromatin: receiver and quarterback for cellular signals. Cell *152*, 685-689.

Kazantsev, A.G., and Thompson, L.M. (2008). Therapeutic application of histone deacetylase inhibitors for central nervous system disorders. Nat Rev Drug Discov *7*, 854-868.

Kessner, D., Chambers, M., Burke, R., Agus, D., and Mallick, P. (2008) ProteoWizard: open source software for rapid proteomics tools development. Bioinformatics *24*, 2534-2536.

Kirienko, N.V., Ausubel, F.M., and Ruvkun, G. (2015). Mitophagy confers resistance to siderophore-mediated killing by Pseudomonas aeruginosa. Proc Natl Acad Sci U S A *112*, 1821-1826.

Kooistra, S.M., and Helin, K. (2012). Molecular mechanisms and potential functions of histone demethylases. Nat Rev Mol Cell Biol *13*, 297-311.

Kouzarides, T. (2007). Chromatin modifications and their function. Cell *128*, 693-705.

Krautkramer, K.A., Reiter, L., Denu, J.M., and Dowell, J.A. (2015). Quantification of SAHA-Dependent Changes in Histone Modifications Using Data-Independent Acquisition Mass Spectrometry. J Proteome Res.

Lane, D.J., Merlot, A.M., Huang, M.L., Bae, D.H., Jansson, P.J., Sahni, S., Kalinowski, D.S., and Richardson, D.R. (2015). Cellular iron uptake, trafficking and metabolism: Key molecules and mechanisms and their roles in disease. Biochim Biophys Acta *1853*, 1130-1144.

Laplante, M., and Sabatini, D.M. (2012). mTOR signaling in growth control and disease. Cell *149*, 274-293.

Larsson, O., Morita, M., Topisirovic, I., Alain, T., Blouin, M.J., Pollak, M., and Sonenberg, N. (2012). Distinct perturbation of the translatome by the antidiabetic drug metformin. Proc Natl Acad Sci U S A *109*, 8977-8982.

Lin, S., and Garcia, B.A. (2012). Examining histone posttranslational modification patterns by high-resolution mass spectrometry. Methods Enzymol *512*, 3-28.

Lok, C.N., and Ponka, P. (1999). Identification of a hypoxia response element in the transferrin receptor gene. J Biol Chem *274*, 24147-24152.

Lowell, B.B., and Shulman, G.I. (2005). Mitochondrial dysfunction and type 2 diabetes. Science *307*, 384-387.

Lozoff, B., Jimenez, E., and Wolf, A.W. (1991). Long-term developmental outcome of infants with iron deficiency. N Engl J Med *325*, 687-694.

MacAskill, A.F., and Kittler, J.T. (2010). Control of mitochondrial transport and localization in neurons. Trends Cell Biol *20*, 102-112.

MacLean, B., Tomazela, D. M., Shulman, N., Chambers, M., Finney, G. L., Frewen, B., Kern, R., Tabb, D. L., Liebler, D. C., and MacCoss, M. J. (2010). Skyline: an open source document editor for creating and analyzing targeted proteomics experiments. Bioinformatics *26*, 966-968.

Marks, P.A., and Breslow, R. (2007). Dimethyl sulfoxide to vorinostat: development of this histone deacetylase inhibitor as an anticancer drug. Nat Biotechnol *25*, 84-90.

McLean, E., Cogswell, M., Egli, I., Wojdyla, D., and de Benoist, B. (2009). Worldwide prevalence of anaemia, WHO Vitamin and Mineral Nutrition Information System, 1993-2005. Public Health Nutr *12*, 444-454.

Mick, D.U., Fox, T.D., and Rehling, P. (2011). Inventory control: cytochrome c oxidase assembly regulates mitochondrial translation. Nat Rev Mol Cell Biol *12*, 14-20.

Morita, M., Gravel, S.P., Chenard, V., Sikstrom, K., Zheng, L., Alain, T., Gandin, V., Avizonis, D., Arguello, M., Zakaria, C.*, et al.* (2013). mTORC1 controls mitochondrial activity and biogenesis through 4E-BP-dependent translational regulation. Cell Metab *18*, 698-711.

Mouchiroud, L., Eichner, L.J., Shaw, R.J., and Auwerx, J. (2014). Transcriptional coregulators: fine-tuning metabolism. Cell Metab *20*, 26-40.

Netz, D.J., Mascarenhas, J., Stehling, O., Pierik, A.J., and Lill, R. (2014). Maturation of cytosolic and nuclear iron-sulfur proteins. Trends Cell Biol *24*, 303-312.

Nicholls, D.G., Darley-Usmar, V.M., Wu, M., Jensen, P.B., Rogers, G.W., and Ferrick, D.A. (2010). Bioenergetic profile experiment using C2C12 myoblast cells. J Vis Exp.

Nunnari, J., and Suomalainen, A. (2012). Mitochondria: in sickness and in health. Cell *148*, 1145-1159.

Pagliarini, D.J., Calvo, S.E., Chang, B., Sheth, S.A., Vafai, S.B., Ong, S.E., Walford, G.A., Sugiana, C., Boneh, A., Chen, W.K.*, et al.* (2008). A mitochondrial protein compendium elucidates complex I disease biology. Cell *134*, 112-123.

Pasini, D., Malatesta, M., Jung, H.R., Walfridsson, J., Willer, A., Olsson, L., Skotte, J., Wutz, A., Porse, B., Jensen, O.N.*, et al.* (2010). Characterization of an antagonistic switch between histone H3 lysine 27 methylation and acetylation in the transcriptional regulation of Polycomb group target genes. Nucleic Acids Res *38*, 4958-4969.

Ponka, P., and Lok, C.N. (1999). The transferrin receptor: role in health and disease. Int J Biochem Cell Biol *31*, 1111-1137.

Quiros, P.M., Espanol, Y., Acin-Perez, R., Rodriguez, F., Barcena, C., Watanabe, K., Calvo, E., Loureiro, M., Fernandez-Garcia, M.S., Fueyo, A.*, et al.* (2014). ATP-dependent Lon protease controls tumor bioenergetics by reprogramming mitochondrial activity. Cell Rep *8*, 542-556.

Quiros, P.M., Langer, T., and Lopez-Otin, C. (2015). New roles for mitochondrial proteases in health, ageing and disease. Nat Rev Mol Cell Biol *16*, 345-359.

Ramanathan, A., and Schreiber, S.L. (2009). Direct control of mitochondrial function by mTOR. Proc Natl Acad Sci U S A *106*, 22229-22232.

Rensvold, J.W., Ong, S.E., Jeevananthan, A., Carr, S.A., Mootha, V.K., and Pagliarini, D.J. (2013). Complementary RNA and protein profiling identifies iron as a key regulator of mitochondrial biogenesis. Cell Rep *3*, 237-245.

Richardson, D.R., Lane, D.J., Becker, E.M., Huang, M.L., Whitnall, M., Suryo Rahmanto, Y., Sheftel, A.D., and Ponka, P. (2010). Mitochondrial iron trafficking and the integration of iron metabolism between the mitochondrion and cytosol. Proc Natl Acad Sci U S A *107*, 10775-10782.

Robinson, P.J., An, W., Routh, A., Martino, F., Chapman, L., Roeder, R.G., and Rhodes, D. (2008). 30 nm chromatin fibre decompaction requires both H4-K16 acetylation and linker histone eviction. J Mol Biol *381*, 816-825.

Rouault, T.A. (2015). Iron-sulfur proteins hiding in plain sight. Nat Chem Biol *11*, 442-445.

Rouault, T.A., and Tong, W.H. (2005). Iron-sulphur cluster biogenesis and mitochondrial iron homeostasis. Nat Rev Mol Cell Biol *6*, 345-351.

Scarpulla, R.C. (2008). Transcriptional paradigms in mammalian mitochondrial biogenesis and function. Physiol Rev *88*, 611-638.

Scarpulla, R.C. (2012). Nucleus-encoded regulators of mitochondrial function: integration of respiratory chain expression, nutrient sensing and metabolic stress. Biochim Biophys Acta *1819*, 1088-1097.

Schiavi, A., Maglioni, S., Palikaras, K., Shaik, A., Strappazzon, F., Brinkmann, V., Torgovnick, A., Castelein, N., De Henau, S., Braeckman, B.P.*, et al.* (2015). Iron-Starvation-Induced Mitophagy Mediates Lifespan Extension upon Mitochondrial Stress in C. elegans. Curr Biol *25*, 1810-1822.

Schmidt, O., Pfanner, N., and Meisinger, C. (2010). Mitochondrial protein import: from proteomics to functional mechanisms. Nat Rev Mol Cell Biol *11*, 655-667.

Schwanhausser, B., Busse, D., Li, N., Dittmar, G., Schuchhardt, J., Wolf, J., Chen, W., and Selbach, M. (2011). Global quantification of mammalian gene expression control. Nature *473*, 337-342.

Shechter, D., Dormann, H.L., Allis, C.D., and Hake, S.B. (2007). Extraction, purification and analysis of histones. Nat Protoc *2*, 1445-1457.

Sheftel, A.D., Mason, A.B., and Ponka, P. (2012). The long history of iron in the Universe and in health and disease. Biochim Biophys Acta *1820*, 161-187.

Shimobayashi, M., and Hall, M.N. (2014). Making new contacts: the mTOR network in metabolism and signalling crosstalk. Nat Rev Mol Cell Biol *15*, 155-162.

Shogren-Knaak, M., Ishii, H., Sun, J.M., Pazin, M.J., Davie, J.R., and Peterson, C.L. (2006). Histone H4-K16 acetylation controls chromatin structure and protein interactions. Science *311*, 844-847.

Smith, B.C., and Denu, J.M. (2009). Chemical mechanisms of histone lysine and arginine modifications. Biochim Biophys Acta *1789*, 45-57.

Stiburek, L., Cesnekova, J., Kostkova, O., Fornuskova, D., Vinsova, K., Wenchich, L., Houstek, J., and Zeman, J. (2012). YME1L controls the accumulation of respiratory chain subunits and is required for apoptotic resistance, cristae morphogenesis, and cell proliferation. Mol Biol Cell *23*, 1010-1023.

Stotland, A., and Gottlieb, R.A. (2015). Mitochondrial quality control: Easy come, easy go. Biochim Biophys Acta.

Uldry, M., Yang, W., St-Pierre, J., Lin, J., Seale, P., and Spiegelman, B.M. (2006). Complementary action of the PGC-1 coactivators in mitochondrial biogenesis and brown fat differentiation. Cell Metab *3*, 333-341.

Vafai, S.B., and Mootha, V.K. (2012). Mitochondrial disorders as windows into an ancient organelle. Nature *491*, 374-383.

Vega, R.B., Horton, J.L., and Kelly, D.P. (2015). Maintaining ancient organelles: mitochondrial biogenesis and maturation. Circ Res *116*, 1820-1834.

Venkatesh, S., and Workman, J.L. (2015). Histone exchange, chromatin structure and the regulation of transcription. Nat Rev Mol Cell Biol *16*, 178-189.

Wallace, D.C. (1999). Mitochondrial diseases in man and mouse. Science *283*, 1482-1488.

Wallace, D.C. (2005). A mitochondrial paradigm of metabolic and degenerative diseases, aging, and cancer: a dawn for evolutionary medicine. Annu Rev Genet *39*, 359-407.

Wallace, D.C., and Fan, W. (2010). Energetics, epigenetics, mitochondrial genetics. Mitochondrion *10*, 12-31.

Xu, W.S., Parmigiani, R.B., and Marks, P.A. (2007). Histone deacetylase inhibitors: molecular mechanisms of action. Oncogene *26*, 5541-5552.

Yoon, Y.S., Yoon, D.S., Lim, I.K., Yoon, S.H., Chung, H.Y., Rojo, M., Malka, F., Jou, M.J., Martinou, J.C., and Yoon, G. (2006). Formation of elongated giant mitochondria in DFO-induced cellular senescence: involvement of enhanced fusion process through modulation of Fis1. J Cell Physiol *209*, 468-480.

Youle, R.J., and Narendra, D.P. (2011). Mechanisms of mitophagy. Nat Rev Mol Cell Biol *12*, 9-14.

Zentner, G.E., and Henikoff, S. (2013). Regulation of nucleosome dynamics by histone modifications. Nat Struct Mol Biol *20*, 259-266.

Zhou, V.W., Goren, A., and Bernstein, B.E. (2011). Charting histone modifications and the functional organization of mammalian genomes. Nat Rev Genet *12*, 7-18.

Zurita Rendon, O., and Shoubridge, E.A. (2012). Early complex I assembly defects result in rapid turnover of the ND1 subunit. Hum Mol Genet *21*, 3815-3824.

3.7 Figures

Figure 1: Iron Deprivation Causes Discordance Between Mitochondrial Transcripts, Proteins and Metabolic Activity

(A-C) Timecourse analyses of OxPhos mRNA and protein abundance in C2C12 mouse myoblasts following DFO treatment as assessed by real-time qPCR and immunoblotting (immunoblots are shown in Figure S1) and quantified with densitometry, respectively. For real-time qPCR relative quantification, the 0 hour timepoint was used as the calibrator sample and *Rplp0* as the endogenous control, and for each timepoint, the level of the mRNAs and proteins from the DFO treated samples are shown relative to the untreated samples. Data are displayed as mean ± SEM of biological triplicate measurements (*$p < 0.05$, **$p < 0.01$, Student's t test).

(A) OxPhos proteins that decrease before their corresponding mRNAs.

(B) OxPhos protein (Cox4i1) that decreases without any change in its corresponding mRNA.

(C) OxPhos mRNAs that decrease but show no change in their corresponding proteins.

(D) Oxygen consumption rate/extracellular acidification rate (OCR/ECAR) of myoblasts treated with the indicated concentrations of DFO. Data are displayed as mean ± SD of 22-24 replicates. See also Figure S1.

Figure 1

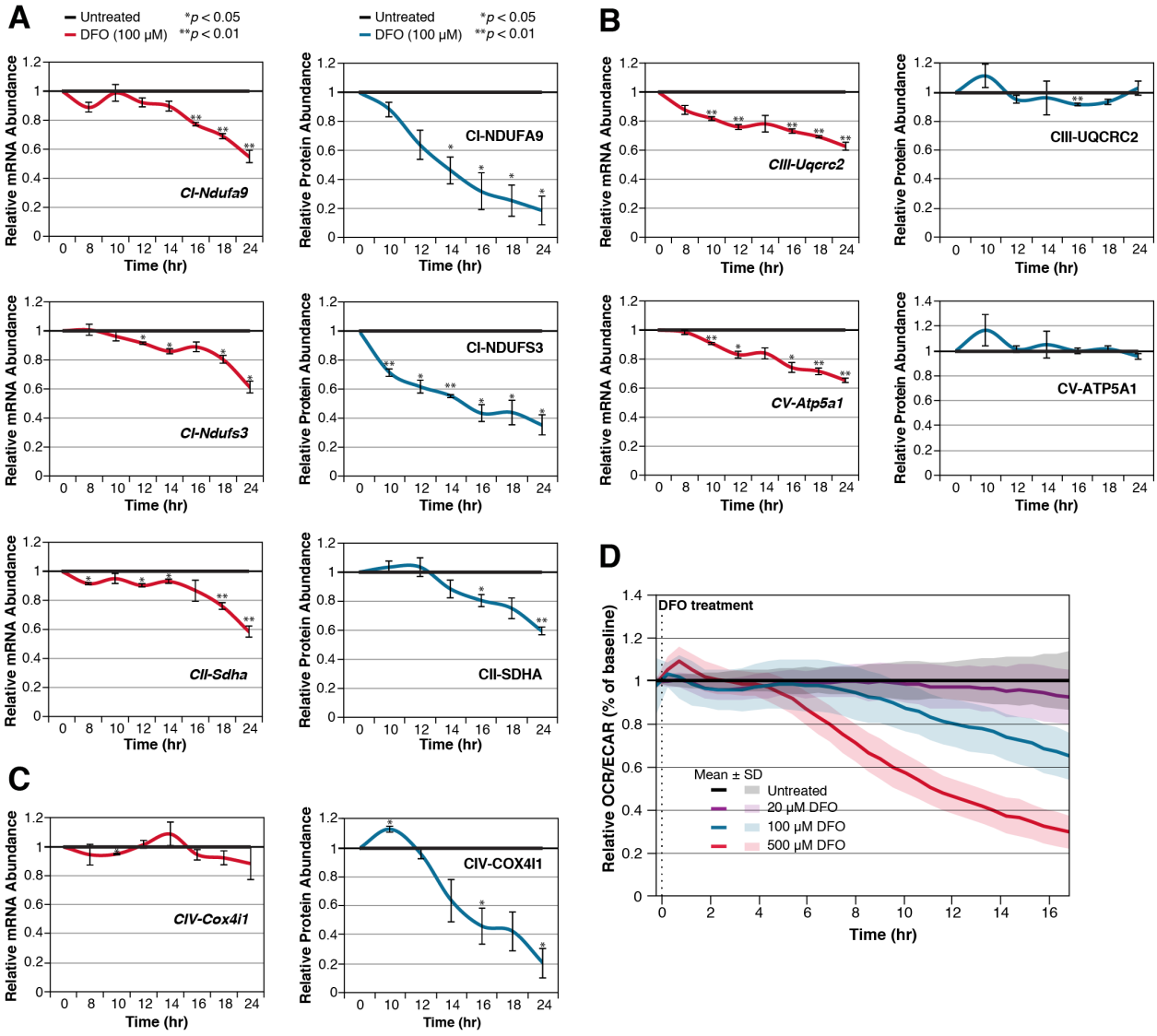
A
Untreated
DFO (100 μM)
*p < 0.05
**p < 0.01
Relative mRNA Abundance
Relative Protein Abundance
Time (hr)
CI-Ndufa9
CI-NDUFA9
CI-Ndufs3
CI-NDUFS3
CII-Sdha
CII-SDHA
CIV-Cox4i1
CIV-COX4I1
B
CIII-Uqcrc2
CIII-UQCRC2
CV-Atp5a1
CV-ATP5A1
C
D
DFO treatment
Relative OCR/ECAR (% of baseline)
Mean ± SD
Untreated
20 μM DFO
100 μM DFO
500 μM DFO

Figure 2: Iron Deprivation Leads to a Decrease in nDNA Mitochondrial Gene Transcription

(A) Ethylene uridine (EU) pulse-chase strategy for analysis of transcript decay.

(B) Timecourse analysis of mRNA degradation and calculated half-lives from DFO treated C2C12 myoblasts as assessed by real-time qPCR. Data are displayed as mean ± SEM of biological triplicate measurements (*$p < 0.05$, Student's t test).

(C) Ethylene uridine (EU) pulse labeling strategy for analysis of transcript synthesis.

(D) Timecourse analysis of mRNA synthesis in C2C12 myoblasts following DFO treatment as assessed by real-time qPCR. Data are displayed as mean ± SEM of biological triplicate measurements (*$p < 0.05$, **$p < 0.01$, Student's t test).

See also Figure S2.

Figure 2

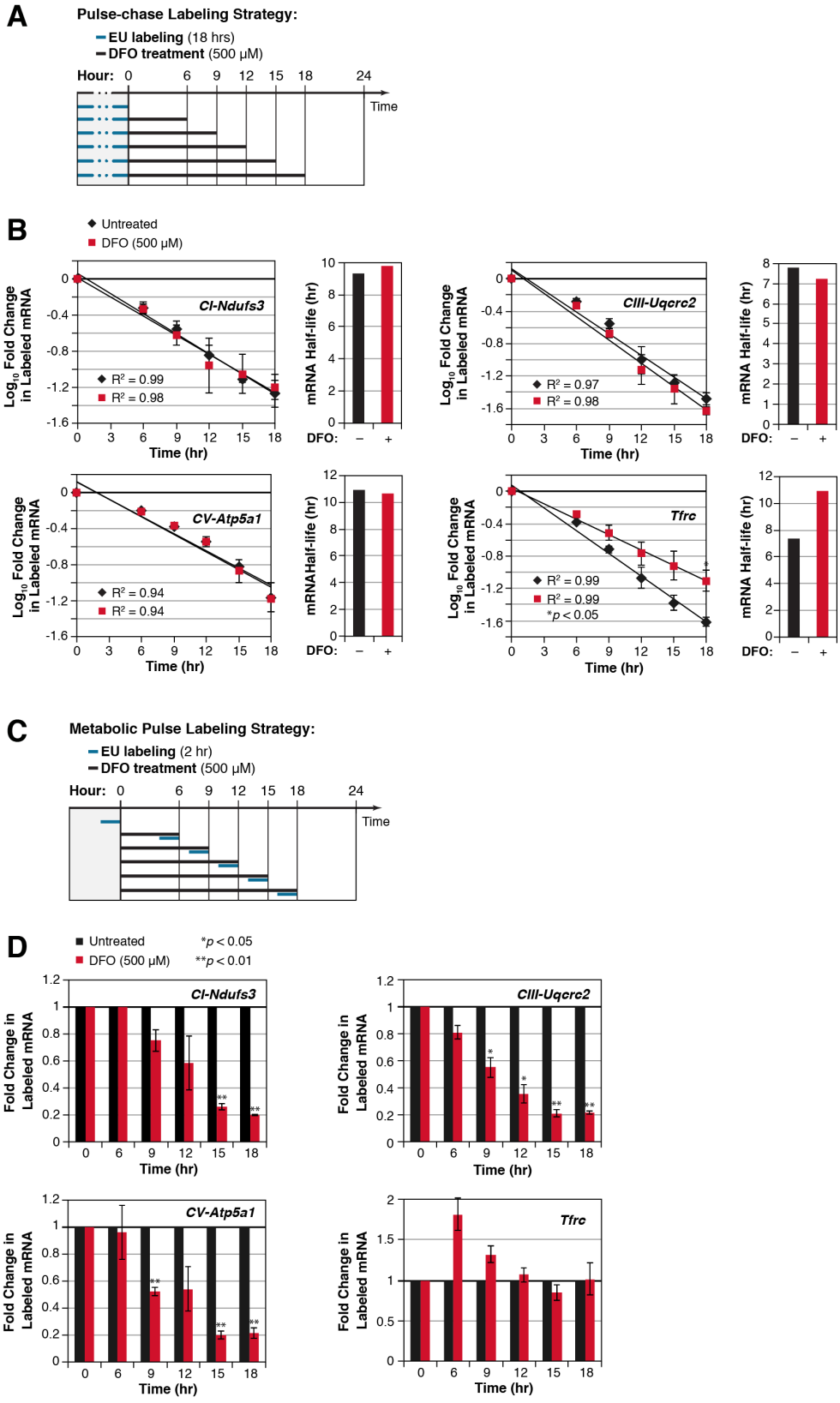
A
Pulse-chase Labeling Strategy:
EU labeling (18 hrs)
DFO treatment (500 μM)
Hour: 0 6 9 12 15 18 24
Time
B
Untreated
DFO (500 μM)
Cl-Ndufs3
CIII-Uqcrc2
CV-Atp5a1
Tfrc
Log10 Fold Change in Labeled mRNA
mRNA Half-life (hr)
Time (hr)
DFO: – +
R² = 0.99
R² = 0.98
R² = 0.97
R² = 0.94
*p < 0.05
C
Metabolic Pulse Labeling Strategy:
EU labeling (2 hr)
DFO treatment (500 μM)
Hour: 0 6 9 12 15 18 24
Time
D
Untreated
DFO (500 μM)
*p < 0.05
**p < 0.01
Fold Change in Labeled mRNA
Cl-Ndufs3
CIII-Uqcrc2
CV-Atp5a1
Tfrc
Time (hr)

Figure 3. The Mitochondrial Transcriptional Response to Iron Deprivation is Independent of PGC-1α and HIF-1α

(A) Level of the indicated mRNAs in wild type or PGC-1α$^{-/-}$ brown preadipocytes after 100 μM DFO treatment for 24 hrs. Data are displayed as the mean of technical triplicate measurements. **(B)** Level of the indicated mRNAs in wild type or HIF-1α$^{-/-}$ MEFs after 100 μM DFO treatment for 24 hrs. Data are displayed as mean of technical triplicate measurements.

Figure 3

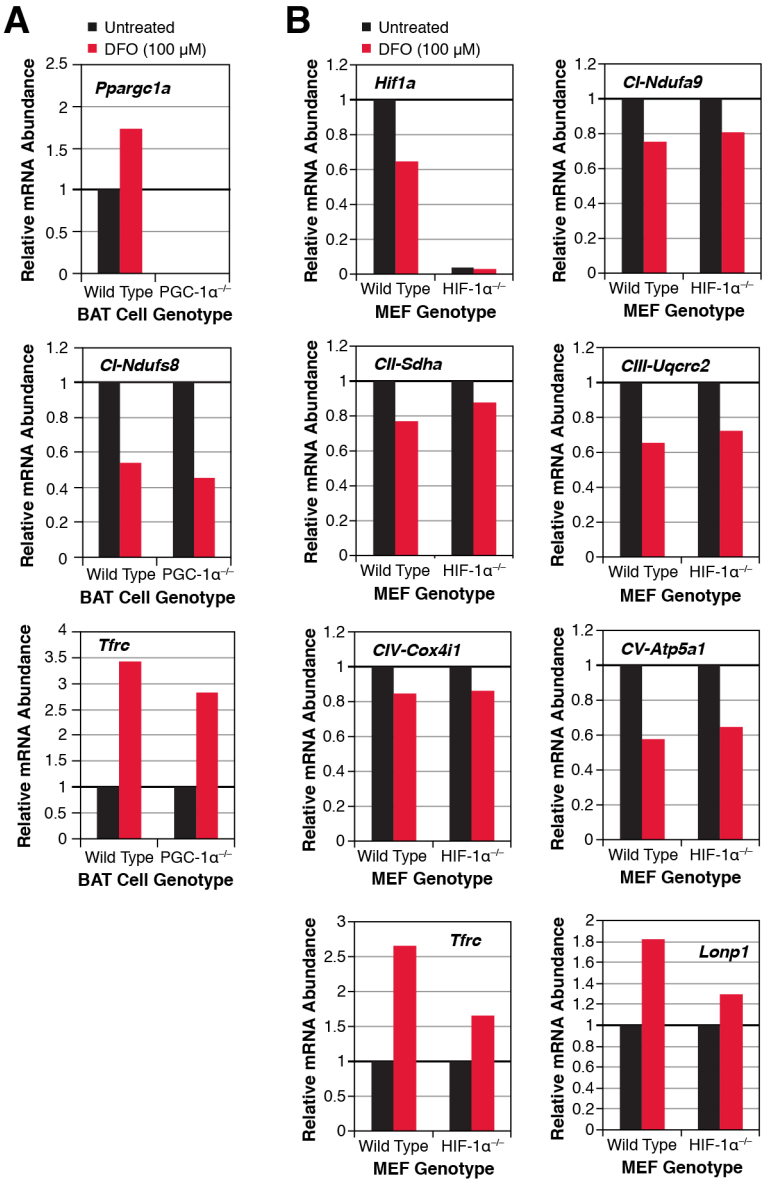
A
B
Untreated
DFO (100 μM)
Relative mRNA Abundance
Ppargc1a
Hif1a
Cl-Ndufa9
Cl-Ndufs8
CII-Sdha
CIII-Uqcrc2
Tfrc
CIV-Cox4i1
CV-Atp5a1
Tfrc
Lonp1
Wild Type
PGC-1α−/−
HIF-1α−/−
BAT Cell Genotype
MEF Genotype

Figure 4. mTOR Inhibition Does Not Induce a Similar Mitochondrial Response to Iron Deprivation

Level of the indicated proteins and phosphoproteins from C2C12 mouse myoblasts treated with the indicated concentrations of **(A)** rapamycin or **(B)** PP242 ± 100 μM DFO for 24 hrs as assessed by immunoblotting.

Figure 4

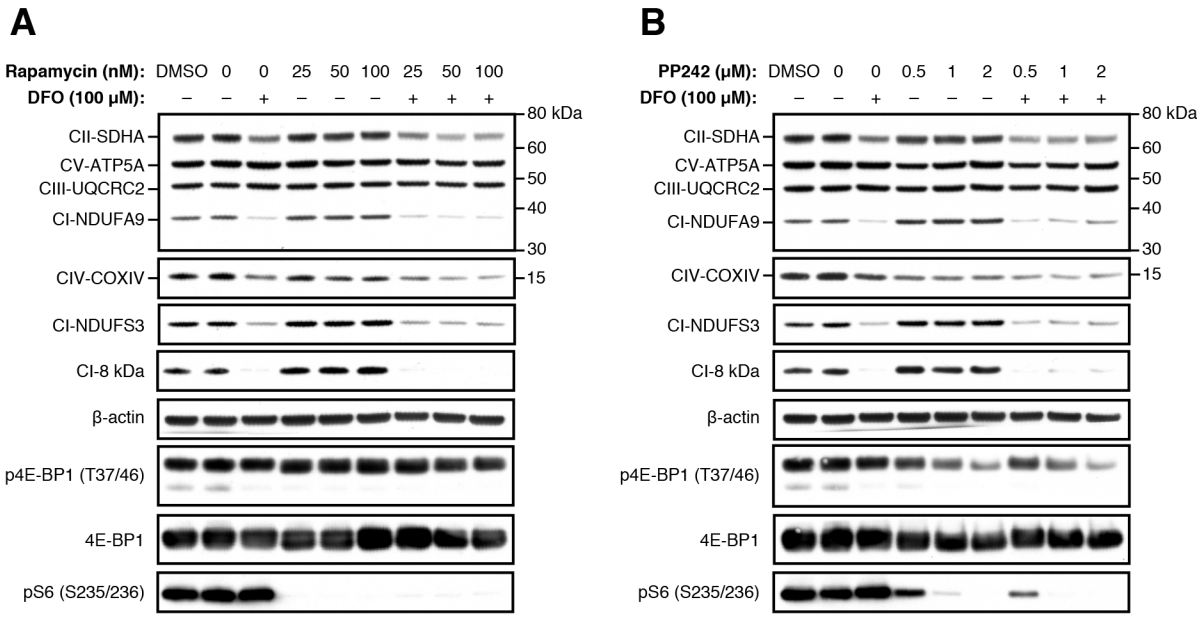
A
Rapamycin (nM): DMSO 0 0 25 50 100 25 50 100
DFO (100 μM): – – + – – – + + +
80 kDa
60
50
40
30
15
CII-SDHA
CV-ATP5A
CIII-UQCRC2
CI-NDUFA9
CIV-COXIV
CI-NDUFS3
CI-8 kDa
β-actin
p4E-BP1 (T37/46)
4E-BP1
pS6 (S235/236)
B
PP242 (μM): DMSO 0 0 0.5 1 2 0.5 1 2
DFO (100 μM): – – + – – – + + +
80 kDa
60
50
40
30
15
CII-SDHA
CV-ATP5A
CIII-UQCRC2
CI-NDUFA9
CIV-COXIV
CI-NDUFS3
CI-8 kDa
β-actin
p4E-BP1 (T37/46)
4E-BP1
pS6 (S235/236)

Figure 5. LONP1 Protease Knockdown Does Not Affect the Mitochondrial Response to Iron Deprivation

(A) Protein and **(B)** mRNA levels in HEK 293 cells after 1 day, 2 days and 5 days of siRNA mediated knockdown of LONP1 or treatment with siRNA non-targeting (NT) control ± 100 μM DFO treatment for 24 hrs. Data are displayed as the mean of technical triplicate measurements. See also Figure S3.

Figure 5

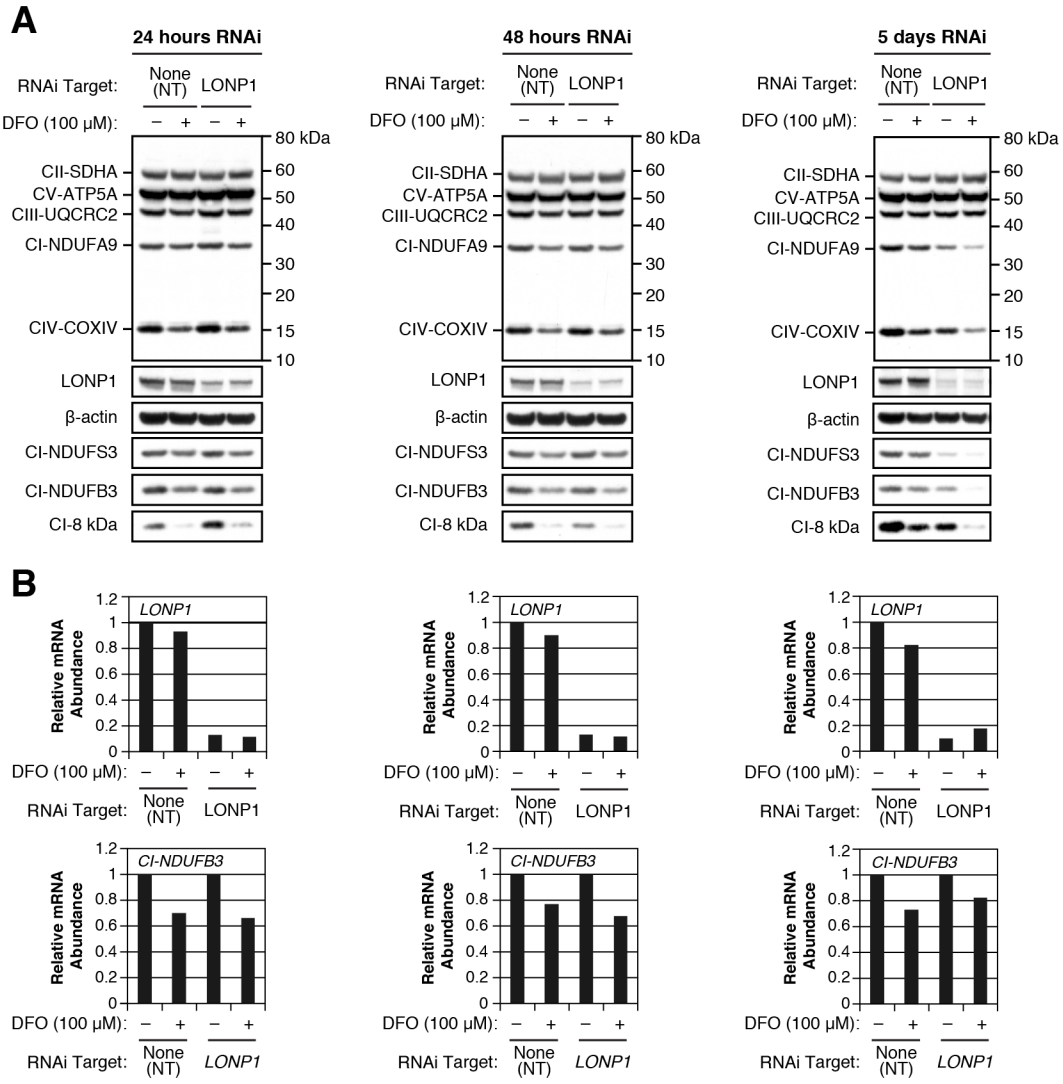
A
24 hours RNAi
48 hours RNAi
5 days RNAi
RNAi Target:
None (NT)
LONP1
DFO (100 μM):
– + – +
80 kDa
CII-SDHA
CV-ATP5A
CIII-UQCRC2
CI-NDUFA9
CIV-COXIV
LONP1
β-actin
CI-NDUFS3
CI-NDUFB3
CI-8 kDa
60
50
40
30
20
15
10
B
Relative mRNA Abundance
LONP1
CI-NDUFB3
1.2
1
0.8
0.6
0.4
0.2
0
LONP1

Figure 6: Iron Deprivation Causes Dynamic Changes in Histone Acetylation and Methylation

(A) Experimental workflow for the analysis of mitochondrial response and recovery following iron deprivation. Myoblasts were treated with 100 μM DFO for 24 hrs then passaged every 24 hrs in DFO free media. Histone modifications were examined at 12 hrs (day 0.5) and 24 hrs (day 1) following DFO treatment, then 48 hr (day 3) and 96 hr (day 5) following the passage of DFO treated myoblasts into DFO-free media.

(B-E) Heatmaps displaying the $\log_2$ fold-change for unmodified, acetylated and methylated histone H3 and H4 peptides from histone extracts as assessed by LC-MS/MS. Red indicates higher abundance and blue indicates lower abundance. Data are displayed as the mean of biological triplicate measurements (*$p < 0.05$, **$p < 0.01$, ***$p < 0.001$, Student's t test).

(F) Level of the indicated histone post-translational modifications (PTMs) from histone extracts as assessed by immunoblotting.

See also Figure S4.

Figure 6

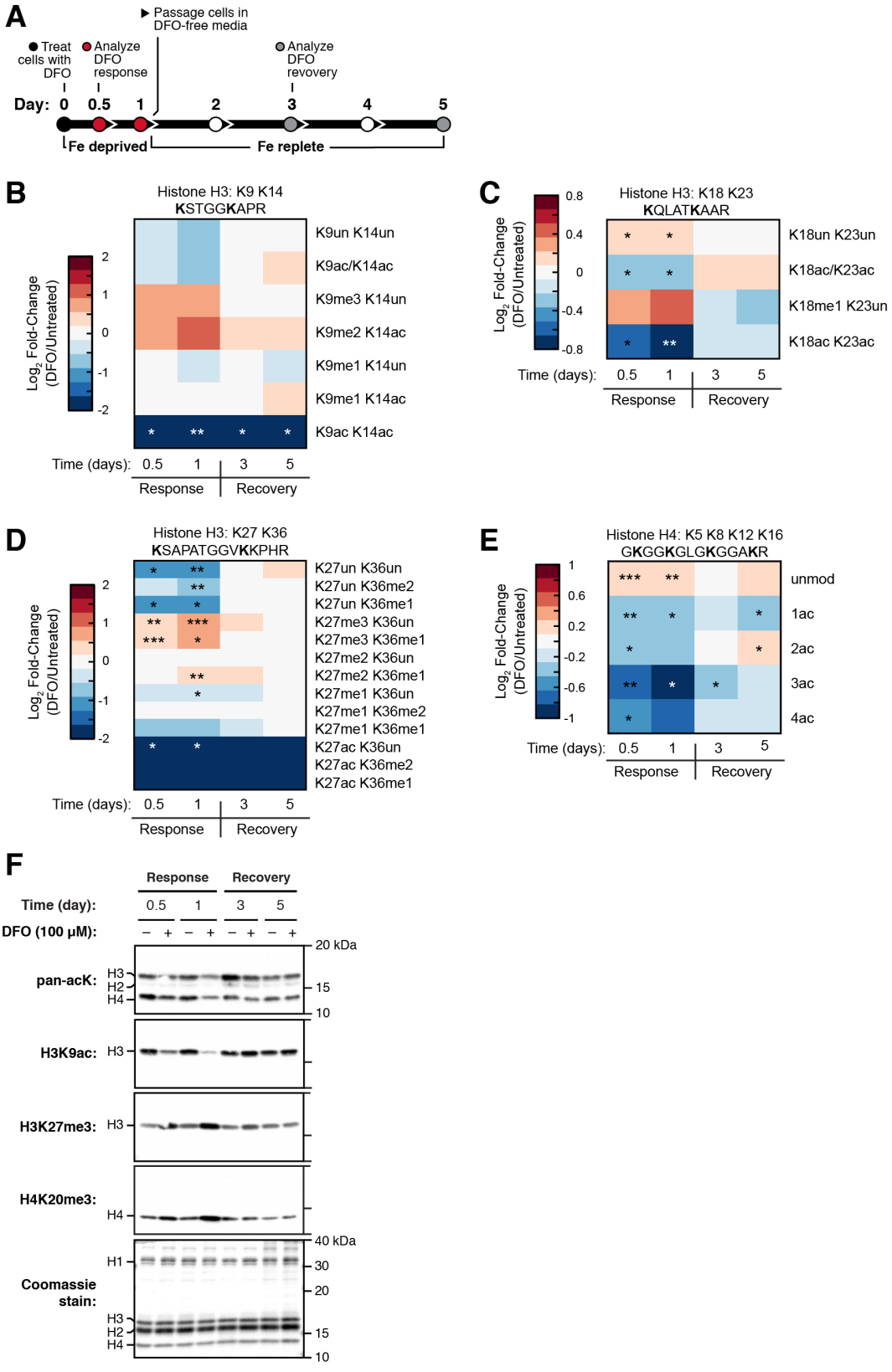
A
Passage cells in DFO-free media
Treat cells with DFO
Analyze DFO response
Analyze DFO revovery
Day: 0 0.5 1 2 3 4 5
Fe deprived
Fe replete
B
Histone H3: K9 K14
KSTGGKAPR
Log2 Fold-Change (DFO/Untreated)
K9un K14un
K9ac/K14ac
K9me3 K14un
K9me2 K14ac
K9me1 K14un
K9me1 K14ac
K9ac K14ac
Time (days): 0.5 1 3 5
Response
Recovery
C
Histone H3: K18 K23
KQLATKAAR
K18un K23un
K18ac/K23ac
K18me1 K23un
K18ac K23ac
D
Histone H3: K27 K36
KSAPATGGVKKPHR
K27un K36un
K27un K36me2
K27un K36me1
K27me3 K36un
K27me3 K36me1
K27me2 K36un
K27me2 K36me1
K27me1 K36un
K27me1 K36me2
K27me1 K36me1
K27ac K36un
K27ac K36me2
K27ac K36me1
E
Histone H4: K5 K8 K12 K16
GKGGKGLGKGGAKR
unmod
1ac
2ac
3ac
4ac
F
Response
Recovery
Time (day): 0.5 1 3 5
DFO (100 µM): − + − + − + − +
pan-acK:
H3K9ac:
H3K27me3:
H4K20me3:
Coomassie stain:
20 kDa
15
10
40 kDa
30
20
H1
H2
H3
H4

Figure 7: Acetylation at nDNA-Encoded Mitochondrial Genes is Decreased Upon Iron Deprivation

(A) Chromatin immunoprecipitation (ChIP) followed by real-time qPCR analysis of H3K9ac and H3K27me3 levels within 1 kilobase after the transcription start site (TSS) of the indicated genes from C2C12 cells treated with 100 μM DFO for 24 hrs. Data are displayed as the mean of technical triplicate measurements.

Figure 7

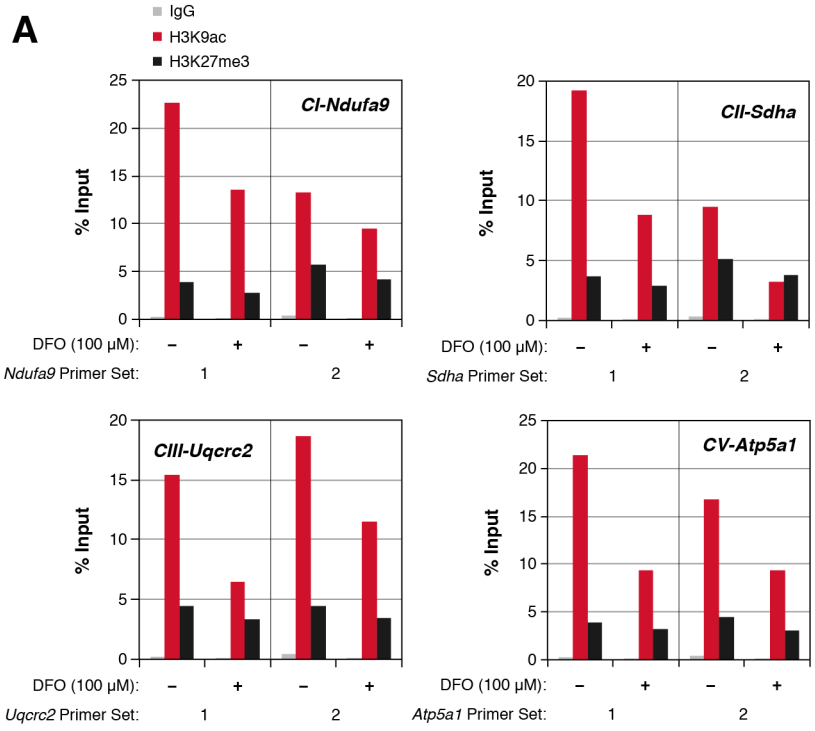
A
IgG
H3K9ac
H3K27me3
CI-Ndufa9
CII-Sdha
CIII-Uqcrc2
CV-Atp5a1
% Input
DFO (100 μM): – + – +
Ndufa9 Primer Set: 1 2
Sdha Primer Set: 1 2
Uqcrc2 Primer Set: 1 2
Atp5a1 Primer Set: 1 2

Figure 8: Histone Deacetylase Inhibition Blocks the Iron-Deprivation Induced Mitochondrial Biogenesis Response

C2C12 myoblasts were treated with the indicated concentrations of the histone deacetylase (HDAC) inhibitor SAHA (suberoylanilide hydroxamic acid) ± 100 μM DFO for 24 hrs.

(A) Abundance of the indicated mRNAs as assessed by real-time qPCR. Data are displayed as mean ± SEM of biological triplicate measurements (*$p < 0.05$, **$p < 0.01$, Student's t test).

(B) Abundance of the indicated proteins as assessed by immunoblotting.

(C) Abundance of the indicated histone post-translational modifications (PTMs) from histone extracts as assessed by immunoblotting.

See also Figure S5.

Figure 8

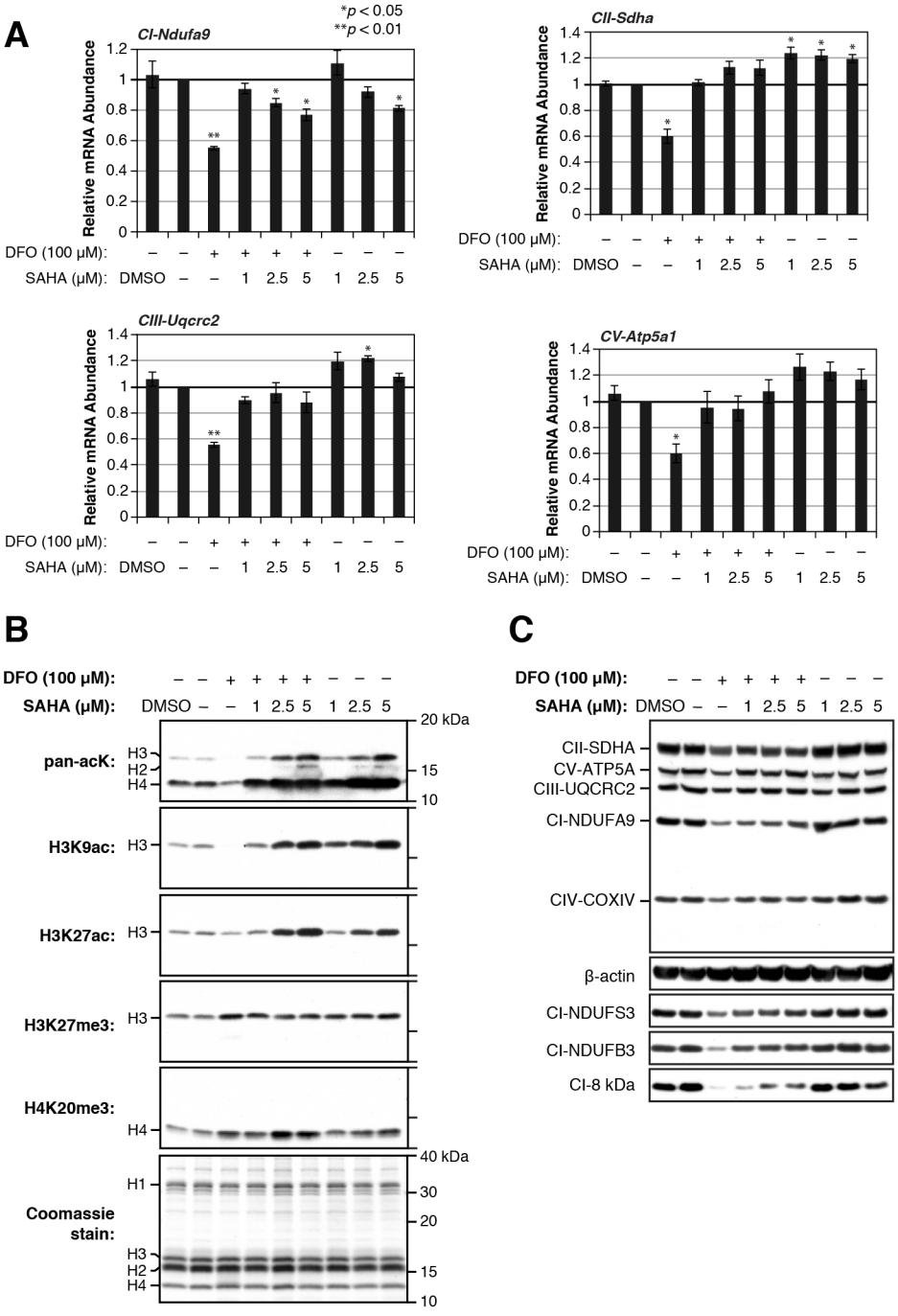
A
*p < 0.05
**p < 0.01
CI-Ndufa9
CII-Sdha
CIII-Uqcrc2
CV-Atp5a1
Relative mRNA Abundance
DFO (100 μM):
SAHA (μM): DMSO
B
DFO (100 μM):
SAHA (μM): DMSO
pan-acK:
H3K9ac:
H3K27ac:
H3K27me3:
H4K20me3:
Coomassie stain:
H1
H2
H3
H4
20 kDa
15
10
40 kDa
30
20
C
DFO (100 μM):
SAHA (μM): DMSO
CII-SDHA
CV-ATP5A
CIII-UQCRC2
CI-NDUFA9
CIV-COXIV
β-actin
CI-NDUFS3
CI-NDUFB3
CI-8 kDa

Figure 9. Mitochondrial mRNA and Protein Expression are Decrease in a Mouse Model of Iron Deficiency

(A) Schematic of the mouse analysis. Mice were maintained on a normal-diet or an iron-deficient diet for three weeks, after which four tissues were processed for real-time qPCR and immunoblot analysis.

(B) Abundance of the indicated mRNAs and **(C)** level of the indicated proteins in the liver, soleus muscle, and heart of pair-fed (n = 6) and iron-deprived mice (n = 5). Data are displayed as mean ± SEM of biological triplicate measurements (*$p < 0.05$, **$p < 0.01$, ***$p < 0.001$, Student's t test).

Figure 9

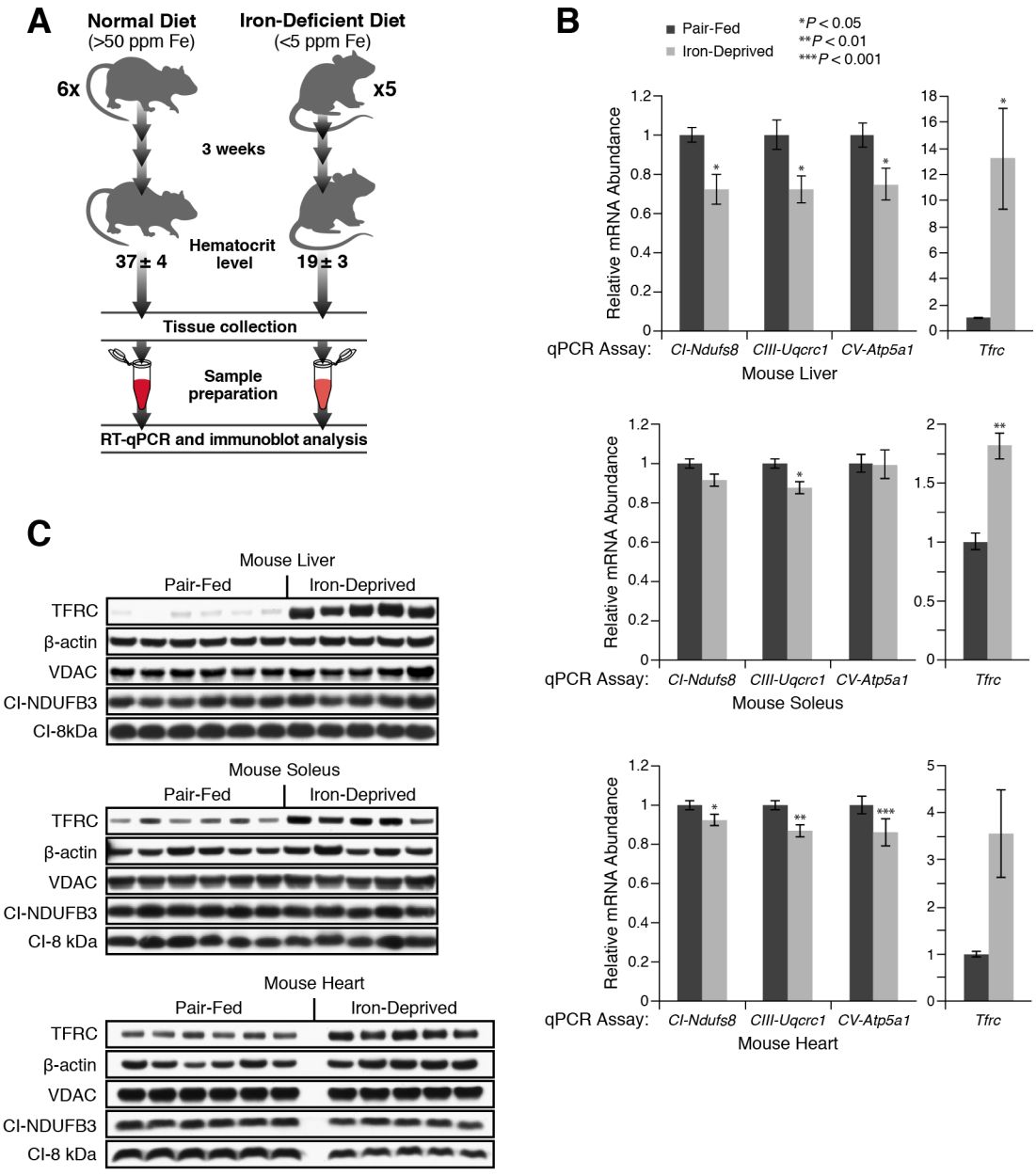
A
Normal Diet
(>50 ppm Fe)
Iron-Deficient Diet
(<5 ppm Fe)
6x
x5
3 weeks
Hematocrit level
37 ± 4
19 ± 3
Tissue collection
Sample preparation
RT-qPCR and immunoblot analysis
B
Pair-Fed
Iron-Deprived
*P < 0.05
**P < 0.01
***P < 0.001
Relative mRNA Abundance
qPCR Assay:
CI-Ndufs8
CIII-Uqcrc1
CV-Atp5a1
Tfrc
Mouse Liver
Mouse Soleus
Mouse Heart
C
Mouse Liver
Pair-Fed
Iron-Deprived
TFRC
β-actin
VDAC
CI-NDUFB3
CI-8kDa
Mouse Soleus
CI-8 kDa
Mouse Heart

Figure 10: Proposed Models for the Mitochondrial Biogenesis Adaptive Response to Iron Deprivation

(A) Model 1: Iron deprivation has independent effects on mitochondrial proteins/function and on histone PTMs. The histone PTM changes lead to decreased transcription and levels of mitochondrial transcripts. The reduction in mitochondrial transcripts further decreases the level of mitochondrial proteins.

(B) Model 2: Iron deprivation first affect mitochondrial proteins and function, and through retrograde signaling leads to changes in histone PTMs, decreased transcription and a reduction in mitochondrial transcripts. Decreased levels of mitochondrial transcripts further affect mitochondrial proteins and function.

Figure 10

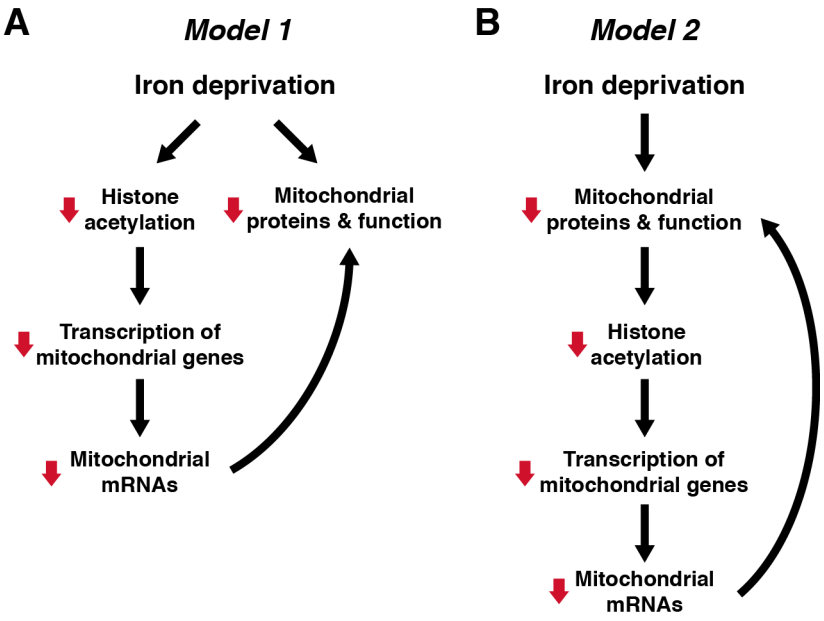
A
Model 1
Iron deprivation
Histone acetylation
Mitochondrial proteins & function
Transcription of mitochondrial genes
Mitochondrial mRNAs
B
Model 2
Iron deprivation
Mitochondrial proteins & function
Histone acetylation
Transcription of mitochondrial genes
Mitochondrial mRNAs

3.8 Supplemental Figures

Figure S1: Proposed Models for the Mitochondrial Biogenesis Adaptive Response to Iron Deprivation, Related to Figure 1

(A) Timecourse analysis of the indicated proteins from C2C12 myoblasts treated with 100 μM DFO for 24 hrs as assessed by immunoblotting and **(B)** quantified with densitometry. For each timepoint, the level of the proteins from the DFO treated samples are shown relative to the untreated samples.

(C) Additional replicate measuring the oxygen consumption rate/extracellular acidification rate (OCR/ECAR) ratio of myoblasts treated with the indicated concentrations of DFO. Data are displayed as mean ± SD of 22-24 replicates.

Figure S1

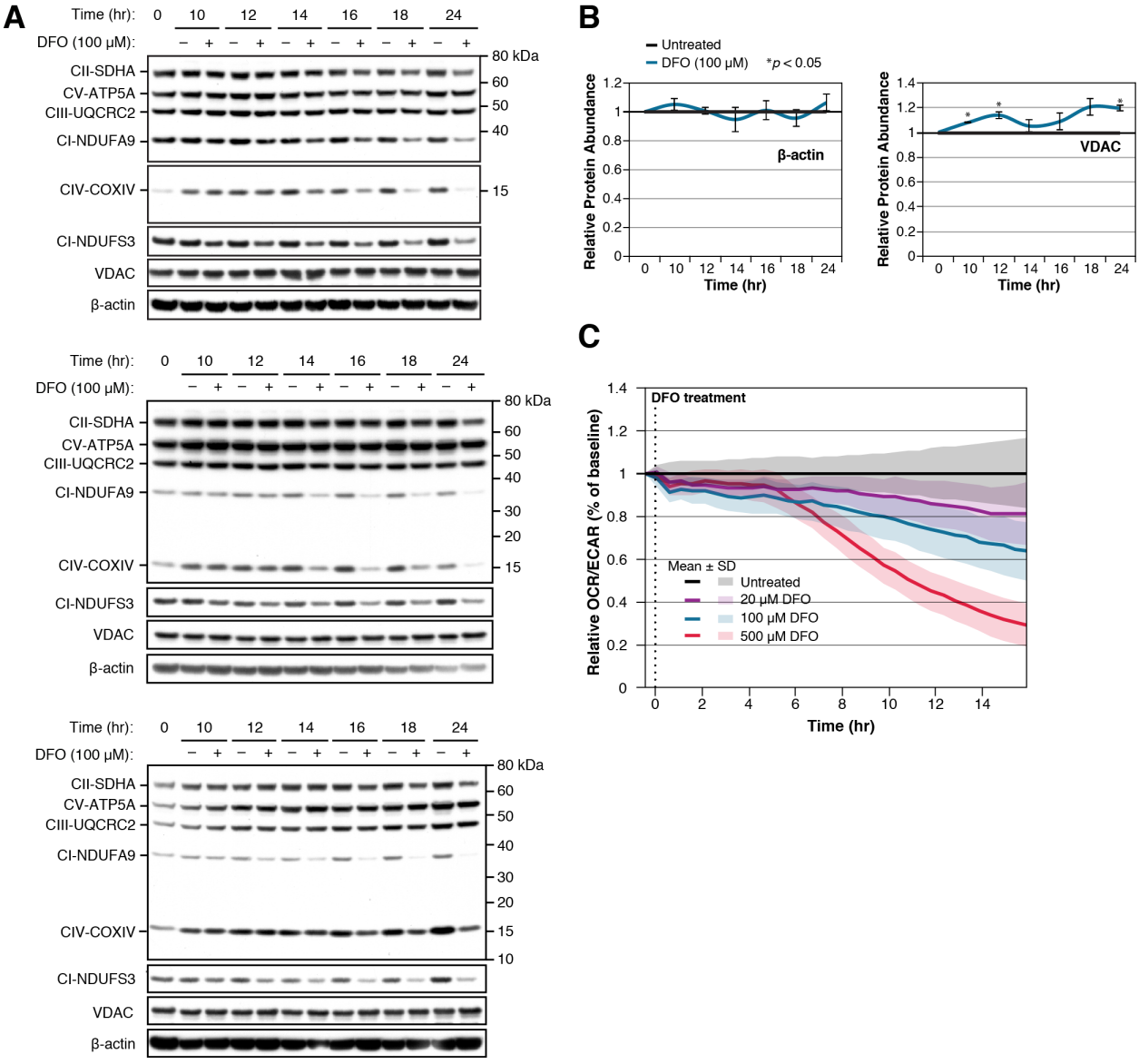
A
Time (hr): 0 10 12 14 16 18 24
DFO (100 μM): – + – + – + – + – + – +
CII-SDHA
CV-ATP5A
CIII-UQCRC2
CI-NDUFA9
CIV-COXIV
CI-NDUFS3
VDAC
β-actin
80 kDa
60
50
40
30
20
15
10
B
Untreated
DFO (100 μM)
*p < 0.05
Relative Protein Abundance
β-actin
VDAC
Time (hr)
C
DFO treatment
Relative OCR/ECAR (% of baseline)
Mean ± SD
Untreated
20 μM DFO
100 μM DFO
500 μM DFO
Time (hr)

Figure S2: Iron Deprivation Decreases the Synthesis of Nuclear-Encoded Mitochondrial mRNAs but Does Not Increase mRNA Degradation, Related to Figure 2

(A) Timecourse analysis of mRNA degradation and calculated half-lives from DFO treated C2C12 myoblasts as assessed by real-time qPCR. Data are displayed as mean ± SEM of biological triplicate measurements.

(B) Average half-life of transcripts encoding protein subunits from each OxPhos complex (calculated from Schwanhäusser, et al., 2011).

(C) Timecourse analysis of mRNA synthesis in C2C12 myoblasts following DFO treatment as assessed by real-time qPCR. Data are displayed as mean ± SEM of biological triplicate measurements (*$p < 0.05$, **$p < 0.01$, Student's t test).

Figure S2

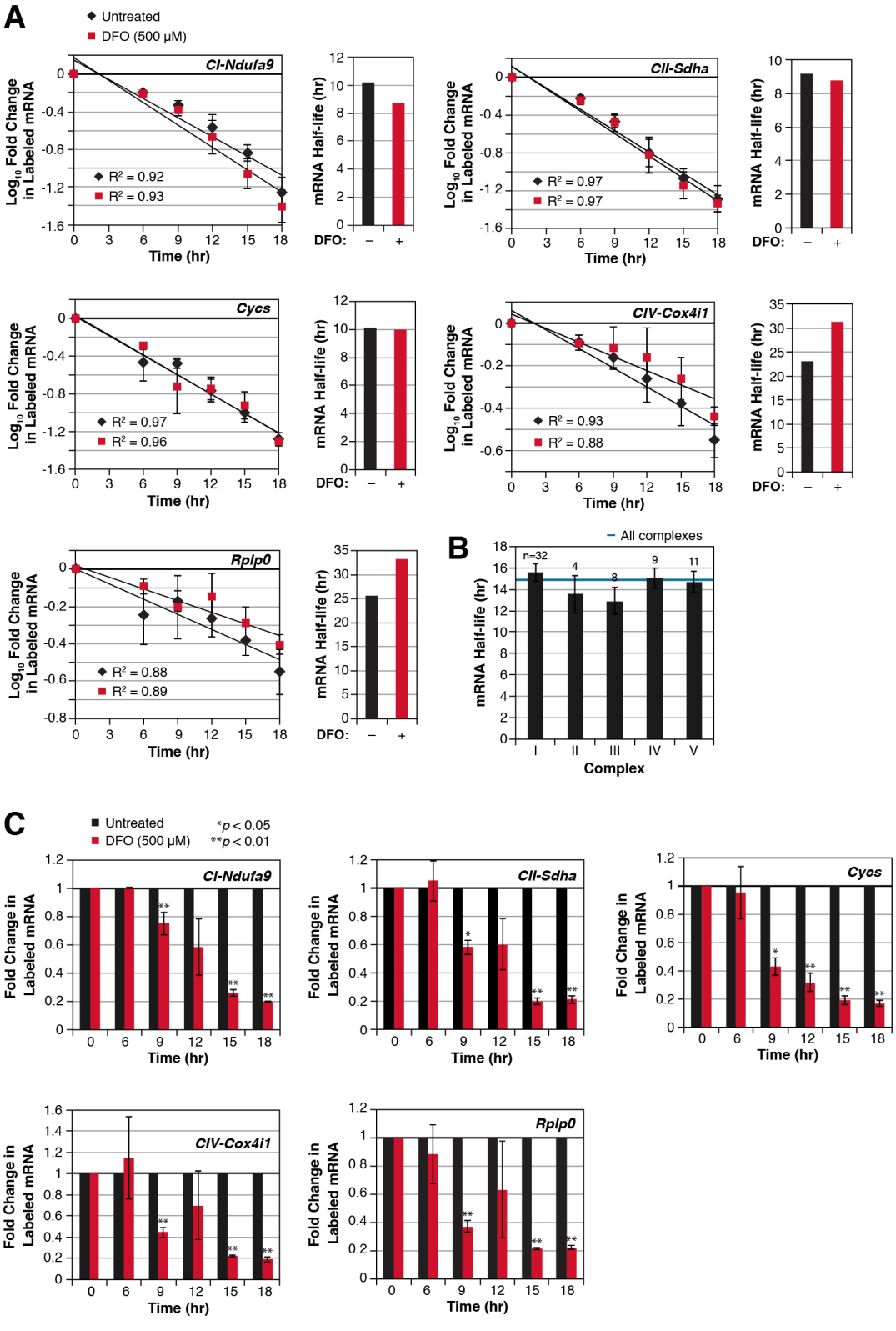
A
Untreated
DFO (500 μM)
CI-Ndufa9
CII-Sdha
Cycs
CIV-Cox4i1
Rplp0
Log10 Fold Change in Labeled mRNA
mRNA Half-life (hr)
Time (hr)
DFO: – +
R² = 0.92
R² = 0.93
R² = 0.97
R² = 0.97
R² = 0.97
R² = 0.96
R² = 0.93
R² = 0.88
R² = 0.88
R² = 0.89
B
All complexes
n=32
4
8
9
11
Complex
I
II
III
IV
V
C
Untreated
DFO (500 μM)
*p < 0.05
**p < 0.01
Fold Change in Labeled mRNA
Time (hr)

Figure S3: Iron Deprivation Changes the Expression of Mitochondrial Proteases, Related to Figure 5

(A) Abundance of transcripts encoding the major mitochondrial quality control proteases in C2C12 myoblasts at the indicated time points following treatment with 100 μM DFO as assessed by real-time qPCR. Data are displayed as mean ± SEM of biological triplicate measurements (*$p < 0.05$, **$p < 0.01$, Student's t test).

(B) Protein and **(C)** mRNA levels in HEK 293 cells after 48 hrs of siRNA mediated knockdown of the indicated proteins or treatment with siRNA non-targeting (NT) control ± 100 μM DFO treatment for 24 hrs. Data are displayed as the mean of technical triplicate measurements.

Figure S3

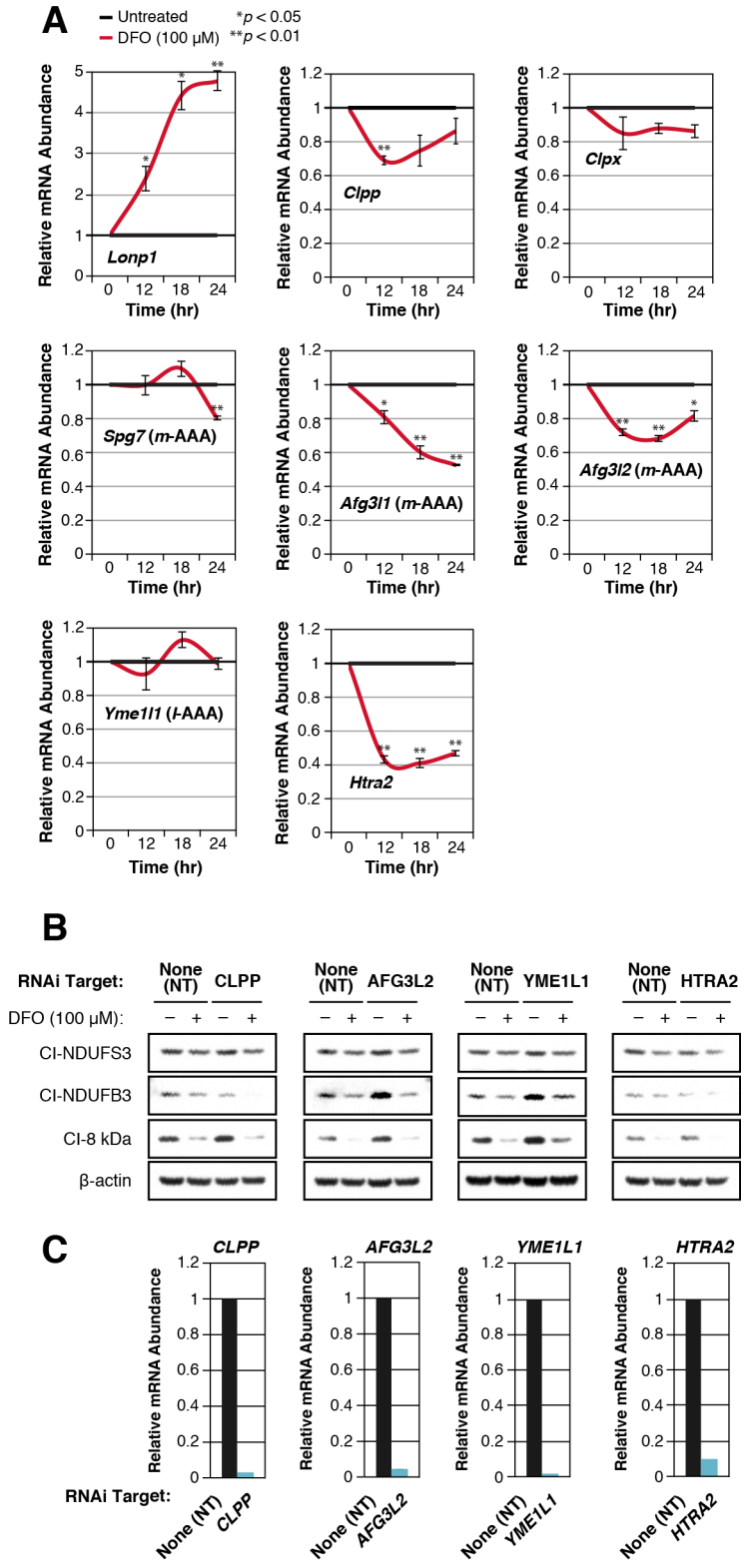
A
Untreated
DFO (100 μM)
*p < 0.05
**p < 0.01
Relative mRNA Abundance
Time (hr)
Lonp1
Clpp
Clpx
Spg7 (m-AAA)
Afg3l1 (m-AAA)
Afg3l2 (m-AAA)
Yme1l1 (i-AAA)
Htra2
B
RNAi Target:
None (NT)
CLPP
AFG3L2
YME1L1
HTRA2
DFO (100 μM):
CI-NDUFS3
CI-NDUFB3
CI-8 kDa
β-actin
C
CLPP
AFG3L2
YME1L1
HTRA2
RNAi Target:
None (NT)

Figure S4: Dynamic Changes in Histone Acetylation and Methylation during Iron Deprivation and Recovery, Related to Figure 6

(A) Heatmap displaying the $\log_2$ fold-change for unmodified, acetylated and methylated histone H3 and H4 peptides from histone extracts of myoblasts treated with 100 μM DFO for 24 hrs then passaged every 24 hrs in DFO free media as assessed by LC-MS/MS. Histone modifications were examined at 12 hrs (day 0.5) and 24 hrs (day 1) following DFO treatment, then 48 hr (day 3) and 96 hr (day 5) following the passage of DFO treated myoblasts into DFO-free media. Red indicates higher abundance and blue indicates lower abundance. Data are displayed as the mean of biological triplicate measurements.

Figure S4

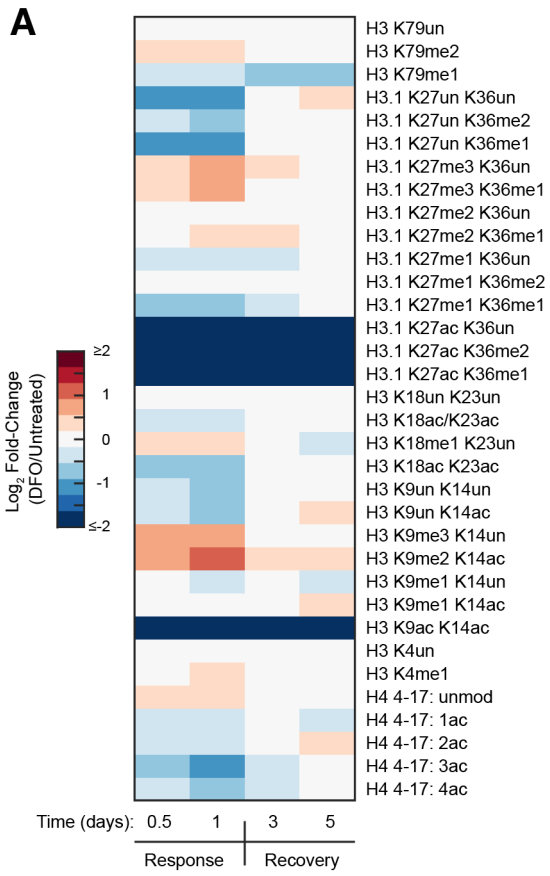
A
H3 K79un
H3 K79me2
H3 K79me1
H3.1 K27un K36un
H3.1 K27un K36me2
H3.1 K27un K36me1
H3.1 K27me3 K36un
H3.1 K27me3 K36me1
H3.1 K27me2 K36un
H3.1 K27me2 K36me1
H3.1 K27me1 K36un
H3.1 K27me1 K36me2
H3.1 K27me1 K36me1
H3.1 K27ac K36un
H3.1 K27ac K36me2
H3.1 K27ac K36me1
H3 K18un K23un
H3 K18ac/K23ac
H3 K18me1 K23un
H3 K18ac K23ac
H3 K9un K14un
H3 K9un K14ac
H3 K9me3 K14un
H3 K9me2 K14ac
H3 K9me1 K14un
H3 K9me1 K14ac
H3 K9ac K14ac
H3 K4un
H3 K4me1
H4 4-17: unmod
H4 4-17: 1ac
H4 4-17: 2ac
H4 4-17: 3ac
H4 4-17: 4ac
Log2 Fold-Change (DFO/Untreated)
≥2
1
0
-1
≤-2
Time (days): 0.5 1 3 5
Response
Recovery

Figure S5: The Mitochondrial Biogenesis Response to Iron Deprivation is Prevented with HDAC Inhibitors SAHA and TSA, Related to Figure 8

Abundance of the indicated **(A)** mRNAs and **(B)** proteins from C2C12 myoblasts were treated with the indicated concentrations of the histone deacetylase (HDAC) inhibitor SAHA (suberoylanilide hydroxamic acid) ± 100 μM DFO for 24 hrs as assessed by real-time qPCR and immunoblotting, respectively. Data are displayed as mean ± SEM of biological triplicate measurements (*$p < 0.05$, **$p < 0.01$, Student's t test).

Abundance of the indicated **(C)** mRNAs and **(D)** proteins from C2C12 myoblasts were treated with the indicated concentrations of the histone deacetylase (HDAC) inhibitor TSA (trichostatin A) ± 100 μM DFO for 24 hrs as assessed by real-time qPCR and immunoblotting, respectively. Data are displayed as the mean of technical triplicate measurements.

Figure S5

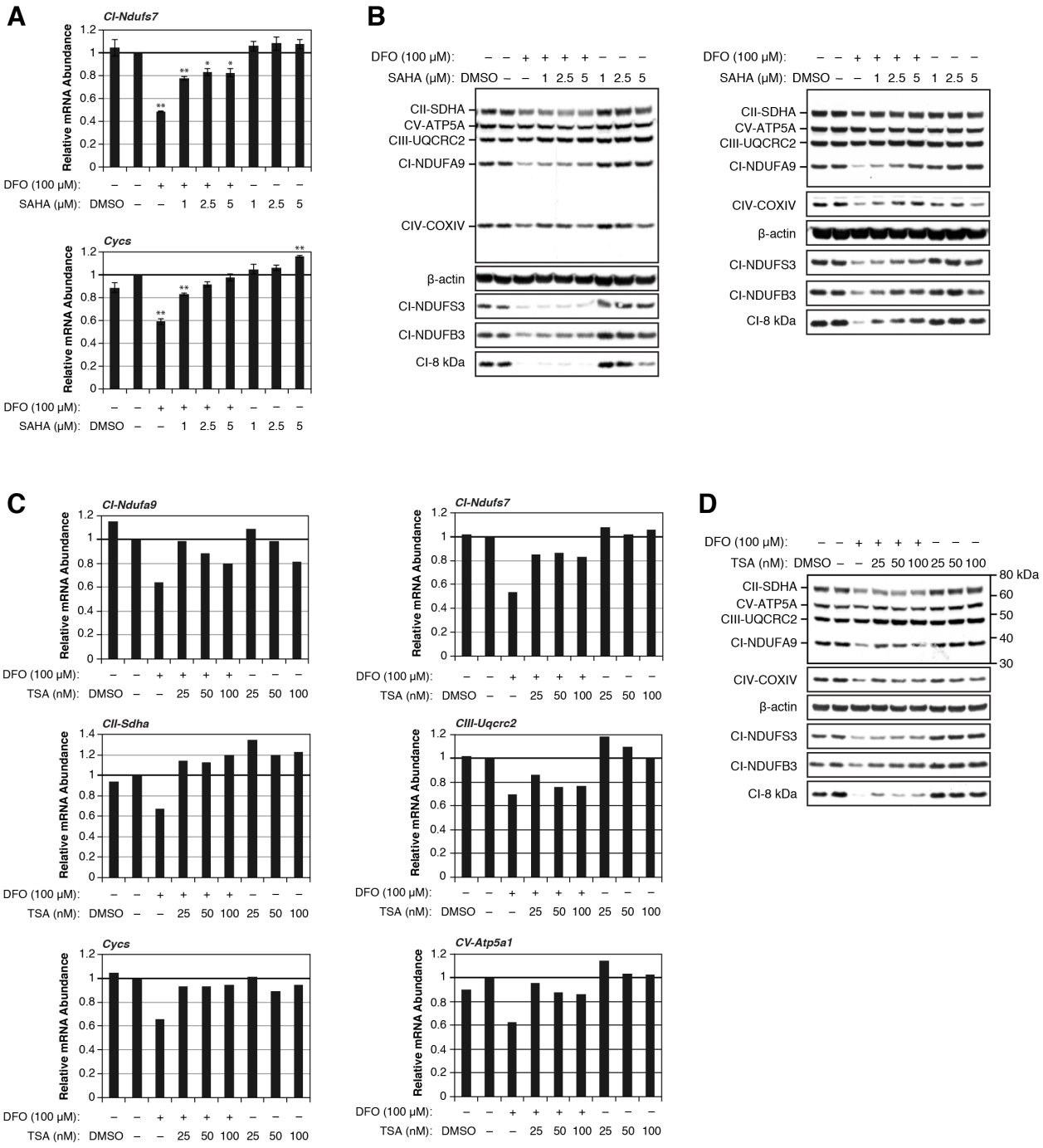
A
Cl-Ndufs7
Relative mRNA Abundance
DFO (100 μM): – – + + + + – – –
SAHA (μM): DMSO – – 1 2.5 5 1 2.5 5
Cycs
Relative mRNA Abundance
DFO (100 μM): – – + + + + – – –
SAHA (μM): DMSO – – 1 2.5 5 1 2.5 5
B
DFO (100 μM): – – + + + + – – –
SAHA (μM): DMSO – – 1 2.5 5 1 2.5 5
CII-SDHA
CV-ATP5A
CIII-UQCRC2
CI-NDUFA9
CIV-COXIV
β-actin
CI-NDUFS3
CI-NDUFB3
CI-8 kDa
DFO (100 μM): – – + + + + – – –
SAHA (μM): DMSO – – 1 2.5 5 1 2.5 5
CII-SDHA
CV-ATP5A
CIII-UQCRC2
CI-NDUFA9
CIV-COXIV
β-actin
CI-NDUFS3
CI-NDUFB3
CI-8 kDa
C
Cl-Ndufa9
Relative mRNA Abundance
DFO (100 μM): – – + + + + – – –
TSA (nM): DMSO – – 25 50 100 25 50 100
Cll-Sdha
Relative mRNA Abundance
DFO (100 μM): – – + + + + – – –
TSA (nM): DMSO – – 25 50 100 25 50 100
Cycs
Relative mRNA Abundance
DFO (100 μM): – – + + + + – – –
TSA (nM): DMSO – – 25 50 100 25 50 100
Cl-Ndufs7
Relative mRNA Abundance
DFO (100 μM): – – + + + + – – –
TSA (nM): DMSO – – 25 50 100 25 50 100
Clll-Uqcrc2
Relative mRNA Abundance
DFO (100 μM): – – + + + + – – –
TSA (nM): DMSO – – 25 50 100 25 50 100
CV-Atp5a1
Relative mRNA Abundance
DFO (100 μM): – – + + + + – – –
TSA (nM): DMSO – – 25 50 100 25 50 100
D
DFO (100 μM): – – + + + + – – –
TSA (nM): DMSO – – 25 50 100 25 50 100
80 kDa
60
50
40
30
CII-SDHA
CV-ATP5A
CIII-UQCRC2
CI-NDUFA9
CIV-COXIV
β-actin
CI-NDUFS3
CI-NDUFB3
CI-8 kDa

CHAPTER FOUR: Conclusions and Future Directions

4.1 Summary

Iron deprivation has dramatic effects on mitochondria, including changes in morphology, composition and activity. While these effects are well documented, the mechanisms of how cells adapt to iron deprivation-induced mitochondrial dysfunction are less understood. We have found that iron-deprivation results in an adaptive decrease in mitochondrial biogenesis. Importantly, our discoveries have opened up new and exciting avenues for future research. One area of future research is to identify the regulators responsible for controlling the changes in histone acetylation and methylation that occur during iron deficiency and to examine if these post-translational changes also occur in an animal model of iron deficiency. Additional future research directions are to determine whether translation and/or protein degradation contributes to the loss of mitochondrial proteins upon iron depletion, and to identify the key form of iron whose loss is sensed and initiates the mitochondrial biogenesis response. Other future research directions include determining the contribution of retrograde signaling to this response and to understand the significance of the persistent epigenetic changes that are observed during iron response and recovery.

4.2 Conclusions

Mitochondria are dynamic cellular organelles that are critical for the survival of nearly every eukaryotic cell type. Besides being responsible for generating the majority of cellular ATP through the TCA cycle and oxidative phosphorylation (OxPhos), mitochondria also have a central role in fatty acid oxidation, ketone body formation, pyrimidine synthesis, reactive oxygen species generation and programmed cell death. The mitochondrion is also critically important for iron metabolism, as it contains enzymes and transporters necessary for heme biosynthesis and

iron-sulfur (Fe-S) cluster biogenesis. Heme and Fe-S clusters are necessary for many cellular processes, including the TCA cycle and the electron transport chain. The production of mitochondria, termed mitochondrial biogenesis, is a complex process that involves the orchestrated transcription, translation, import, and assembly of approximately twelve hundred proteins encoded by two genomes (Mick et al., 2011; Pagliarini et al., 2008; Scarpulla, 2008; Schmidt et al., 2010). Moreover, mitochondrial biogenesis can be tailored in response to environmental conditions (Hock and Kralli, 2009; Scarpulla, 2011).

Our discoveries have revealed a fundamental role for iron in mitochondrial biogenesis (Rensvold et al., 2013). First, we found, through parallel quantitative proteomic and microarray analyses, that induction of mitochondrial biogenesis by overexpression of the transcriptional coactivator PGC-1α in C2C12 mouse myotubes results in drastic changes in the abundance of proteins involved in regulating cellular iron levels. The transferrin receptor, which transports transferrin-bound iron into cells, was greatly increased, whereas ferritin light chain, a component of the ferritin complex that stores cellular iron, was decreased. These results implied that iron might be a vital nutrient during mitochondrial biogenesis. Indeed, when we combined PGC-1α overexpression and treatment with the cell-permeable iron chelator deferoxamine (DFO), we observed a reduction in the abundance of transcripts and proteins induced by the PGC-1α mitochondrial biogenesis program.

Second, we discovered that mitochondrial biogenesis is altered directly in response to iron deprivation. Specifically, our quantitative proteomic analysis revealed that DFO treatment alone has a powerfully negative effect on the expression of mitochondrial proteins. These mitochondrial protein alterations appeared to stem from altered gene expression, as comparison of mRNA abundances from our microarray analyses showed that almost without exception,

mitochondrial transcripts that were increased by PGC-1α overexpression were comparably decreased by DFO treatment. However, careful timecourse analyses of mRNA and protein abundance showed that the decreases in protein abundance occur before the changes in their corresponding transcripts, suggesting that iron deprivation initiates separate responses leading to the mitochondrial mRNA and protein changes *or* that the mRNA changes are in response to the decreases in mitochondrial function and proteins. Moreover, we discovered that for the OxPhos proteins unaffected by our iron chelation treatment (complexes III and V), their transcripts were nonetheless reduced (and this observation is supported by our original microarray and mass spectrometry analyses). Next, we determined the level of gene expression at which iron deprivation operates (i.e., transcription or mRNA turnover) to cause the observed decrease in mitochondrial transcripts. To do so, we utilized RNA pulse-chase and labeling approaches, and from these analyses, determined that iron deprivation affects the synthesis of new OxPhos-encoding transcripts but has no measurable effect on transcript turnover. Cellular iron levels are known to regulate the expression of multiple genes at the post-transcriptional level via iron responsive elements (IREs) in the untranslated regions (UTRs) of specific mRNAs (Anderson et al., 2012). However, little is known about a role for iron in the regulation of mammalian transcriptional programs. Collectively, our large-scale analyses of mRNA and protein abundance reveal that the removal of iron is sufficient to cause a global downregulation of mitochondrial gene expression, and suggest that cells might actively calibrate their mitochondrial content to available free iron.

Our microarray and proteomic data show that iron chelation has an approximately equal and opposite effect on mitochondrial biogenesis to that of PGC overexpression. Using immunoblot analyses, we demonstrated that the decrease in abundance of the mitochondrial

proteins was proportional to the concentration of DFO, indicating that cells might coordinate their mitochondrial protein content to cellular iron levels. Proteins from other cellular compartments and a mitochondrial outer membrane protein were unaffected, indicating that this effect is specific for certain mitochondrial proteins. In addition, a variety of mammalian cell lines showed similar decreases when treated with DFO. As the tested cell lines differ in cell type, tissue of origin and species, this result suggests that mammalian cells may universally calibrate their mitochondrial content to iron levels. Additionally, we discovered that the effects on cellular gene expression and respiratory capacity can be fully reversed upon the reintroduction of iron, suggesting that the response to iron deprivation is an adaptive cellular response rather than mere irreversible cellular damage.

Finally, we tested whether known regulators of mitochondrial biogenesis could explain the response to DFO. Since iron deprivation can inactivate the iron dependent prolyl hydroxylases that target HIF-1α for ubiquitination and degradation, DFO treatment could initiate a HIF-1α-dependent decrease in mitochondrial biogenesis. However, we found that HIF-1α, as well as other established regulators of mitochondrial biogenesis, including PGC-1α and PGC-1β, were not necessary for the response. Further, using a MS-based quantitative proteomics approach, we found that iron chelation caused dynamic changes in histone tail acetylation and methylation, including an overall decrease in histone tail acetylation. Using chromatin immunoprecipitation followed by real-time quantitative PCR (ChIP-qPCR) we found decreases in histone H3 lysine 9 acetylation (H3K9ac) at mitochondrial genes and that the effect of iron chelation on mitochondrial transcript levels was fully reversed with HDAC inhibition, consistent with histone post-translational modification (PTM)-mediated regulation of gene expression.

Our results suggest that decreased mitochondrial biogenesis, driven by changes in histone PTMs, is a regulated and important adaptive cellular response to iron deprivation. Here, I propose that this response is just one part of a broad, highly orchestrated mitochondrial regulatory program initiated by iron depletion. Indeed, other studies have found that iron deficiency also results in changes to mitochondrial dynamics and an increase in mitochondrial autophagy (Allen et al., 2013; Schiavi et al., 2015; Yoon et al., 2006). The contribution of these different mechanisms to mitochondrial regulation likely depends on the duration or intensity of iron deprivation. At the timepoints that we see a reduction in mitochondrial gene expression, we do not observe any obvious changes in mitochondrial morphology and only a slight increase in mitochondrial mass (Rensvold et al., 2013). Moreover, the reported changes in mitochondrial dynamics, morphology and autophagy were observed at higher concentrations or longer lengths of iron chelation than what was used in our experiments. This suggests that decreased mitochondrial biogenesis is probably the first of these responses as cells try to reduce the production of mitochondrial proteins (a substantial number of which depend on iron) until iron levels are restored. If iron depletion persists and mitochondrial dysfunction continues to decline, mitochondria fuse (or decrease fission) in an attempt to maintain or restore function (Yoon et al., 2006). Concurrently, mitochondrial protein composition becomes considerably altered, especially for the inner membrane localized OxPhos machinery, likely contributing to a loss of cristae, mitochondrial swelling and an increase in mitochondrial mass (Dallman and Goodman, 1970). Following this, possibly in an effort to eliminate damaged mitochondria or to recycle iron for other cellular uses, elimination of mitochondria by autophagy increases (Allen et al., 2013; Kirienko et al., 2015; Schiavi et al., 2015). Ultimately, if iron levels do not return to normal, mitochondrial function is not restored and mitochondrial membrane potential is lost, cells

undergo intrinsic, mitochondrial-dependent apoptosis via membrane permeabilization, swelling and release of apoptotic factors, including cytochrome *c* (Yu et al., 2007). Altogether, our results demonstrate that iron is essential for the mitochondrial biogenesis program and indicate that histone PTM regulation of mitochondrial gene expression is an early adaptive response to iron deprivation.

4.3 Future Directions

4.3.1 Regulation of Histone Post-Translational Modifications in Response to Iron Deprivation

Our large-scale mass spectrometry (MS)-based analysis of histone tail post-translational modifications (PTMs) revealed that dynamic changes in lysine acetylation and methylation accompany iron deprivation. Additionally, we discovered that the effect of iron deprivation on mitochondrial biogenesis is dependent on histone acetylation levels, as treatment of iron-deprived cells with the clinically used histone deacetylase (HDAC) inhibitors, suberoylanilide hydroxamic acid (SAHA) or trichostatin A (TSA), blocked the effect of iron deprivation on mitochondrial gene expression and histone acetylation levels. The enzymes that regulate acetylation include acetyl-CoA-dependent lysine acetyltransferases (HATs), and the NAD^+- or iron/zinc-dependent deacetylases (HDACs) (Smith and Denu, 2009). In humans, 18 HDACs have been identified and organized into 4 classes, including class I (HDAC1, HDAC2, HDAC3 and HDAC8), class IIa (HDAC4, HDAC5, HDAC7 and HDAC9), class IIb (HDAC6 and HDAC10), class III (sirtuins 1–7) and class IV (HDAC11). SAHA (also known as vorinostat) and TSA chelate zinc in the active site of Class I, II, and IV HDACs but do not inhibit Class III HDACs (Marks and Breslow, 2007; Witt et al., 2009; Xu et al., 2007). Our data suggest that an increase the activity of class I, II and/or IV HDACs could be responsible for the decreases in

histone acetylation and mitochondrial gene expression we see during iron chelation. Consequently, future studies should examine the role of chromatin modifying enzymes, including HATs, HDACs, lysine methyltransfereases and lysine demethylases, in the mitochondrial response to iron deprivation. Loss-of-function analyses using RNAi mediated knockdown or CRISPR/Cas9 (clustered regularly interspaced short palindromic repeats/CRISPR associated protein 9) gene inactivation could be used to identify if a specific HDAC or HDAC class is response for these changes. Conversely, a decrease in HAT activity could also result in our observations, and HDAC inhibition may simply be blocking the normal turnover of histone acetylation. Again, loss-of-function techniques targeting HATs could be to assess this hypothesis. Similarly, as we observed increases in histone tail lysine methylation in both our MS and immunoblot analyses, some of which are strongly associated with repression of gene expression, iron deprivation may be causing the changes in mitochondrial gene expression through a decrease in histone demethylase activity. Of note, most lysine demethylase reactions are catalyzed by the Jumonji C (JmjC)-domain containing demethlyases that require α-ketoglutarate, O_2 and Fe^{2+} (Kooistra and Helin, 2012; Mosammaparast and Shi, 2010). There are a variety of commercially available demethylase inhibitors that could be used to test if a decrease in histone demethylase activity is sufficient to cause a similar mitochondrial response (Hojfeldt et al., 2013).

4.3.2 Analysis of protein translation and degradation during iron deprivation

Our original genome scale analyses revealed that iron deprivation causes a coordinated decrease in mitochondrial transcripts and proteins. However, from our timecourse analyses we also found that many of the mitochondrial proteins decrease before their corresponding

transcripts. This result suggests that the decrease in the abundance of mitochondrial proteins, at least initially, is not due to the decrease in transcripts but due to regulation of protein translation, degradation or both. Therefore, future research should determine whether iron deprivation affects the synthesis or degradation (or both) of mitochondrial proteins. Notably, a recent global analysis of protein turnover found that the average half-life of OxPhos protein complexes was approximately 100 hours with complex I subunits having the lowest half-lives at about 50 hours and complex V the greatest at over 200 hours (Figure 1A) (Schwanhausser et al., 2011). Interestingly, our measurements show that iron chelation causes up to an 80% loss (in the case of complex I) of mitochondrial proteins after 24 hours. If iron chelation were to only affect translation, then based on the protein half-lives, 50 hours or more would be required to cause just a 50% loss of protein abundance, indicating that a decrease in translation alone would be insufficient to cause our observations and that an increase in protein degradation is likely contributing to the mitochondrial response to iron. Despite this, when we treated cells with small interfering RNAs (siRNAs) targeting the major mitochondrial quality control proteases, we found that the knockdown of any one protease did not alter the response to DFO. Traditional approaches for the analysis of protein synthesis and degradation could be used to address these inconsistencies. Unfortunately, we found that cycloheximide treatment (to determine protein half-lives) when combined with DFO treatment results in severe cell death, making this approach impractical. Moreover, we observed a similar problem when using the proteasome inhibitor MG132, which also inhibits the mitochondrial LONP1 protease. We suspect that traditional ^{35}S-methionine pulse labeling and pulse-chase approaches would be more effective for our experimental system, and would complement the approach we used for determining that iron

chelation affects the synthesis of mitochondrial transcripts and does not affect transcript turnover.

While ^{35}S-methionine labeling would likely be a suitable approach for addressing whether iron deprivation affects the synthesis or degradation of mitochondrial proteins, it suffers from several disadvantages, most notably being very low-throughput and having the risks associated with radioactivity. Here, I propose the use of MS-based quantitative proteomics to determine whether the observed effect of iron deprivation on mitochondrial protein abundance is due to a translation defect or due to increased protein turnover (Figure 1B). This approach would be analogous to traditional ^{35}S-methionine pulse labeling approaches; however, it would enable the survey of a wide range of cellular and mitochondrial proteins and the quantification of their changes with high accuracy. New advances in labeling methods for quantitative proteomics, such as the neutron encoded (NeuCode) labeling system, invented by Professor Josh Coon (UW-Madison) (Hebert et al., 2013b), would be well suited for this purpose. NeuCode exploits the subtle mass differences caused by nuclear binding energy variation in stable isotopes. These mass differences are synthetically encoded into amino acids and incorporated into proteins from cells in culture via metabolic labeling, similar to the stable isotope labeling by amino acids in cell culture (SILAC) method. The key advancement here is that high mass accuracy mass spectrometers can resolve these tiny mass differences. When combined with the typical SILAC labeling approach, NeuCode can increase the multiplexing capacity from 3 to at least 9, all while typically increasing the number of overall identifications (Hebert et al., 2013b; Merrill et al., 2014; Rose et al., 2013). As such, NeuCode promises to deliver the best features of previous quantitative approaches: the high quantitative accuracy of SILAC with the larger mulitiplexing

cababilites of tagging methods that are applied after sample collection, such as isobaric tagging, thereby enabling more comprehensive and more accurate experiments to be conducted.

For the NeuCode pulse-labeling analysis of protein synthesis, different NeuCode heavy labels could be added to control (untreated) and iron chelator (DFO) treated cells just prior to sample collection (e.g., 3 hours), allowing for the synthesis of new proteins with the heavy labels (Figure 1B). Importantly, the duration of the labeling period should be empirically determined as to maximize the detection and signal of the nascent proteins while minimizing any contribution of degradation to the abundance of these proteins. Further, time points should be within the first 12 hours of treatment, since there is little change in most mRNA levels at this time. Different time points would be collected and the relative amount of proteins made during the short labeling period in untreated and DFO treated cells could then be compared at each time point. After harvesting, equal numbers of cells from each condition at each time point would then be combined. Following that, a mitochondrial enrichment step could be performed to ensure maximum coverage of mitochondrial proteins before analysis. By using 9 NeuCode labels (4 time points × 2 conditions + 1 × t_0 time point = 9), the relative protein synthesis +/− DFO treatment could be assessed in one MS run (Figure 1B). If the decreased protein levels we observed within 12 hours following iron deprivation are due to decreased protein synthesis, then the DFO-treated cells should produce less heavy-labeled protein during each short heavy label incubation period. On the other hand, if there is no difference in the synthesis rates, then the decreased protein levels are probably due to an increased rate of protein turnover.

For the NeuCode pulse-chase analysis of protein degradation, cells would first be labeled with different NeuCode heavy labels (the “pulse”), and after 100% incorporation of the labels, the cells would be switched to unlabeled growth media (the “chase”) and treated +/− DFO

(Figure 1B). Different time points would be collected and the relative amount of heavy labeled proteins at each time point could be determined as well as the relative rate of protein loss. Similar to the strategy above, after harvesting, equal numbers of cells from each condition at each time point would be combined, followed by a mitochondrial enrichment to ensure maximum coverage of mitochondrial proteins before analysis. If the decrease in mitochondrial proteins following DFO treatment is caused by an increase in protein degradation, less remaining heavy labeled proteins would be detected in the DFO treated cells and there would be an increase in the relative rate of protein loss (Figure 1B).

Importantly, the results of these analyses would help to focus candidate-based approaches in identifying regulators involved in this response (i.e., focusing on know regulators of translation or protein degradation). For example, if the loss of mitochondrial proteins observed during iron deprivation is due to increased protein degradation, we might suspect a key role for a mitochondrial protease. Alternatively, if the protein changes are due to alterations in protein synthesis, we might suspect a key role for the translation machinery. In either case, the resulting data would establish a robust foundation for further exploring the nature of this cellular stress response.

4.3.3 Identification of the form of cellular iron whose depletion triggers the mitochondrial biogenesis response

Treatment of tissue culture cells with the iron chelator DFO results in a rapid, downregulation of mitochondrial transcripts and proteins. Additionally, we found that overexpression of ferroportin, a plasma membrane protein that pumps iron out of cells, results in a decreased abundance of mitochondrial proteins, indicating that the effect is dependent on iron

levels and is not merely a DFO specific effect. We also observed that ferroportin overexpression reduces ferritin levels, confirming that ferroportin expression causes a decrease in cellular iron.

Mammalian cells contain many forms of iron whose levels dictate cellular activity. These forms include protein cofactors such as heme and Fe-S clusters and protein bound di-iron and monoiron centers. In addition, iron is found in the chelatable, "labile iron pool" (LIP) and is stored in the cytosolic protein ferritin and mitochondrial protein mitoferrin (Hentze et al., 2010; Richardson et al., 2010). Different forms of iron can function as indicators of cellular iron status and are sensed by specific proteins that control cellular processes. For example, the cytoplasmic enzyme aconitase senses Fe-S cluster levels, the E3 ubiquitin ligase substrate specificity component FBXL5 senses changes in the level of the cytosolic iron pool and the transcriptional repressor BACH1 senses heme levels (Hentze et al., 2010; Mense and Zhang, 2006).

As cellular iron forms are known to function as indicators of iron status, I propose that depletion of a key form of cellular iron initiates the remodeling of the mitochondrial proteome. As such, future experiments should determine whether a decrease in the level of cellular heme, mitochondrial or cytosolic derived Fe-S clusters, or the mitochondrial or cytosolic iron pool triggers the mitochondrial biogenesis response to iron deprivation. To identify this key form of cellular iron, a combination of genetic and pharmacological approaches could be used. DFO likely decreases the level of all cellular forms of iron. Therefore, differentially altering the levels of heme, Fe-S clusters and the cellular iron pools, would be necessary to determine which form of iron (or loss thereof) is responsible for the decrease in mitochondrial biogenesis. Heme levels could be altered using pharmacological inhibitors, such as succinylacetone (SA), to block heme synthesis, and the level of Fe-S clusters and mitochondrial iron could be altered using RNAi to knockdown the level of key proteins involved in Fe-S cluster biogenesis and cellular iron

transport. Importantly, the levels of cellular and mitochondrial iron, cytosolic and mitochondrial derived Fe-S clusters, and cellular heme should be monitored in response to each treatment as loss of one form of iron can cause changes in others. For example, defects in mitochondrial Fe-S biogenesis have been shown to cause accumulation of iron in mitochondria and a consequent depletion of cytosolic iron (Rouault and Tong, 2005). We have observed a dose dependent decrease in mitochondrial protein abundance upon treatment with the heme biosynthesis inhibitor SA (Figure 2A). However, without knowing how heme levels are affected at each concentration of SA, and whether other forms of iron are affected, we cannot conclude that depletion of heme causes the mitochondrial biogenesis response. Of note, using SA treatment without tracking the different forms of cellular iron may have contributed to the misidentification of RBCK1 (HOIL-1) as the ubiquitin ligase that targets iron regulatory protein 2 (IRP2) for degradation (Ishikawa et al., 2005; Yamanaka et al., 2003; Zumbrennen et al., 2008). There are a wide variety of established fluorescence-based and enzyme-coupled assays that can be used to measure heme, Fe-S and iron levels, and when combined with the treatments listed above, these assays can be used to determine which form of iron is consistently decreased when the levels of mitochondrial transcripts and proteins are decreased. The results of these analyses would help to motivate future research in identifying a possible protein sensor that is responsible initiating the mitochondrial response to iron deprivation (i.e., focusing on know heme-, Fe-S cluster- or iron-binding protein sensors). Overall, the results of these experiments would provide important groundwork for future exploration of this adaptive response.

4.3.4 Analysis of Histone Post-Translational Modifications in an Animal Model of Iron Deficiency

Our analyses of iron deprivation in cultured mouse cells and iron deficient mice identified decreases in mitochondrial gene expression at both the mRNA and protein level. Specifically, in all 3 tissues analyzed, we observed significant decreases in transcripts for at least one of the mitochondrial genes examined, with the greatest decreases occurring in liver. We have also discovered that iron deprivation in tissue cultured cells leads to dynamic changes in histone tail lysine acetylation and methylation. Accordingly, an important future research direction would be to determine whether these changes in histone PTMs also occur in an animal model of iron deficiency. However, the effects we observed in mice were not as large as might have been expected based on other reports in the literature. In order to increase the possibility of observing changes in histone PTMs, the effect of iron deficiency on the mitochondrial biogenesis response in mice should first be maximized. This objective would likely be accomplished through increasing the severity of iron deficiency. To accomplish this, the mice could be kept on the iron deficient diet for a longer period of time or they could be treated with an iron chelator, such as DFO. Another option would be to make the mouse mothers iron deficient (either through diet or chelation) during gestation and/or nursing and continue the newborns on an iron deficient diet after weaning (Dallman, 1969). Genetic perturbation of proteins involved in maintaining iron homeostasis, such as a tissue specific knockout of the transferrin receptor or the iron regulatory proteins (Fleming et al., 2011), the latter of which has already been shown to cause severe mitochondrial defects (Galy et al., 2010), would provide another approach. Additionally, these same studies could be performed in rats instead of mice. Rats are the traditional animal model for studying the effects of iron deficiency as their rapid growth rate results in severe anemia when on

an iron deficient diet (Dallman, 1986). Finally, research using the nematode *Caenorhabditis elegans* has proven successful in analyzing changes in mitochondrial autophagy in response to iron deprivation (Kirienko et al., 2015; Schiavi et al., 2015). As such, this organism may also be suitable for studying the mitochondrial biogenesis response and possible changes in histone acetylation and methylation.

4.3.5 Iron Deprivation Induced Mitochondrial Retrograde Signaling

We have observed that iron depletion leads to drastic effects on mitochondrial function and the nuclear epigenome. Specifically, iron deprivation results in a rapid, dose-dependent loss of nuclear- and mitochondrial-encoded transcripts, proteins and mitochondrial oxidative capacity that is fully reversible upon the reintroduction of iron (Rensvold et al., 2013). From detailed timecourse analyses we found that, in many cases, OxPhos proteins decrease before their matching transcripts. This suggests that iron deprivation may cause separate effects on the transcription of nuclear encoded mitochondrial genes and on mitochondrial protein levels *or* that the decreases in mitochondrial function and proteins occurs first, and this leads to the transcriptional changes, possibly suggesting mitochondrial to nuclear retrograde signaling. Consequently, an important future research direction would be to examine the potential role of retrograde signaling in this response.

Mitochondrial retrograde signaling involves communication from the mitochondrion to the nucleus that occurs during normal and disease states. Mitochondrial dysfunction can trigger retrograde signaling as an adaptive response, allowing mitochondria to communicate changes in their metabolic status to the nucleus, resulting in changes to nuclear gene expression and cellular function. Retrograde communication can include calcium signaling, reactive oxygen species

(ROS), mitochondrial dependent metabolites and the mitochondrial unfolded protein response (UPR^{mt}) (Guha and Avadhani, 2013; Wallace and Fan, 2010). As outlined below, several of these signaling processes have the potential to be involved in the mitochondrial adaptation to iron deprivation.

First, iron deprivation induced changes to mitochondrial oxidative metabolism and its metabolic products could alter the activities of chromatin modifying enzymes that drive the repression of nuclear nuclear-encoded mitochondrial genes. In addition to changes in mitochondrial gene expression, we also observed dynamic changes in histone tail lysine acetylation and methylation in response to iron deprivation. The enzymes that regulate these modifications include acetyl-CoA-dependent lysine acetyltransferases, NAD^+ and iron/zinc dependent deacetylases (HDACs), SAM (*S*-adenosyl-L-methionine)-dependent lysine/arginine methyltransfereases, and FAD and iron-O_2-α-ketoglutarate dependent lysine demethylases. Since these enzymes use central metabolites and metal ions, they are susceptible to changes in nutrient availability and metabolism that alter the level of those co-substrates. Indeed, there is building evidence that changes to acetyl-CoA, SAM, NAD(H), O_2, α-ketglutarate and metal ions might lie at the center of profound epigenetic alterations, especially from environmental and nutritional changes (Fan et al., 2015; Gut and Verdin, 2013; Kaelin and McKnight, 2013). Therefore, a first step in identifying a connection between mitochondrial metabolites and histone modification would be to determine whether mitochondrial dependent metabolites are affected during iron deprivation. Importantly, advances in MS-based metabolomics have enabled sensitive measurement of the compounds that constitute most of energy and redox metabolism, amino acid synthesis and degradation, fatty acid metabolism and nucleotide metabolism (Patti et al., 2012) and would likely be a useful approach for this future direction. Many of these key metabolites

are important for epigenetic modification and thus, could constitute a direct metabolic signaling pathway from mitochondria-to-nucleus.

Mitochondrial generated ROS also known to be an important retrograde signal. During hypoxia, ROS generated from complex III are necessary for the stabilization of HIF-1α and subsequent changes in gene expression that help cells to adapt to lower oxygen levels (Klimova and Chandel, 2008). Several studies have reported that inhibition of heme synthesis or iron chelation treatment (DFO) in cell culture, and dietary iron deprivation in rats increases the levels of intracellular ROS using the cell permeable fluorescent dye, dichlorodihydrofluorescin (DCFH) (Atamna et al., 2001; Walter et al., 2002; Yoon et al., 2006). However, other studies have shown that DFO stabilization of HIF-1α does not require ROS production but instead acts downstream of complex III (Chandel et al., 2000). Additionally, DFO has a much higher affinity for ferric iron (Fe^{3+}) over ferrous iron (Fe^{2+}), and therefore is thought to render the bound iron metabolically inactive such that it cannot participate in the generation of ROS (Kalinowski and Richardson, 2005). Using cytosolic and mitochondrial targeted reduction-oxidation (redox)-sensitive GFP (roGFPs) (Hanson et al., 2004; Meyer and Dick, 2010), we observed that DFO actually decreases the redox state of mitochondria and causes no change to the cytosolic state at both 6 hours and 24 hours following treatment (Figure 3A). As a control, we treated cells with $CoCl_2$, which has previously been shown to cause increased ROS. With this treatment we observed a significant increase in the redox state in both the cytosol and mitochondria (Figure 3A). While iron deprivation may cause an increase in cellular ROS under certain circumstances, these results suggest that mitochondrial generated ROS are unlikely to function as a retrograde signal during iron deprivation.

Another important mitochondrial retrograde response is the UPR^{mt}, which is induced during mitochondrial dysfunction that stems from protein folding stress and leads to the induction of mitochondrial chaperones, proteases and assembly factors to promote the recovery from the stress (Jovaisaite and Auwerx, 2015; Schulz and Haynes, 2015). The UPR^{mt} also restricts the expression of other mitochondrial genes, such as those encoding for OxPhos and TCA cycle proteins, until the proteotoxic stress is resolved (Nargund et al., 2015). Future research should address whether the UPR^{mt} is also involved in the mitochondria biogenesis response to iron deprivation. Key signaling mechanisms of this adaptive response have been described in *C. elegans*. Of particular note is the transcription factor ATFS-1. Under normal conditions ATFS-1 is imported into mitochondria where it is degraded by LON protease. However, during mitochondrial protein folding stress, mitochondrial protein import is impaired and instead of being imported into mitochondria, ATFS-1 traffics to the nucleus, where it initiates the transcriptional programs described above. A recent study found that induction of the UPR^{mt} in *C. elegans* exposed to the pathogen *Pseudomonas aeruginosa* is linked to the innate immune response (Pellegrino et al., 2014). Interestingly, exposure of *C. elegans* to *P. aeruginosa* mutants that lack genes involved in siderophore (iron chelating compounds) production resulted in less UPR^{mt} activation. Mammalian cells initiate similar transcriptional changes as *C. elegans* during proteotoxic stress, including increases in select mitochondrial proteases and chaperones, however the signaling mechanisms are not as well understood. As a first step in determining if the UPR^{mt} is involved in iron deprivation-induced mitochondrial transcriptional regulation, we analyzed the expression of mitochondrial chaperones, proteases and transcriptional regulators that are linked to the UPR^{mt} following DFO treatment (Figure 3B) (Jovaisaite et al., 2014; Mohrin et al., 2015). From these analyses we found increases in the expression of several of

these genes as well as a large increase in the transcription factor CHOP (Figure 3B), suggesting that the UPR^{mt} might be activated during iron deprivation. Additional gain- and loss-of-function experiments should be performed to determine if these regulators are important for the mitochondrial biogenesis response to iron depletion. Second, known activators of the UPR^{mt}, such as mtDNA depletion, overexpression of aggregation prone mutant protein ornithine transcarbamylase (OTC) and doxycycline inhibition of mitochondrial translation, should be used to determine if they lead to similar changes in OxPhos transcription and changes to histone PTMs as we observe with DFO.

4.3.6 Heritable Epigenetic Effects of Iron Deprivation

From our large-scale, quantitative mass spectrometry-based analysis of histone tail acetylation and methylation during DFO response and recovery, we discovered that changes in histone PTMs are largely coordinated with changes in mitochondrial gene expression and function. However, we also found that several PTMs did not return to untreated levels following the reintroduction of iron. Specifically, the abundance of histone H3 K9ac+K14ac and K27ac peptides were decreased throughout iron chelation response and recovery. Intriguingly, these experiments suggest that a few of the iron deprivation induced epigenetic changes may be preserved and have lasting effects on gene regulatory programs. Future research should examine these PTMs in depth and determine whether they have an impact on gene expression and if they are associated with changes to cellular physiology.

The most direct approach to determine if the PTMs that are maintained following a prior bout of iron depletion are associated with changes to cellular function would be to perform a large-scale analysis gene expression, such as microarray, RNA sequencing or MS-based

proteomic analyses. These analyses would be able to detect any transcripts or proteins whose levels do not recover following iron deprivation and could therefore potentially be regulated by the persistent epigenetic changes. Apart from performing additional experiments, we can also infer possible effects of the persistent epigenetic changes based on previously reported phenotypes associated with prior iron deficiency or the effects of maternal iron deficiency on offspring. Various studies using historic events of extreme food scarcity, including the Dutch Hongerwinter (Hunger Winter) (1944-1945), the Great Chinese Famine (1958-1961) and the Överkalix, Sweden periods of feast and famine (~1800-1900), have found links between prenatal or childhood nutrition and increased risk of obesity and schizophrenia and prevalence of diabetes and cardiovascular disease that may also have transgenerational effects (Kaati et al., 2002; Li et al., 2010; Lumey et al., 2011; Ravelli et al., 1998; Ravelli et al., 1999; Ravelli et al., 1976; Roseboom et al., 2000; St Clair et al., 2005; Susser and Lin, 1992). Interestingly, Dutch Hunger Winter individuals who were prenatally exposed to famine had decreased DNA methylation of the IGF2 (insulin-like growth factor 2) gene (Heijmans et al., 2008), providing evidence that nutrient deprivation early in development can cause persistent changes in epigenetic modifications. Iron deficiency anemia in humans, during gestation or early life, is associated with defects in cognitive and motor development leading to learning and memory deficits that persist after iron deficiency despite iron treatment (Fretham et al., 2011; McCann and Ames, 2007; Zimmermann and Hurrell, 2007). Moreover, animal models of early iron deficiency anemia have supported these findings from human studies. Additionally, rats born from iron-deprived mothers were found to be more susceptible to obesity when fed a high-fat diet.

Additionally, the concept of mitochondrial hormesis (mitohormesis) may provide insight into the persistent epigenetic changes. Mitohormesis is the idea that temporary, non-lethal

mitochondrial stress can result in adaptive cellular changes that provide defense from larger, subsequent stresses (Yun and Finkel, 2014). For example, activation of the UPR^{mt} in *C. elegans* during mitochondrial stress induced by RNAi knockdown of specific mitochondrial genes may be linked to lifespan extension (i.e., resistance to the effects of aging). In the case of iron deprivation, it is possible that the iron chelation induced epigenetic changes that remain following iron repletion may function to confer protection from future stress, such as another bout of iron deficiency.

4.4 Impact

Starting from the broad aim of understanding how cells regulate their mitochondrial content in response to nutrient availability, we have identified and characterized an adaptive mitochondrial biogenesis response to iron deprivation utilizing a combination of unbiased, large-scale analyses and focused, hypothesis-driven experiments. Our exploration of this response has opened up new and exciting avenues of research that may lead to greater understanding of the basic molecular mechanisms that regulate mitochondrial biogenesis as well as new therapies that reduce the prevalence and burden of iron deficiency. Moreover, our work may provide valuable insight into disease pathogenesis, as mitochondrial dysfunction occurs in many common human disorders.

4.5 Experimental Procedures

4.5.1 Cell Culture

Brown preadipocytes were maintained in high glucose DMEM with 20% FBS and 1 × PS (Invitrogen) at 37°C and 5% CO_2. All other cell lines were maintained in high glucose DMEM with 10% FBS and 1 × PS (Invitrogen). Deferoxamine mesylate salt (DFO), succinylacetone (SA, 4,6-dioxoheptanoic acid) and cobalt(II) chloride hexahydrate ($CoCl_2 \cdot 6H_2O$) were obtained from Sigma-Aldrich.

4.5.2 Relative Quantification Real Time-qPCR

Total RNA was purified from cultured cells using the RNeasy Mini Kit (QIAGEN). First-strand cDNA was synthesized from purified RNA (500 ng) using the SuperScript III Synthesis System for RT-PCR (Invitrogen). Real time-quantitative PCR was performed using SYBR green-based detection (Applied Biosystems) with *Rplp0* as the endogenous control for analysis of cultured cells. Primer sequences are listed below.

4.5.3 Primers used for SYBR Green Real-Time qPCR

SYBR green primers were designed using the Roche Universal ProbeLibrary Assay Design Center tool or the Integrated DNA Technologies RealTime qPCR Assay tool.

Mouse:

Afg3l1:

Left: gcccaggaaattcagtacctc Right: cctttccctcctctgttgc

Afg3l2:

Left: ggtttatattgctgagagcgatg Right: atgagtacggtgggcaacat

Atf5:

Left: tttttatgaagaggaataagatgaggt Right: ggaggctgcaccaacaat

Cebpb:

Left: tgatgcaatccggatcaa Right: cacgtgtgttgcgtcagtc

Clpp:

Left: gcaacaagaagcccattcat Right: gtactgcattgtgtcgtagatgg

Clpx:

Left: tggtgcctttaatggcttaga Right: ggtgttccaaagccgagata

Ddit3:

Left: gcgacagagccagaataaca Right: gatgcacttccttctggaaca

Dnaja3:

Left: acaagccaagcagaagaagc Right: tttcccactggcatccttac

Hspa9:

Left: gttatggagggcaaacaagc Right: aggggtagttctggcacctt

Hspd1:

Left: cagagctgggtccctcact Right: ggactgtgggtagtcgaagc

Hspe1:

Left: ggcccgagttcagagtcc Right: tgtcaaagagcggaagaaactt

Htra2:

Left: ttggagtgatgatgctgacc Right: ttggctcacggagctgtagt

Lonp1:

Left: tggcgtcttcctaaagagagat Right: tcccgtatggtagatttcatcc

Nrf1:

Left: gacgctgctttcagtccttc Right: gtgttcagtttgggtcactcc

Rplp0:

Left: actggtctaggacccgagaag Right: tcccaccttgtctccagtct

Sirt7:

Left: tgtcatgcaactcctcatgaat Right: ggtcgccaaggagaagatt

Spg7:

Left: tgatggaccatgaagcaaag Right: tttccagaagggcattcg

Tfrc:

Left: tcctttccttgcatattctgg Right: ccaaataaggatagtctgcatcc

Trap1:

Left: aaggaggaaaagtttgaggaca Right: ttctcatccacgccattaga

Yme1l1:

Left: cggtagaccctgtccagatg Right: ttcaaccacttcctgtaactcttg

4.5.4 Immunoblotting

For immunoblotting, protein lysates were prepared in RIPA buffer composed of 150 mM NaCl, 1% IGEPAL CA-630, 0.5% sodium deoxycholate, 0.1% SDS, 50 mM Tris (pH 8.0), 0.4 mM EDTA (pH 8.0), 10% glycerol and a protease inhibitor cocktail (Roche Diagnostics), and 15 μg of cleared whole-cell lysate, as determined by BCA assay (Thermo Scientific), was separated on a 4-12% Novex NuPAGE Bis-Tris Mini Gel (Invitrogen), transferred to PVDF and probed with primary antibodies (listed below).

4.5.5 Primary Antibodies used for Immunoblotting

Antigen	**Supplier**	**Product Number**
β-actin	Abcam	ab8224
CI subunit 8 kDa	Abcam	ab110245
COXIV	Abcam	ab14744
Cytochrome c	Abcam	ab110325
NDUFB3	Proteintech Group	12358-1-AP
VDAC	Abcam	ab18988

4.5.6 roGFP Measurements

HEK 293FT cells were seeded at 12.5×10^3 cells/well on black, clear bottom 96 well plates coated with poly-D-lysine (500 µg/mL for 1 hr at 37°C then washed with PBS) and the following day were transfected with 100 ng of ro1 (roGFP1, cytosolic) or pRA306 (roGFP1, mitochondrial) using Lipofectamine LTX (Invitrogen) at 0.35 µL/well with PLUS reagent at 0.1 µL/well based on the manufacturer's recommendations. The next day the cells were treated with DFO or $CoCl_2$, and after 24 hrs the growth media was exchanged for PBS and roGFP fluorescence was measured using a BioTek Synergy 2 Microplate Reader with 360/40 and 485/20 excitation, and 528/20 emission filter sets. The fluorescence emission values at the 360/40 (oxidized) and 485/20 (reduced) excitations were used to calculate oxidized/reduced (ox/red) ratios. **Athavi Jeevananthan (Pagliarini Lab) performed the roGFP experiments.**

4.5.7 Statistics

p Values were calculated by Student's two-tailed t test as indicated in the figure legends.

4.6 Acknowledgements

We would like to thank the members of the R.S.E., J.M.D. and D.J.P. laboratories for helpful discussions and assistance regarding this project, and we would like to thank James Remington (University of Oregon) for providing the roGFP constructs.

4.7 References

Allen, G.F., Toth, R., James, J., and Ganley, I.G. (2013). Loss of iron triggers PINK1/Parkin-independent mitophagy. EMBO Rep *14*, 1127-1135.

Anderson, C.P., Shen, M., Eisenstein, R.S., and Leibold, E.A. (2012). Mammalian iron metabolism and its control by iron regulatory proteins. Biochim Biophys Acta *1823*, 1468-1483.

Atamna, H., Liu, J., and Ames, B.N. (2001). Heme deficiency selectively interrupts assembly of mitochondrial complex IV in human fibroblasts: revelance to aging. J Biol Chem *276*, 48410-48416.

Chandel, N.S., McClintock, D.S., Feliciano, C.E., Wood, T.M., Melendez, J.A., Rodriguez, A.M., and Schumacker, P.T. (2000). Reactive oxygen species generated at mitochondrial complex III stabilize hypoxia-inducible factor-1alpha during hypoxia: a mechanism of O2 sensing. J Biol Chem *275*, 25130-25138.

Dallman, P.R. (1969). Iron restriction in the nursing rat: early effects upon tissue heme proteins, hemoglobin and liver iron. J Nutr *97*, 475-480.

Dallman, P.R. (1986). Biochemical basis for the manifestations of iron deficiency. Annu Rev Nutr *6*, 13-40.

Dallman, P.R., and Goodman, J.R. (1970). Enlargement of mitochondrial compartment in iron and copper deficiency. Blood *35*, 496-505.

Fan, J., Krautkramer, K.A., Feldman, J.L., and Denu, J.M. (2015). Metabolic regulation of histone post-translational modifications. ACS Chem Biol *10*, 95-108.

Fleming, R.E., Feng, Q., and Britton, R.S. (2011). Knockout mouse models of iron homeostasis. Annu Rev Nutr *31*, 117-137.

Fretham, S.J., Carlson, E.S., and Georgieff, M.K. (2011). The role of iron in learning and memory. Adv Nutr *2*, 112-121.

Galy, B., Ferring-Appel, D., Sauer, S.W., Kaden, S., Lyoumi, S., Puy, H., Kolker, S., Grone, H.J., and Hentze, M.W. (2010). Iron regulatory proteins secure mitochondrial iron sufficiency and function. Cell Metab *12*, 194-201.

Guha, M., and Avadhani, N.G. (2013). Mitochondrial retrograde signaling at the crossroads of tumor bioenergetics, genetics and epigenetics. Mitochondrion *13*, 577-591.

Gut, P., and Verdin, E. (2013). The nexus of chromatin regulation and intermediary metabolism. Nature *502*, 489-498.

Hanson, G.T., Aggeler, R., Oglesbee, D., Cannon, M., Capaldi, R.A., Tsien, R.Y., and Remington, S.J. (2004). Investigating mitochondrial redox potential with redox-sensitive green fluorescent protein indicators. J Biol Chem *279*, 13044-13053.

Hebert, A.S., Merrill, A.E., Bailey, D.J., Still, A.J., Westphall, M.S., Strieter, E.R., Pagliarini, D.J., and Coon, J.J. (2013). Neutron-encoded mass signatures for multiplexed proteome quantification. Nat Methods *10*, 332-334.

Heijmans, B.T., Tobi, E.W., Stein, A.D., Putter, H., Blauw, G.J., Susser, E.S., Slagboom, P.E., and Lumey, L.H. (2008). Persistent epigenetic differences associated with prenatal exposure to famine in humans. Proc Natl Acad Sci U S A *105*, 17046-17049.

Hentze, M.W., Muckenthaler, M.U., Galy, B., and Camaschella, C. (2010). Two to tango: regulation of Mammalian iron metabolism. Cell *142*, 24-38.

Hock, M.B., and Kralli, A. (2009). Transcriptional control of mitochondrial biogenesis and function. Annu Rev Physiol *71*, 177-203.

Hojfeldt, J.W., Agger, K., and Helin, K. (2013). Histone lysine demethylases as targets for anticancer therapy. Nat Rev Drug Discov *12*, 917-930.

Ishikawa, H., Kato, M., Hori, H., Ishimori, K., Kirisako, T., Tokunaga, F., and Iwai, K. (2005). Involvement of heme regulatory motif in heme-mediated ubiquitination and degradation of IRP2. Mol Cell *19*, 171-181.

Jovaisaite, V., and Auwerx, J. (2015). The mitochondrial unfolded protein response-synchronizing genomes. Curr Opin Cell Biol *33*, 74-81.

Jovaisaite, V., Mouchiroud, L., and Auwerx, J. (2014). The mitochondrial unfolded protein response, a conserved stress response pathway with implications in health and disease. J Exp Biol *217*, 137-143.

Kaati, G., Bygren, L.O., and Edvinsson, S. (2002). Cardiovascular and diabetes mortality determined by nutrition during parents' and grandparents' slow growth period. Eur J Hum Genet *10*, 682-688.

Kaelin, W.G., Jr., and McKnight, S.L. (2013). Influence of metabolism on epigenetics and disease. Cell *153*, 56-69.

Kalinowski, D.S., and Richardson, D.R. (2005). The evolution of iron chelators for the treatment of iron overload disease and cancer. Pharmacol Rev *57*, 547-583.

Kirienko, N.V., Ausubel, F.M., and Ruvkun, G. (2015). Mitophagy confers resistance to siderophore-mediated killing by Pseudomonas aeruginosa. Proc Natl Acad Sci U S A *112*, 1821-1826.

Klimova, T., and Chandel, N.S. (2008). Mitochondrial complex III regulates hypoxic activation of HIF. Cell Death Differ *15*, 660-666.

Kooistra, S.M., and Helin, K. (2012). Molecular mechanisms and potential functions of histone demethylases. Nat Rev Mol Cell Biol *13*, 297-311.

Li, Y., He, Y., Qi, L., Jaddoe, V.W., Feskens, E.J., Yang, X., Ma, G., and Hu, F.B. (2010). Exposure to the Chinese famine in early life and the risk of hyperglycemia and type 2 diabetes in adulthood. Diabetes *59*, 2400-2406.

Lumey, L.H., Stein, A.D., and Susser, E. (2011). Prenatal famine and adult health. Annu Rev Public Health *32*, 237-262.

Marks, P.A., and Breslow, R. (2007). Dimethyl sulfoxide to vorinostat: development of this histone deacetylase inhibitor as an anticancer drug. Nat Biotechnol *25*, 84-90.

McCann, J.C., and Ames, B.N. (2007). An overview of evidence for a causal relation between iron deficiency during development and deficits in cognitive or behavioral function. Am J Clin Nutr *85*, 931-945.

Mense, S.M., and Zhang, L. (2006). Heme: a versatile signaling molecule controlling the activities of diverse regulators ranging from transcription factors to MAP kinases. Cell Res *16*, 681-692.

Merrill, A.E., Hebert, A.S., MacGilvray, M.E., Rose, C.M., Bailey, D.J., Bradley, J.C., Wood, W.W., El Masri, M., Westphall, M.S., Gasch, A.P.*, et al.* (2014). NeuCode labels for relative protein quantification. Mol Cell Proteomics *13*, 2503-2512.

Meyer, A.J., and Dick, T.P. (2010). Fluorescent protein-based redox probes. Antioxid Redox Signal *13*, 621-650.

Mick, D.U., Fox, T.D., and Rehling, P. (2011). Inventory control: cytochrome c oxidase assembly regulates mitochondrial translation. Nat Rev Mol Cell Biol *12*, 14-20.

Mohrin, M., Shin, J., Liu, Y., Brown, K., Luo, H., Xi, Y., Haynes, C.M., and Chen, D. (2015). Stem cell aging. A mitochondrial UPR-mediated metabolic checkpoint regulates hematopoietic stem cell aging. Science *347*, 1374-1377.

Mosammaparast, N., and Shi, Y. (2010). Reversal of histone methylation: biochemical and molecular mechanisms of histone demethylases. Annu Rev Biochem *79*, 155-179.

Nargund, A.M., Fiorese, C.J., Pellegrino, M.W., Deng, P., and Haynes, C.M. (2015). Mitochondrial and nuclear accumulation of the transcription factor ATFS-1 promotes OXPHOS recovery during the UPR(mt). Mol Cell *58*, 123-133.

Pagliarini, D.J., Calvo, S.E., Chang, B., Sheth, S.A., Vafai, S.B., Ong, S.E., Walford, G.A., Sugiana, C., Boneh, A., Chen, W.K.*, et al.* (2008). A mitochondrial protein compendium elucidates complex I disease biology. Cell *134*, 112-123.

Patti, G.J., Yanes, O., and Siuzdak, G. (2012). Innovation: Metabolomics: the apogee of the omics trilogy. Nat Rev Mol Cell Biol *13*, 263-269.

Pellegrino, M.W., Nargund, A.M., Kirienko, N.V., Gillis, R., Fiorese, C.J., and Haynes, C.M. (2014). Mitochondrial UPR-regulated innate immunity provides resistance to pathogen infection. Nature *516*, 414-417.

Ravelli, A.C., van der Meulen, J.H., Michels, R.P., Osmond, C., Barker, D.J., Hales, C.N., and Bleker, O.P. (1998). Glucose tolerance in adults after prenatal exposure to famine. Lancet *351*, 173-177.

Ravelli, A.C., van Der Meulen, J.H., Osmond, C., Barker, D.J., and Bleker, O.P. (1999). Obesity at the age of 50 y in men and women exposed to famine prenatally. Am J Clin Nutr *70*, 811-816.

Ravelli, G.P., Stein, Z.A., and Susser, M.W. (1976). Obesity in young men after famine exposure in utero and early infancy. N Engl J Med *295*, 349-353.

Rensvold, J.W., Ong, S.E., Jeevananthan, A., Carr, S.A., Mootha, V.K., and Pagliarini, D.J. (2013). Complementary RNA and protein profiling identifies iron as a key regulator of mitochondrial biogenesis. Cell Rep *3*, 237-245.

Richardson, D.R., Lane, D.J., Becker, E.M., Huang, M.L., Whitnall, M., Suryo Rahmanto, Y., Sheftel, A.D., and Ponka, P. (2010). Mitochondrial iron trafficking and the integration of iron metabolism between the mitochondrion and cytosol. Proc Natl Acad Sci U S A *107*, 10775-10782.

Rose, C.M., Merrill, A.E., Bailey, D.J., Hebert, A.S., Westphall, M.S., and Coon, J.J. (2013). Neutron encoded labeling for peptide identification. Anal Chem *85*, 5129-5137.

Roseboom, T.J., van der Meulen, J.H., Osmond, C., Barker, D.J., Ravelli, A.C., Schroeder-Tanka, J.M., van Montfrans, G.A., Michels, R.P., and Bleker, O.P. (2000). Coronary heart disease after prenatal exposure to the Dutch famine, 1944-45. Heart *84*, 595-598.

Rouault, T.A., and Tong, W.H. (2005). Iron-sulphur cluster biogenesis and mitochondrial iron homeostasis. Nat Rev Mol Cell Biol *6*, 345-351.

Scarpulla, R.C. (2008). Transcriptional paradigms in mammalian mitochondrial biogenesis and function. Physiol Rev *88*, 611-638.

Scarpulla, R.C. (2011). Metabolic control of mitochondrial biogenesis through the PGC-1 family regulatory network. Biochim Biophys Acta *1813*, 1269-1278.

Schiavi, A., Maglioni, S., Palikaras, K., Shaik, A., Strappazzon, F., Brinkmann, V., Torgovnick, A., Castelein, N., De Henau, S., Braeckman, B.P.*, et al.* (2015). Iron-Starvation-Induced Mitophagy Mediates Lifespan Extension upon Mitochondrial Stress in C. elegans. Curr Biol *25*, 1810-1822.

Schmidt, O., Pfanner, N., and Meisinger, C. (2010). Mitochondrial protein import: from proteomics to functional mechanisms. Nat Rev Mol Cell Biol *11*, 655-667.

Schulz, A.M., and Haynes, C.M. (2015). UPR-mediated cytoprotection and organismal aging. Biochim Biophys Acta.

Schwanhausser, B., Busse, D., Li, N., Dittmar, G., Schuchhardt, J., Wolf, J., Chen, W., and Selbach, M. (2011). Global quantification of mammalian gene expression control. Nature *473*, 337-342.

Smith, B.C., and Denu, J.M. (2009). Chemical mechanisms of histone lysine and arginine modifications. Biochim Biophys Acta *1789*, 45-57.

St Clair, D., Xu, M., Wang, P., Yu, Y., Fang, Y., Zhang, F., Zheng, X., Gu, N., Feng, G., Sham, P.*, et al.* (2005). Rates of adult schizophrenia following prenatal exposure to the Chinese famine of 1959-1961. JAMA *294*, 557-562.

Susser, E.S., and Lin, S.P. (1992). Schizophrenia after prenatal exposure to the Dutch Hunger Winter of 1944-1945. Arch Gen Psychiatry *49*, 983-988.

Wallace, D.C., and Fan, W. (2010). Energetics, epigenetics, mitochondrial genetics. Mitochondrion *10*, 12-31.

Walter, P.B., Knutson, M.D., Paler-Martinez, A., Lee, S., Xu, Y., Viteri, F.E., and Ames, B.N. (2002). Iron deficiency and iron excess damage mitochondria and mitochondrial DNA in rats. Proc Natl Acad Sci U S A *99*, 2264-2269.

Witt, O., Deubzer, H.E., Milde, T., and Oehme, I. (2009). HDAC family: What are the cancer relevant targets? Cancer Lett *277*, 8-21.

Xu, W.S., Parmigiani, R.B., and Marks, P.A. (2007). Histone deacetylase inhibitors: molecular mechanisms of action. Oncogene *26*, 5541-5552.

Yamanaka, K., Ishikawa, H., Megumi, Y., Tokunaga, F., Kanie, M., Rouault, T.A., Morishima, I., Minato, N., Ishimori, K., and Iwai, K. (2003). Identification of the ubiquitin-protein ligase that recognizes oxidized IRP2. Nat Cell Biol *5*, 336-340.

Yoon, Y.S., Yoon, D.S., Lim, I.K., Yoon, S.H., Chung, H.Y., Rojo, M., Malka, F., Jou, M.J., Martinou, J.C., and Yoon, G. (2006). Formation of elongated giant mitochondria in DFO-induced cellular senescence: involvement of enhanced fusion process through modulation of Fis1. J Cell Physiol *209*, 468-480.

Yu, Y., Kovacevic, Z., and Richardson, D.R. (2007). Tuning cell cycle regulation with an iron key. Cell Cycle *6*, 1982-1994.

Yun, J., and Finkel, T. (2014). Mitohormesis. Cell Metab *19*, 757-766.

Zimmermann, M.B., and Hurrell, R.F. (2007). Nutritional iron deficiency. Lancet *370*, 511-520.

Zumbrennen, K.B., Hanson, E.S., and Leibold, E.A. (2008). HOIL-1 is not required for iron-mediated IRP2 degradation in HEK293 cells. Biochim Biophys Acta *1783*, 246-252.

4.8 Figures

Figure 1: Analysis of Mitochondrial Protein Synthesis and Degradation Upon Iron Chelation

(A) Average half-life of transcripts encoding protein subunits from each OxPhos complex (calculated from Schwanhäusser, et al., 2011).

(B) 9-plex NeuCode metabolic labeling strategies for MS-based proteomic analysis of mitochondrial protein synthesis and degradation. Experimental workflow for analysis of mitochondrial protein synthesis and degradation involves performing pulse-labeling and pulse-chase strategies, respectively, followed by mitochondrial enrichment and high-resolution MS-based quantitative proteomics with 9-plex NeuCode. If DFO treatment causes a decrease in synthesis and/or an increase in degradation we will measure a lower abundance of the labeled proteins in DFO treated cells. Each color designates one of 9 unique NeuCode labels.

Figure 1

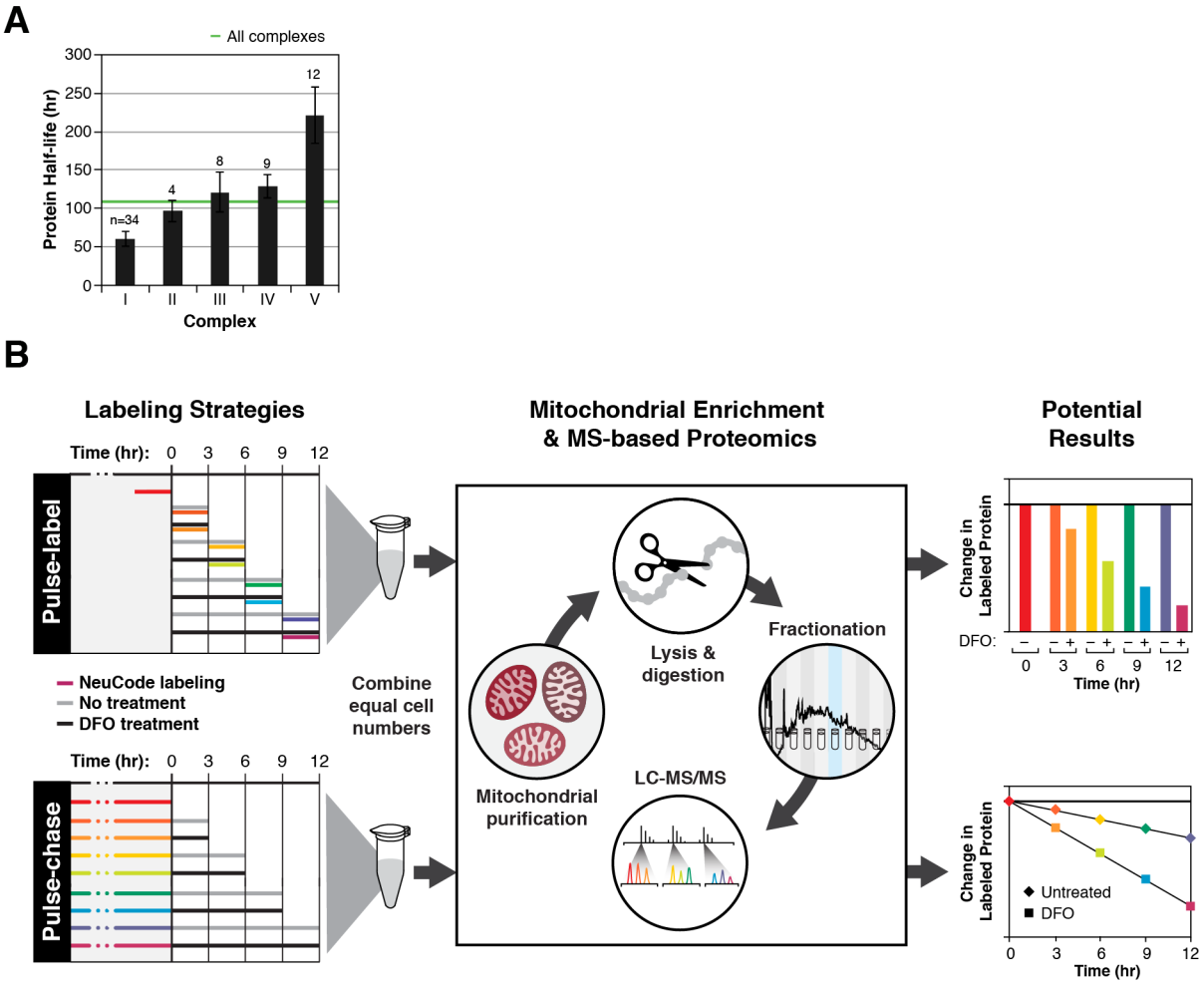
A
All complexes
Protein Half-life (hr)
300
250
200
150
100
50
0
n=34
4
8
9
12
I
II
III
IV
V
Complex
B
Labeling Strategies
Mitochondrial Enrichment & MS-based Proteomics
Potential Results
Time (hr): 0 3 6 9 12
Pulse-label
NeuCode labeling
No treatment
DFO treatment
Time (hr): 0 3 6 9 12
Pulse-chase
Combine equal cell numbers
Mitochondrial purification
Lysis & digestion
Fractionation
LC-MS/MS
Change in Labeled Protein
DFO:
0 3 6 9 12
Time (hr)
Change in Labeled Protein
Untreated
DFO
0 3 6 9 12
Time (hr)

Figure 2: Succinylacetone Inhibition of Heme Synthesis Causes Similar Decreases in Mitochondrial Protein Abundance as Iron Chelation

(A) Level of the indicated proteins from C2C12 mouse myoblasts treated with the indicated concentrations of deferoxamine (DFO) and succinylacetone (SA) for 24 hrs as assessed by immunoblotting.

Figure 2

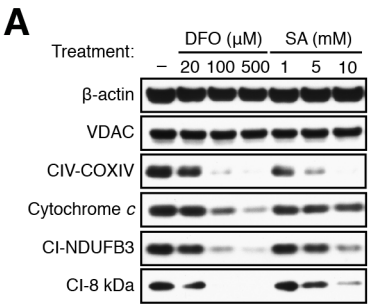
A
Treatment:
DFO (μM)
SA (mM)
–
20
100
500
1
5
10
β-actin
VDAC
CIV-COXIV
Cytochrome c
CI-NDUFB3
CI-8 kDa

Figure 3: Analysis of Mitochondrial Retrograde Signals and Adaptations in Response to Iron Depletion

(A) Redox signal from HEK 293FT cells transfected with reduction-oxidation sensitive GFP targeted to the cytosol (roGFP) or mitochondria (mito-roGFP) after 6 or 24 hrs following treatment with 100 μM DFO or $CoCl_2$. Data are displayed as the mean of biological triplicate measurements (*$p < 0.05$, **$p < 0.01$, Student's t test). **roGFP experiments were performed by Athavi Jeevananthan.**

(B) Abundance of transcripts encoding the major mitochondrial chaperones and proteases, and transcriptional regulators linked to the UPR^{mt} in C2C12 myoblasts following treatment with 100 μM DFO for 24 hrs as assessed by real-time qPCR. Data are displayed as mean of triplicate measurements.

Figure 3

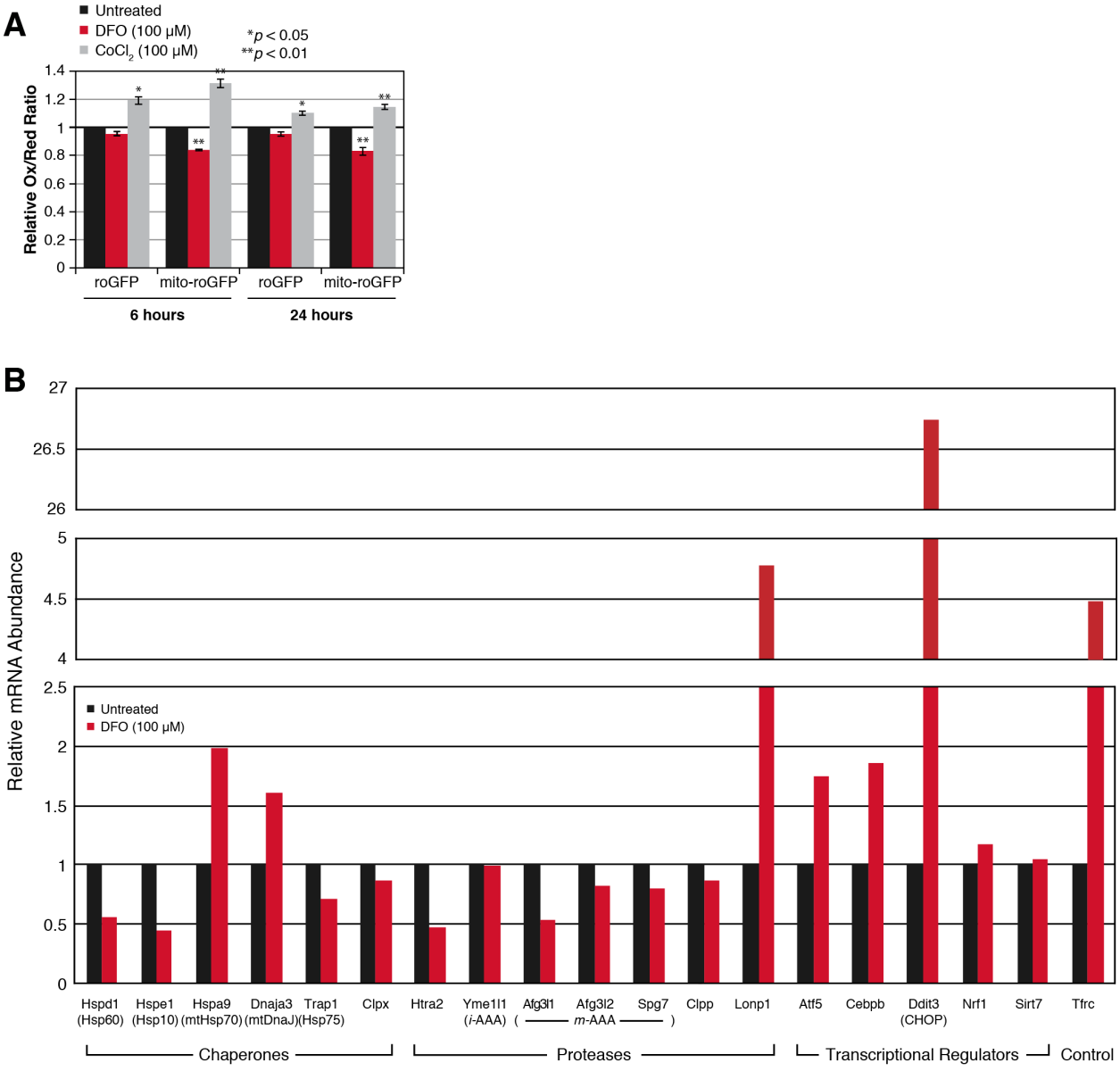
A
Untreated
DFO (100 μM)
CoCl2 (100 μM)
*p < 0.05
**p < 0.01
Relative Ox/Red Ratio
roGFP
mito-roGFP
roGFP
mito-roGFP
6 hours
24 hours
B
Relative mRNA Abundance
Untreated
DFO (100 μM)
Hspd1 (Hsp60)
Hspe1 (Hsp10)
Hspa9 (mtHsp70)
Dnaja3 (mtDnaJ)
Trap1 (Hsp75)
Clpx
Htra2
Yme1l1 (i-AAA)
Afg3l1
Afg3l2
m-AAA
Spg7
Clpp
Lonp1
Atf5
Cebpb
Ddit3 (CHOP)
Nrf1
Sirt7
Tfrc
Chaperones
Proteases
Transcriptional Regulators
Control